DESIGN OF COMPACT MICROSTRIP ANTENNA FOR BIOMEDICAL APPLICATIONS

A Thesis

Submitted in fulfilment of the requirement for the award of the degree

of

DOCTOR OF PHILOSOPHY

in

Electronics and Communication Engineering

Submitted by

GURPRINCE SINGH

Reg. No. 901706010

Under the Supervision of

Dr. Jaswinder Kaur
Assistant Professor
TIET, Patiala (Punjab), India

Electronics and Communication Engineering Department

Thapar Institute of Engineering and Technology, Patiala-147004

February-2022

CERTIFICATE

I, **Gurprince Singh** hereby declare that the work contained in the thesis entitled **"DESIGN OF COMPACT MICROSTRIP ANTENNA FOR BIOMEDICAL APPLICATIONS"** being submitted by me to **Department of Electronics and Communication Engineering, Thapar Institute of Engineering and Technology, Patiala** in fulfillment of the award of the degree of "**Doctor of Philosophy**" is a record of authentic research work carried out under the supervision of **Dr. Jaswinder Kaur**. The matter presented in this thesis does not incorporate any material previously published or written by any other person except where due references are made in the text. The results obtained in this thesis have not been submitted in part or full to any other institute or university for the award of degree or diploma.

Gurprince Singh

Date 26-Sept-2023

Gurprince Singh

(Reg. No. 901706010)

This is to certify that the above statement made by the candidate is correct and true to the best of our knowledge and belief. He has worked under our supervision and fulfilled the requirements for the submission of this thesis which has reached the requisite standard.

Jaswinder Kaur

Dr. Jaswinder Kaur

Assistant Professor, ECED

TIET, Patiala-147001, India

Date 26/9/2023

ACKNOWLEDGEMENT

I sincerely thank my creator, the almighty God for the gift of life, knowledge and strength to accomplish this work. This research work is by far the most significant accomplishment in my life and it would be impossible without peoples who supported me and believed in me. I would like to extend my gratitude and my sincere gratitude to my honorable, research advisors, Dr. Jaswinder Kaur for their support and guidance during the course of my study. She is not only a great professor, with deep vision but also and most importantly kind persons. They have always been willing to give me insights and pointers to tackle the problems along the way keeping very keen interest in listening to my problems. They are always there when I needed to see them and attentive when I spoke with them. My respect for them grew and will always grow throughout my entire life. They always pointed me in the right direction when I lost the path and supported me when I was in the right path. I sincerely thank for their exemplary guidance and encouragement. Their trust and support inspired me in the most important moments of making right decisions and I am glad to work with them. Their moral support when I faced hurdles is unforgettable. I would also like to thank the facilities provided by Thapar Institute of Engineering and Technology, Patiala for the successful work.

I would like to thank my committee members and also my completion of acknowledgement remains void without thanking Dr. Alpana Agarwal and my doctoral committee members. I am also thankful to various researchers of the world, who are engaged in sharing their experienced knowledge in the web communities of Research Gate, Wikipedia, and others.

Last but not least I would like to thank my father Mitthu Singh, mother Paramjeet Kaur, and brother Dr. Gurveer Singh, who taught me the value of hard work by their own example and all those persons who directly or indirectly helped me during my work and contributed towards this work.

Gurprince Singh

TIET, Patiala (Punjab), India

ABSTRACT

Implantable Medical Devices (IMDs) have recently become a popular research area because of their potential to improve one's quality of life. IMDs are the devices that are implanted into human tissues for diagnostic, monitoring, and therapy purposes. Biotelemetry for IMDs enables bidirectional data transfer and control signal reception without the need for cables attached to bedside monitors. Because of the rising number of age-related symptoms and the need for telemedicine in old age centers, IMD sector is expected to grow. Among all the components used in these devices, an antenna is a fundamental element for wireless data transmission outside the human body. The current study examines implantable biomedical antennas in depth. One of the biggest challenges in IMDs is that the human body changes the antenna's general properties and absorbs majority of its radiation. Moreover, at lower frequencies it is difficult to lower the proportions of the antenna to meet the size requirements of an implantable device. The antenna material should be biocompatible in order to protect the surrounding body tissues from allergic reactions and the proposed antenna design must also exhibit more expanded SAR distribution to meet the IEEE safety standards.

Therefore, this thesis focuses on design approaches, constraints, simulation techniques and manufacturing and testing of implantable antennas. Compact and biocompatible antennas have been fabricated which can yield the performance parameters good enough to meet the safety standards and size requirements. In-silico, in-vitro and ex-vivo techniques are used for testing and validation of antenna prototypes. For in-vitro testing, skin mimicking solution has been prepared for testing of proposed antenna prototype at particular frequency bands, whereas chicken sample is utilized for ex-vivo testing. Four antennas are designed, fabricated and tested for implanting inside human body at ISM (2.4-2.48 GHz) and MICS (402-405 MHz) bands. To make the antenna compact enough, high dielectric substrate material, slotting technique and shorting pin technique is used. To enhance the biocompatibility of antennas, high dielectric substrates are used for covering the antenna as superstrate layers which also improve some of the antenna parameters especially gain and helps further to reduce the size. All of the proposed antennas in this thesis are novel, miniaturized, within safety limits for human body, can operate successfully within appropriate medical band ranges and have better performance than other antennas available in

recently reported literature. This ensures that the fabricated antenna is ready to use with immediate effect and can prove to be helpful in implantable devices for biotelemetry applications.

LIST OF PUBLICATIONS

1. Singh G, Kaur J. Skin and brain implantable inset-fed antenna at ISM band for wireless biotelemetry applications. Microw Opt Technol Lett. 2020;1–6.https://doi.org/10.1002/mop.32603
2. Singh G, Kaur J. In-silico and in-vitro testing of an implantable superstrate loaded biocompatible antenna for MICS band applications. Microw Opt Technol Lett. 2020;1–7.https://doi.org/10.1002/mop.32687
3. Singh, G., Kaur, J. Design of a compact superstrate-loaded slotted implantable antenna for ISM band applications. Sādhanā 46, 164 (2021). https://doi.org/10.1007/s12046-021-01691-4
4. Singh, G., Kaur, J. & Kaur, S. Detection of breast tumor using inset-fed microstrip patch antenna at MICS band for implantable applications. Sādhanā 46, 244 (2021). https://doi.org/10.1007/s12046-021-01762-6
5. Singh, G., Kaur, J. Small Footprint Biocompatible Antenna for Implantable Devices: Design, In-Silico, In-Vitro and Ex-Vivo Testing. Iran J Sci Technol Trans Electr Eng (2023). https://doi.org/10.1007/s40998-023-00588-8

COMMUNICATED

1. Singh G, Kaur J, Kaur S, Panwar R. Detection of Brain Tumor using microstrip-line fed Hexagonal shaped antenna at ISM band for wearable applications.[under review in WPC journal]

LIST OF ABBREVIATIONS

IMD	Implantable Medical Devices
RF	Radio Frequency
FES	Functional Electrical Stimulators Medical
MICS	Implant Communications Service Industrial
ISM	Scientific and Medical
MBAN	Medical Body Area Networks
WBAN	Wireless Body Area Networks
WMTS	Wireless Medical Telemetry Service Planar
PIFA	Inverted-F Antenna
VF	Volume Factor
PCB	Printed Circuit Board
SMD	Surface Mounted Device
SCS	Spinal Cord Simulators
DBS	Deep Brain Stimulators
WPT	Wireless Power Transfer
MRI	Magnetic Resonance Imaging
CT	Computer Tomography
VNA	Vector Network Analyzer
SAR	Specific Absorption Rate

SPEAG	Schmid and Partner Engineering AG
POPEYE	Posable Phantom for Electromagnetic Systems Evaluations
FSS	Frequency Selective Surface
PDMS	Poly-Di-Methyl-Siloxane
IACUC	Institutional Animal Care And Use Committee
ZOR	Zeroth–Order-Resonance
HFSS	High Frequency Structure Simulator
CST MWS	Computer Simulation Technology Microwave Studio

GLOSSARY OF SYMBOLS

ϵ_r	Relative Permittivity
ϵ	Absolute Permittivity
ϵ_0	Free Space Permittivity
tan δ	Loss Tangent
$\lvert E \rvert$	Electric Field Intensity
σ	Conductivity
π	Pi
ρ	Tissue Density

LIST OF FIGURES

Figure No. **Name of Figure** **Pg. No.**

FIGURE 1.1 DATA TRANSFER THROUGH BIOTELEMETRY FROM BODY IMPLANTABLE DEVICE [4].....2

FIGURE 1.2 BLOCK DIAGRAM OF AN IMPLANTABLE DEVICE AND ITS WIRELESS DATA TRANSMISSION SYSTEM[19].....4

FIGURE 1.3 TYPES OF IMDS (A) FLAT TYPE [21] (B) CAPSULE TYPE [23].....7

FIGURE 1.4 WPT TO AN IMPLANTABLE DEVICE [33].....8

FIGURE 1.5 IN-SILICO TESTING OF ANTENNA INSIDE (A) HOMOGENEOUS LAYER (B) HETEROGENEOUS LAYERS.....8

FIGURE 1.6 TESTING OF IMPLANTABLE DEVICE IN 3D REALISTIC HUMAN MODEL [12].....10

FIGURE 1.7 SOLID BODY PHANTOMS DEVELOPED BY SPEAG (A) WHOLE BODY PHANTOM POPEYE (B) SAM HEAD PHANTOM.....11

FIGURE 1.8 (A) ELASTIC SUPERSTRATE MATERIAL (B) ANTENNA ENCASED INSIDE SUPERSTRATE MATERIAL [44].....12

FIGURE 1.9 IN-SILICO TESTING OF IMPLANTABLE CAPSULE DEVICE IN (A) HOMOGENEOUS PHANTOM [12] (B) HUMAN MODEL NAMED GUSTAV OF CST [26] 13

FIGURE 1.10 IN-VITRO TESTING INSIDE SKIN MIMICKING LIQUID CONTAINED IN A RECTANGULAR BOX [47].....14

FIGURE 1.11 (A) EX-VIVO TESTING INSIDE PORK SAMPLE (A) MEASUREMENT OF FAR FIELD PATTERNS [22] (B) MEASUREMENT OF RETURN LOSS [48].....15

FIGURE 1.12 IN-VIVO TESTING (A) INSIDE DONOR RAT [44] (B) INSIDE DONOR PIG [49] 16

FIGURE 3.1 FLOWCHART OF PROPOSED MICROSTRIP PATCH ANTENNAS AT MICS AND ISM BAND.....35

FIGURE 3.1.1 GEOMETRY OF PROPOSED ANTENNA.....37

(A) RADIATING PATCH.....37

(B) GROUND PLANE.....37

(C) FABRICATED ANTENNA WITHOUT SUPERSTRATE LAYER.....37

(D) FABRICATED ANTENNA WITH SUPERSTRATE LAYER....37

FIGURE 3.1.2 TESTING OF ANTENNA....38

(A) ANTENNA INSIDE SKIN LAYER....38

(B) ANTENNA INSIDE THREE LAYER (SKIN-FAT-MUSCLE)....38

(C) FABRICATED ANTENNA TESTING INSIDE SKIN MIMICKING LIQUID....38

FIGURE 3.1.3 SIMULATED RESULTS OF PROPOSED ANTENNA....40

(A) SAR VALUE FOR 1-GRAM AVERAGE CUBIC TISSUE AT 2MW POWER. 40

(B) COMPARISON OF RETURN LOSS OF PROPOSED ANTENNA WITHIN BRAIN LAYER, SINGLE SKIN LAYER, THREE-LAYER AND WITHOUT SUPERSTRATE....40

FIGURE 3.1.4 SIMULATED GAIN AND SURFACE CURRENT DISTRIBUTION OF PROPOSED ANTENNA INSIDE SKIN 42

(A) 3D GAIN....42

(B) SURFACE CURRENT DISTRIBUTION....42

FIGURE 3.1.5 COMPARISON BETWEEN SIMULATED AND MEASURED RESULTS OF PROPOSED ANTENNA IN SKIN....43

(A) GAIN 43

(B) RETURN LOSS....43

FIGURE 3.2.1 GEOMETRY OF PROPOSED ANTENNA....47

(A) RADIATING PATCH....47

(B) GROUND PLANE 47

(C) FABRICATED ANTENNA WITHOUT SUPERSTRATE LAYER 47

(D) FABRICATED ANTENNA WITH SUPERSTRATE LAYER....47

FIGURE 3.2.2 EVOLUTION OF PROPOSED ANTENNA....48

(A) EVOLUTION STAGES OF PROPOSED ANTENNA 48

(B) RETURN LOSS CURVES FOR FOUR DIFFERENT CASES 48

FIGURE 3.2.3 TESTING OF ANTENNA....49

(A) ANTENNA INSIDE SKIN LAYER....49

(B) ANTENNA INSIDE THREE LAYER (SKIN-FAT-MUSCLE) 49

(C) FABRICATED ANTENNA TESTING INSIDE SKIN MIMICKING LIQUID....49

FIGURE 3.2.4 COMPARISON OF RETURN LOSS OF PROPOSED ANTENNA WITHIN BRAIN LAYER, HOMOGENEOUS SKIN LAYER AND THREE-LAYER PHANTOM....50

FIGURE 3.2.5 SAR VALUE FOR 1-GRAM AVERAGED CUBIC TISSUE AT 1W POWER....51

FIGURE 3.2.6 SIMULATED RESULTS OF PROPOSED ANTENNA....52

(A) GAIN VS FREQUENCY 52

(B) SURFACE CURRENT DISTRIBUTION....52

FIGURE 3.2.7 COMPARISON BETWEEN SIMULATED AND MEASURED RESULTS....53

(A) GAIN AT PHI 90 DEGREE AND PHI 0 DEGREE 53

(B) RETURN LOSS OF PROPOSED ANTENNA IN SKIN....53

FIGURE 4.1 GEOMETRICAL REPRESENTATION OF THE PROPOSED ANTENNA....57

(A) RADIATING PATCH....57

(B) GROUND PLANE 57

(C) FABRICATED ANTENNA WITHOUT SUPERSTRATE LAYER 57

(D) FABRICATED ANTENNA WITH SUPERSTRATE LAYER....57

FIGURE 4.2 EVOLUTION OF THE GROUND PLANE OF PROPOSED ANTENNA 59

FIGURE 4.3 COMPARISON OF RETURN LOSS FOR FOUR DIFFERENT CONFIGURATIONS OF GROUND PLANE OF PROPOSED ANTENNA 60

FIGURE 4.4 PARAMETRIC SWEEP FOR THE DIFFERENT SLOTS EMBEDDED IN THE GROUND PLANE OF PROPOSED ANTENNA 61

(A) RETURN LOSS OF THE PROPOSED ANTENNA WITH VARYING R_1 61

(B) RETURN LOSS OF THE PROPOSED ANTENNA WITH VARYING G_2 61

FIGURE 4.5 SIMULATION SETUP OF PROPOSED ANTENNA....62

(A) ANTENNA INSIDE SKIN LAYER 62

(B) ANTENNA INSIDE THREE LAYER MODEL OF SKIN, FAT AND MUSCLE....62

(C) ANTENNA INSIDE BRAIN LAYER 62

FIGURE 4.6 COMPARISON OF SIMULATED RETURN LOSS CHARACTERISTICS OF THE PROPOSED ANTENNA 63

FIGURE 4.7 SURFACE CURRENT AND SAR OF PROPOSED ANTENNA 65

(A) SURFACE CURRENT DISTRIBUTION ON RADIATING ELEMENT AND GROUND PLANE 65

(B) SAR VALUE FOR 1-GRAM AVERAGED AND 10-GRAM AVERAGED TISSUE 65

FIGURE 4.8 IMPEDANCE VS FREQUENCY PLOT OF PROPOSED ANTENNA.....66

(A) REAL PART 66

(B) IMAGINARY PART.....66

FIGURE 4.9 GAIN PLOT AND RADIATION PATTERN OF THE PROPOSED ANTENNA 67

(A) SIMULATED GAIN VS FREQUENCY 67

(B) SIMULATED CO-POLARIZATION AND CROSS-POLARIZATION FOR E-PLANE AT PHI = 90 DEGREES 67

(C) SIMULATED CO-POLARIZATION AND CROSS-POLARIZATION FOR H-PLANE AT PHI = 0 DEGREES.....67

FIGURE 4.10 TESTING AND SET-UP OF THE PROPOSED ANTENNA 68

(A) FABRICATED ANTENNA TESTING INSIDE SKIN MIMICKING LIQUID 68

(B) COMPARISON OF SIMULATED AND MEASURED RETURN LOSS OF THE PROPOSED ANTENNA IN SKIN 68

FIGURE 5.1 GEOMETRY OF PROPOSED ANTENNA.....72

(A) RADIATING PATCH.....72

(B) GROUND PLANE 72

(C) FABRICATED ANTENNA WITHOUT SUPERSTRATE LAYER 72

(D) FABRICATED ANTENNA WITH SUPERSTRATE LAYER.....72

FIGURE 5.2 EVOLUTION OF PROPOSED ANTENNA.....73

(A) DIFFERENT CASES LEADING TO THE FINAL STRUCTURE OF PROPOSED ANTENNA73

(B) RETURN LOSS CURVES CORRESPONDING TO FOUR DIFFERENT CASES 73

FIGURE 5.3 TESTING OF PROPOSED ANTENNA 74

(A) IN-SILICO TESTING INSIDE SKIN LAYER 74
(B) IN-VITRO TESTING INSIDE SKIN MIMICKING LIQUID 74
(C) EX-VIVO TESTING INSIDE ANIMAL TISSUE (CHICKEN) 74
FIGURE 5.4 SIMULATED RESULTS OF PROPOSED ANTENNA....75
(A) SAR FOR 1-GRAM AVERAGED CUBIC TISSUE AT 1W POWER....75
(B) SAR FOR 10-GRAM AVERAGED CUBIC TISSUE AT 1W POWER....75
FIGURE 5.5 SIMULATED RESULTS OF PROPOSED ANTENNA....76
(A) SURFACE CURRENT DISTRIBUTION....76
(B) 3D PATTERN OF GAIN 76
FIGURE 5.6 RETURN LOSS CURVES OF PROPOSED ANTENNA DURING IN-SILICO, IN-VITRO AND EX-VIVO TESTING 77

LIST OF TABLES

Table No. **Name of Table** **Pg. No.**

TABLE 1.1 PERMITTIVITY AND CONDUCTIVITY OF SOME HUMAN TISSUES AT MICS AND ISM BAND[37] 9

TABLE 3.1.1 DIELECTRIC PROPERTIES OF HUMAN TISSUES AT ISM BAND 39

TABLE 3.1.2 COMPARISON OF SIMULATED AND MEASURED RETURN LOSS AND BANDWITH OF PROPOSED ANTENNA 43

TABLE 3.1.3 COMPARISON OF PROPOSED ANTENNA WITH RECENT LITERATURE 44

TABLE 3.2.1 COMPARISON OF SIMULATED AND MEASURED RETURN LOSS AND BANDWITH OF PROPOSED ANTENNA 51

TABLE 3.2.2 COMPARISON OF PROPOSED ANTENNA WITH RECENT LITERATURE 54

TABLE 4.1 GEOMETRICAL DIMENSIONS OF PROPOSED ANTENNA IN MM 58

TABLE 4.2 PERFORMANCE CHARACTERISTICS OF THE GROUND PLANE OF ANTENNA FOR FOUR DIFFERENT CASES 60

TABLE 4.3 PERFORMANCE CHARACTERISTICS OF THE PROPOSED ANTENNA WITH DIFFERENT VALUES OF R_1 (RADIUS OF CIRCULAR SLOTS) 61

TABLE 4.4 PERFORMANCE CHARACTERISTICS OF THE PROPOSED ANTENNA WITH DIFFERENT VALUES OF G2 (LENGTH OF BIGGER RECTANGULAR SLOT) 62

TABLE 4.5 DIELECTRIC PROPERTIES OF HUMAN TISSUES AT ISM BAND 63

TABLE 4.6 PERFORMANCE OF THE PROPOSED ANTENNA IN BRAIN LAYER, SINGLE SKIN LAYER AND THREE LAYER PHANTOM MODELS 64

TABLE 4.7 SIMULATED AND MEASURED RETURN LOSS AND BANDWITH OF THE PROPOSED ANTENNA INSIDE SINGLE LAYERED SKIN PHANTOM 69

TABLE 4.8 COMPARISON OF PERFORMANCE PARAMETERS OF PROPOSED ANTENNA WITH RECENTLY REPORTED LITERATURE 69

TABLE 5.1 RETURN LOSS AND BANDWIDTH OBTAINED DURING IN-SILICO, IN-VITRO AND EX-VIVO TESTING. 78

TABLE 5.2 COMPARISON OF PROPOSED ANTENNA WITH RECENT AVAILABLE LITERATURE 78

TABLE OF CONTENTS

Page No.

Certificate i

Acknowledgments ii

Abstract iii

List of Publications v

List of Abbreviations vi

Glossary of Symbols viii

List of Figures ix

List of Tables xiv

Table of Contents xvi

CHAPTER 1 1

INTRODUCTION 1

1.1 INTRODUCTION 1

1.2 IMPLANTABLE DEVICE CIRCUITRY AND WORKING 4

1.2.2 Wireless Power Transfer (WPT) in IMDs 7

1.3 TISSUE MODELS 8

1.4 SUPERSTRATE AND SUBSTRATE LAYERS 11

1.5 TESTING OF ANTENNA 12

1.5.1 In-silico testing 13

1.5.2 In-vitro testing 13

1.5.3 Ex-vivo testing 14

1.5.4 In-vivo testing 15

1.6 RESEARCH GAPS 16

1.7 OBJECTIVES 17

1.8 ORGANIZATION OF THESIS 18

CHAPTER 2 20

LITERATURE SURVEY 20

2.1 IN-SILICO TESTING (TESTING INSIDE SOFTWARE) 21

2.2 IN-VITRO TESTING (TESTING INSIDE PHANTOM) 24

2.3 EX-VIVO OR IN-VIVO (TESTING INSIDE ANIMAL) 28

2.4 MOTIVATION 32

CHAPTER 3 34

SKIN AND BRAIN IMPLANTABLE INSET-FED ANTENNAS AT ISM AND MICS BANDS FOR BIOTELEMETRY APPLICATIONS 34

3.1 IMPLANTABLE ANTENNA AT ISM BAND 36

3.1.1 Antenna Design 36

3.1.2 Fabrication and Testing of Antenna 38

3.1.3 Results and Discussions 39

3.2 IMPLANTABLE ANTENNA AT MICS BAND 46

3.2.1 Step by step approach to proposed antenna design 46

3.2.2 Testing of antenna 49

3.2.3 Results and discussions 50

CONCLUSION 54

CHAPTER 4 56

COMPACT IMPLANTABLE ANTENNA AT ISM BAND FOR BIOTELEMETRY APPLICATIONS 56

4.1 ANTENNA DESIGN 56

4.1.1 Evolution of the ground plane of proposed antenna 58

4.1.2 Parametric Sweep with different r_1 and g_2 60

4.2 SIMULATION AND MEASUREMENT SET UP OF THE PROPOSED ANTENNA 62

4.2.1 Surface Current Distribution 64

4.2.2 Specific Absorption Rate (SAR) 64

CONCLUSION 70

CHAPTER 5 71

IN-SILICO, IN-VITRO AND EX-VIVO TESTING OF SMALL FOOTPRINT IMPLANTABLE BIOCOMPATIBLE MICROSTRIP ANTENNA FOR BIOTELEMETRY APPLICATIONS 71

5.1 DESIGN AND EVOLUTION OF PROPOSED ANTENNA 71

5.2 TESTING OF PROPOSED ANTENNA 74

5.3 RESULTS AND DISCUSSION 75

CONCLUSION 79

CHAPTER 6 80

CONCLUSIONS AND FUTURE SCOPE 80

6.1 CONCLUSIONS 80
6.2 FUTURE SCOPE 81

REFERENCES 84

CHAPTER 1
INTRODUCTION

1.1 INTRODUCTION

The market of implantable medical devices (IMD) is thriving and in fact substantially booming in the 21st century. In this modern century, individuals are getting more habitual with the quick paced way of life. They are getting more vulnerable to diseases because of the infrequent visits to hospitals for normal routine checkups. Due to the busy schedule, everyone cannot afford time for his/her regular checkups and sometimes ignore the early stages of dangerous diseases, which may even cause death. Now-a-days, Covid-19 has affected almost every country in the world. Doctor to patient ratio has declined a lot, and it has become almost impossible and risky for hospital staff to physically examine every patient and perform routine checkups. Consequently, the need of body implantable devices for biotelemetry is skyrocketed. Therefore, there is a need to make some advancements in medical technologies to keep track of the patient's health parameters from a distance [1]. Moreover, it is an efficient, easy, and real time approach for patient monitoring [2]. This transfer of human body data, either wired or wireless, is called biomedical telemetry. Biomedical telemetry is used in biomedical engineering, which holds a noteworthy place in the advancement of patient diagnosis. It's been used from the early 1960's since the invention of wearable and battery powered pacemakers. In these starting years, low frequency inductive links were used with a low data rate of 1-30 kbps and a range of less than 10 cm which are considered as drawbacks [3]. To overcome this problem, these devices are now operated on the Radio Frequency (RF) spectrum. Figure 1.1 demonstrates the biotelemetry system of implantable devices in which a receiving antenna receives the signal from implantable antenna and the data is obtained after data processing unit available in the receiver system [4]. The receiver system can be mobile, laptop or any special receiver system particularly designed for receiving data. Some implantable devices that are widely used are functional electrical stimulators (FES) [5], pacemakers [6], cochlear implants [7], retinal implants [8], body temperature monitoring [9], and neural recording [10]. These devices work mainly in two frequency bands: Medical Implant Communications Service (MICS) (402-405 MHz) and Industrial, Scientific and Medical (ISM) (2.4-2.48 GHz) band [11-15].

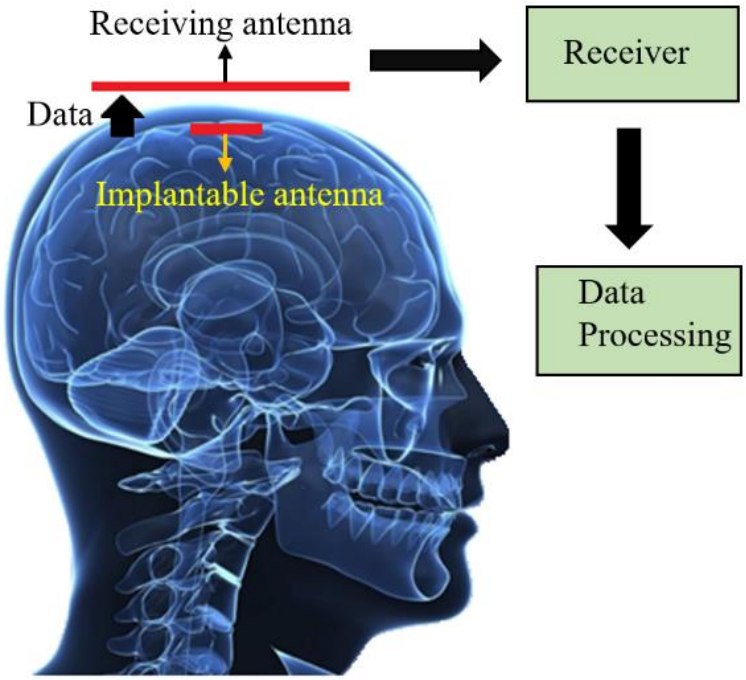

Figure 1.1 Data transfer through biotelemetry from body implantable device [4]

There are basically two types of devices used for biotelemetry, i.e., body implantable and body wearable antennas used for wireless body area networks (WBAN). In body implantable devices the device is implanted directly inside human body, whereas in body wearable, devices are in direct contact with the human body. In our work, the main focus is done on body implantable antenna [11].

The IMD is equipped with a battery, antenna, sensor, etc. [12]. The element used to send and receive signals wirelessly from the body implantable device is known as an implantable antenna. In data transmission, a high-performance implanted antenna is critical. To power the electronic components of IMDs, these implantable antennas are usually coupled with a rectifier. Several studies on implantable antennas for various applications have been published [2] [7]. A quad-band implanted antenna is proposed for multipurpose implants in [13], with single frequency band dedicated for harvesting energy. While, the remaining ones are utilized for transmission of data and wakeup signal [14].

For making these antennas, some common challenges faced are antenna size, biocompatibility, specific absorption rate (SAR) limitations and volume factor. Since implantable devices have size restrictions, all equipment and components within these devices ought to be miniaturized.

Moreover, it's troublesome to get an appreciable and desired radiation performance at low frequencies with a miniaturized structure [13]. As the antenna is to be inserted inside skin, therefore, it must be as small as possible [15]. For creating a compact size antenna, many techniques are used such as Planar Inverted-F Antenna (PIFA) structure [14], meandered [16], shorting pin [16-17], patch stacking [18-20], spiral [21-24] shaped designs and use of high dielectric materials [25-27].

Biocompatibility is important for patient's wellbeing. Human body tissues are conductive in nature which can short circuit to the antenna's metal layer in case of any direct contact. For long haul implantation, biocompatibility and obviating unwanted short circuit is important. The most general utilized methodology for protecting the biocompatibility of any antenna while isolating the metallic structure from human body tissue is to conceal the element with high dielectric superstrate like Rogers RT/duroid 3010 (ϵ_r = 10.2, tan δ = 0.0022), Rogers RT/duroid 3210 (ϵ_r = 10.2, tan δ = 0.003), Rogers RT/duroid 6010 (ϵ_r = 10.2, tan δ = 0.0035) and Alumina (ϵ_r = 9.4, tan δ = 0.006) etc. [1] [17].

The next challenge is due to exposure of the human body to electromagnetic fields i.e., SAR limitation. If the exposure to radiation of electromagnetic waves is above the threshold limit according to IEEE standards, then it has detrimental effects on the human body.

According to IEEE C95. 1-1999 standard, for any 1 gram tissue of cubic shape it has to be kept lower than 1.6 W/kg ($SAR_{1g,max} \leq 1.6$ W/kg), and for any 10 gram tissue of cubic shape, it should be kept lower than 2 W/kg ($SAR_{1g,max} \leq 2$ W/kg) [1][18].

Equation (1.1) depicts that the power absorbed (P_{abs}) by the human body is directly proportional to the electric field intensity [1].

$$P_{abs} = \int \sigma \left| E \right|^2 dV \tag{1.1}$$

Where, $\left| E \right|$ denotes the electric field intensity and σ is denoted by conductivity of human tissue.

Last challenge faced while making an implantable antenna is the volume factor. Volume factor of antenna can be denoted by the ratio of bandwidth of an antenna (kHz) to the volume of antenna (mm^3) as shown in Equation (1.2) [24].

$$\text{Volume factor (VF)} = \text{Bandwidth (in kHz)/Antenna volume } (mm^3) \tag{1.2}$$

1.2 IMPLANTABLE DEVICE CIRCUITRY AND WORKING

Figure 1.2 demonstrates the internal circuitry of IMDs that are developed for communication with external equipments using biotelemetry. The implantable device communication system includes the wireless data transmission link, the human body, and the external receiving system link, which is explained in seven subsections below.

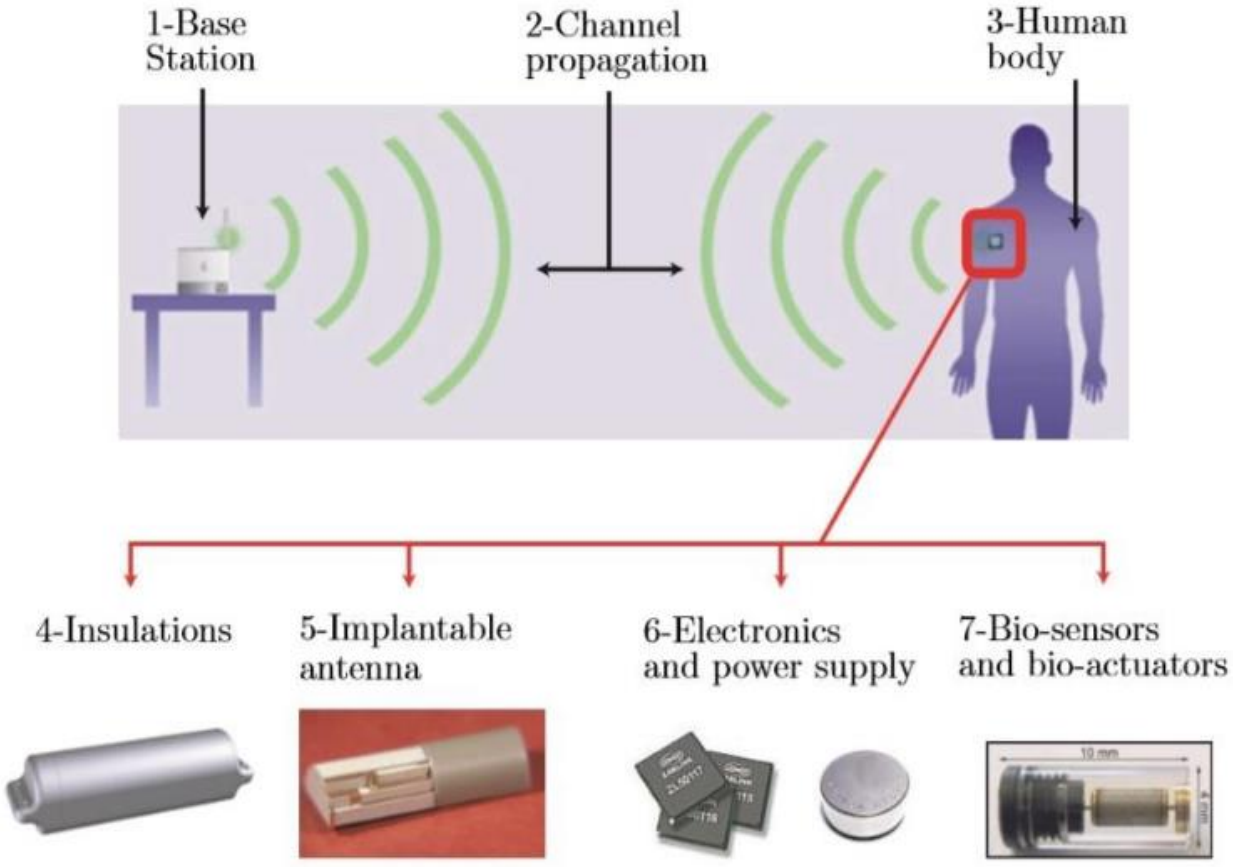

Figure 1.2 Block diagram of an implantable device and its wireless data transmission system[19]

1. Base Station: A base station is generally equipped with a receiver antenna, a controller for driving and storing the measurements.

2. Channel Propagation: The electromagnetic waves are propagated from an implantable device and received by the device at the base station. As the wireless transmission occurs at a low range of 10 to 20 feet [20], this transmission is done for indoor applications.

3. Human body: Human body works as a medium. There are various challenges for wireless transmission in the human body. It is composed of various tissues (skin, brain, fat, bone, muscle, etc.) with variable permittivity and electrical conductivity that changes with weight, age, or by

changing posture [28]. Apart from this, the position of IMD is also very important and plays a major role in wireless data transmission system. At surgery time, the device is placed in the most appropriate position for performing its basic tasks. Because of these factors, an antenna that is implanted inside human tissues may differ from its operational frequencies [18] [21].

4. Insulations: Biocompatible protection is required for every IMD for avoiding any unfavorable reactions with living tissues. Such insulation is critical from the antenna's perspective, as the human body does not provide a conducive environment for Radio Frequency (RF) radiation. Additionally, insulating layers around the antenna or on the human skin's surface can improve electromagnetic transmission from an implanted radiator to the base station.

5. Implantable antenna: An antenna is among the most important components of any wireless data transmission system. Data transfer happens only when the antenna ensures a reliable connection. The radiation efficiency, bandwidth characteristics, compatibility with lossy biological material, and optimal use of accessible volume are some of the most important issues that must be considered while designing an antenna. In general, the goal of an implanted antenna is to take up the least amount of space possible while also promoting device unification with other parts of the device and achieving the required electromagnetic performance [21].

6. Electronics and power supply: In fact, IMDs are made up of several types of electronics (batteries, sensors, and printed circuit boards (PCBs) with surface-mounted devices (SMDs) and micro cameras) that have a high conversion efficiency of 50% (rectifier and antenna). Electrochemical energy sources (batteries) and direct current (dc) power delivery through wires have traditionally been the most frequent sources of power for IMDs [8]. The battery determines how long an IMD can operate and how big it can be.

7. Biosensors and actuators: An antenna links a biosensor and an interface circuit in an implantable system. The interface circuit interprets data from the biosensor and sends relevant results to an external wearable device or a nearby personal computer through the antenna. Biosensors, which use biological material to monitor physiological processes, or bio-actuators, which trigger a physiological reaction to execute a bodily function, in some circumstances both can be included in the IMD depending upon the aim. Actuators are employed in active systems, such as those utilized in the pharmaceutical industry for automated drug delivery systems. Antennas are used as sensors as well. Antenna sensors are an excellent choice for implantable monitoring systems. The

antenna sensor has a unique feature that it may also function as a wireless transmitter, collecting and transmitting signals without the need for an additional connection [11] [12] [22].

1.2.1 Shapes of IMDs

The implant position and construction of each IMD is unique [4]. IMDs contain a variety of electronic and RF components including camera, PCB, battery, sensor, and RF components like filter, antenna, and rectifier. The majority of system level investigations have been reported only on capsule or flat type devices. Fig. 1.3(a) and 1.3(b) demonstrate the structure styles of flat type (skin implantation) and capsule type (deep tissue implantation) devices respectively.

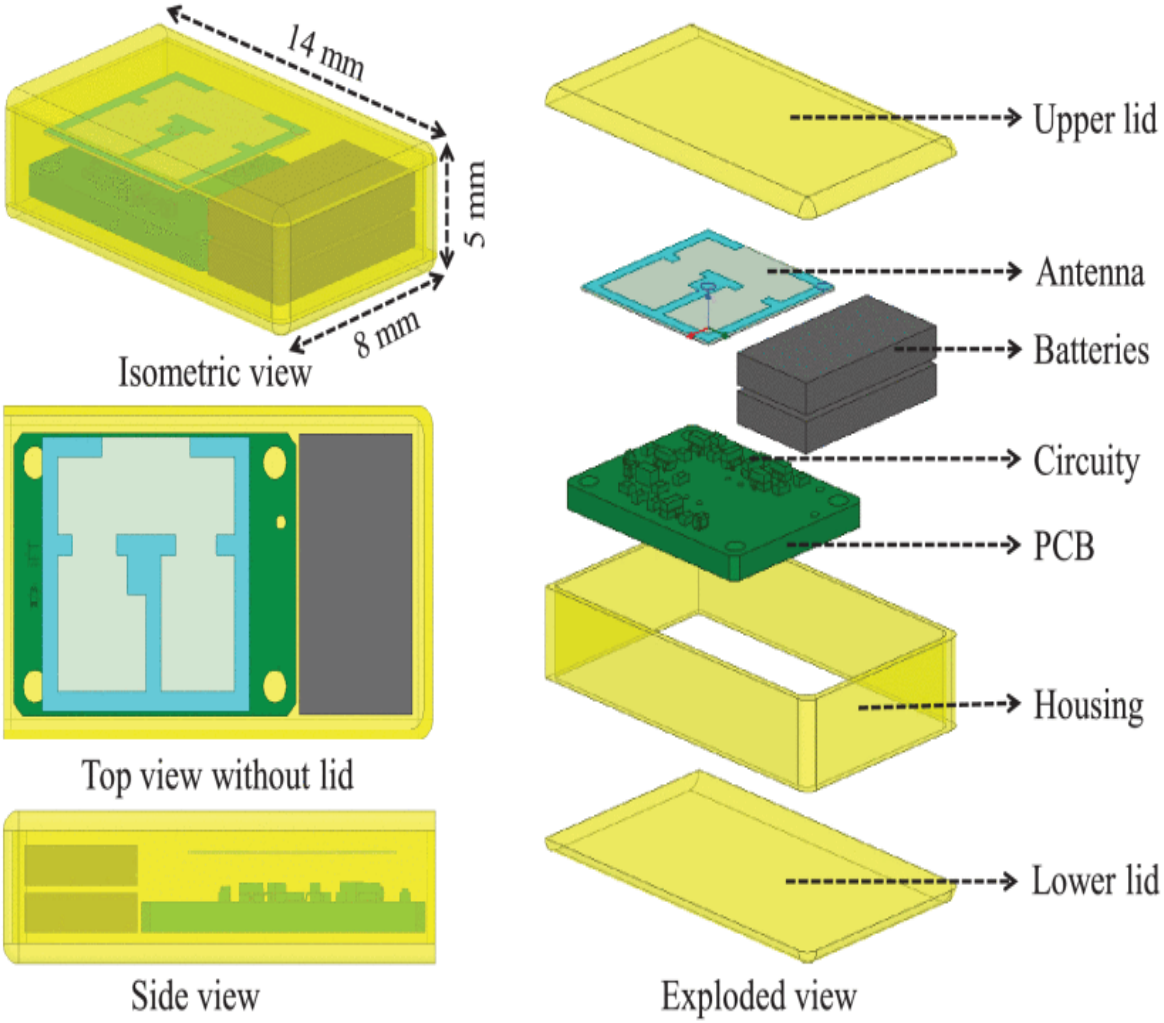

(a)

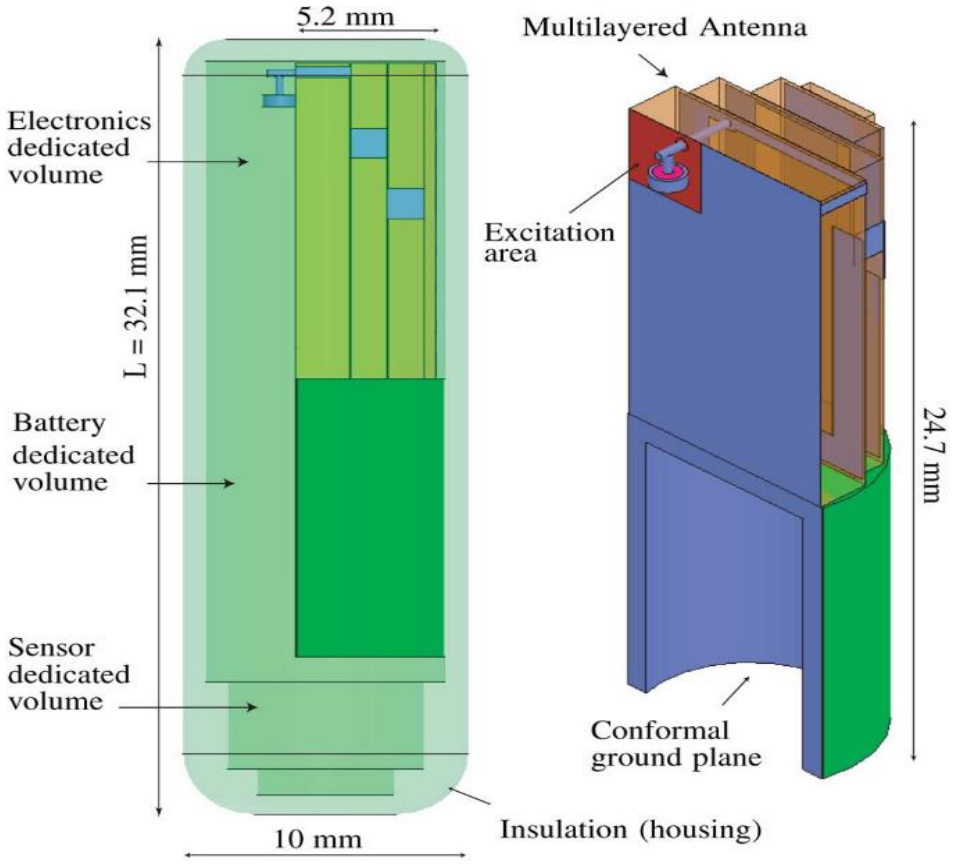

(b)

Figure 1.3 Types of IMDs (a) Flat type [21] (b) Capsule type [23]

Flat-type devices such as spinal cord stimulators (SCSs) and deep brain stimulators (DBSs) are commonly used for skin implantation [14]. In contrast, the capsule-type devices such as capsule endoscopes and leadless pacemakers are commonly used for deep tissue implantation. In [21], a flat-type device that has been developed has an overall dimension of 14 x 8 x 5 mm^3 and in [23], the capsule-type device has an overall dimension of 32.1 x 10 x 5.2 mm^3.

1.2.2 Wireless Power Transfer (WPT) in IMDs

WPT is regarded as a revolutionary method for charging and driving electronic components in a variety of applications, including biomedical engineering[24]–[26]. Figure 1.4 shows WPT from an peripheral transmitter to the IMD inside human body. In [14] and [27], for example, magnetic resonance is used for charging as well as driving the electronic components in IMDs [28] and vehicular batteries [29]. Other methods for driving electronic modules in IMDs include near field inductive coupling [30], [31] and capacitive coupling [32]. These procedures have been used by prosthetics, spinal cord stimulators (SCSs), and cochlear implants [14].

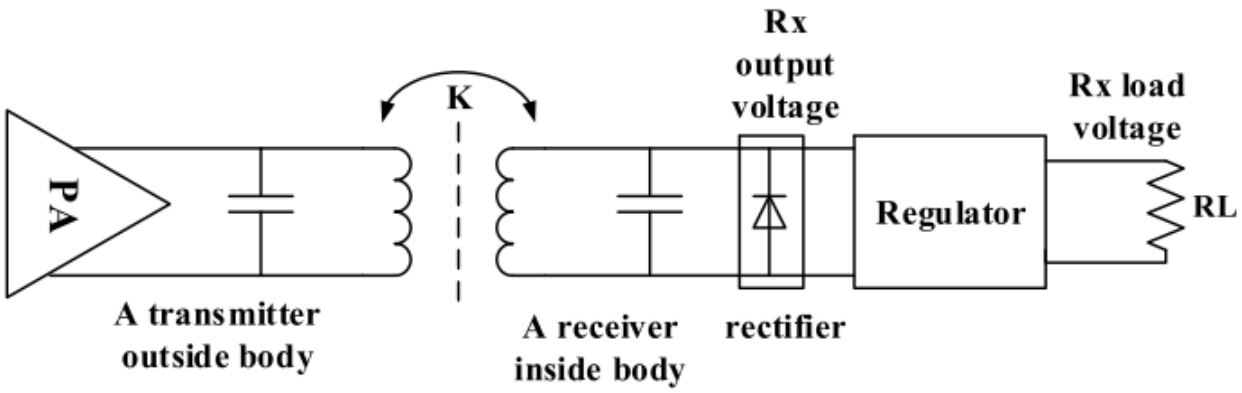

Figure 1.4 WPT to an implantable device [33]

1.3 TISSUE MODELS

Before fabricating an antenna, its performance is analyzed in numerical tissue models by simulating the same inhomogeneous solution of biological tissue with the same permittivity (ϵ_r), conductivity (σ) and mass-density parameters as utilized in the simulation software. These tissue models can be single/homogeneous layer or multi/heterogeneous layers depending on the use of antennas [7].

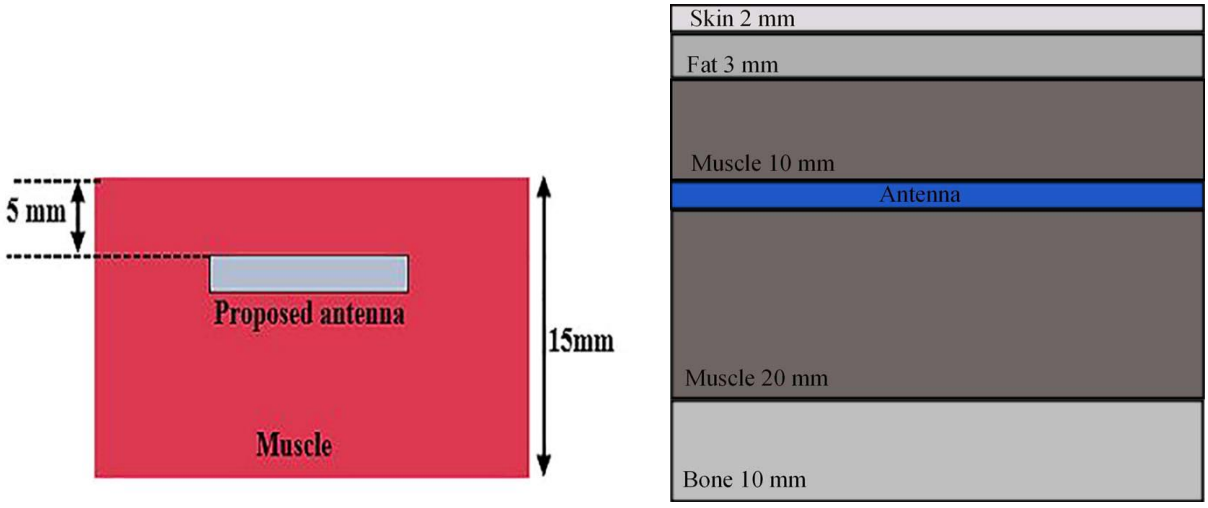

(a) (b)

Figure 1.5 In-silico testing of antenna inside (a) homogeneous layer (b) heterogeneous layers

Inside a single layer skin model, the antennas presented in [10] [11] are tested. In [12][34] , the antenna analyzed inside a three-layered geometrical model of skin, muscle and fat is reported. The electrical properties of human tissue depends upon the frequency of operation. The dielectric and conductivity values of some human tissues at MICS and ISM band are illustrated in Table 1.1. Furthermore, as demonstrated in Figure 1.5(a), the homogeneous muscle layer model is utilized

for testing the proposed antenna [35]. In contrast, in Figure 1.5(b), a 5-layer model is presented that is made up of skin, fat, muscle, and bone [36].

Table 1.1 Permittivity and conductivity of some human tissues at MICS and ISM band[37]

Frequency / Tissue type	ISM band (at 2.45 GHz)		MICS band (at 400 MHz)	
	ϵ_r	σ	ϵ_r	σ
Skin	38.1	1.46	46.79	0.69
Fat	5.28	0.11	5.58	0.04
Muscle	52.73	1.74	57.13	0.796
Bone	11.38	0.394	13.15	0.09

Anatomical models are utilized during simulation to achieve the findings that are close to actual results while performing practical testing. These models are generated by combining Magnetic Resonance Imaging (MRI) and Computer Tomography (CT) records with the electrical characteristics of the human tissues. An antenna's performance is altered when a human body is present nearby because the near-field strongly couples with the surrounding lossy media. So, choosing the right human model or phantom during the antenna design is essential for evaluating an antenna that has been suggested for a particular application. In recent decades, a number of human body models have been published and evaluated in the literature. Some of the most important phantoms utilised for wearable and implantable applications were compiled in the study provided by [38].

The choice of one body model over another is determined by several factors, including the intended application and the time and resources available. In general, choosing a theoretical or canonical phantom in the early stages of antenna design is common for two reasons: saving time and computational resources, and being able to experimentally verify the outcomes with the same model. However, realistic or voxel phantoms are needed at a later validation stage. Simulations in such accurate phantoms must not be underestimated, since minor deviations in the dielectric properties of the tissues lead to unexpected variations in antenna performance [38]. There are different types of body structures for different body parts used in the literature e.g., in [13], a realistic shoulder model has been analyzed. In [14], a more realistic Computer Simulation Technology (CST) Gustav model for chest implantation of antenna has been used. In

[15], the suggested brain implantable antenna is evaluated in the canonical cubic tissue model, the DUKE model, and on the Vector Network Analyzer (VNA), with the results compared using all three techniques. In [12] a realistic three dimensional human model using Remcom XFdtd software was utilized which contains 39 different types of human tissues with a resolution of 5 mm, as depicted in Figure 1.6.

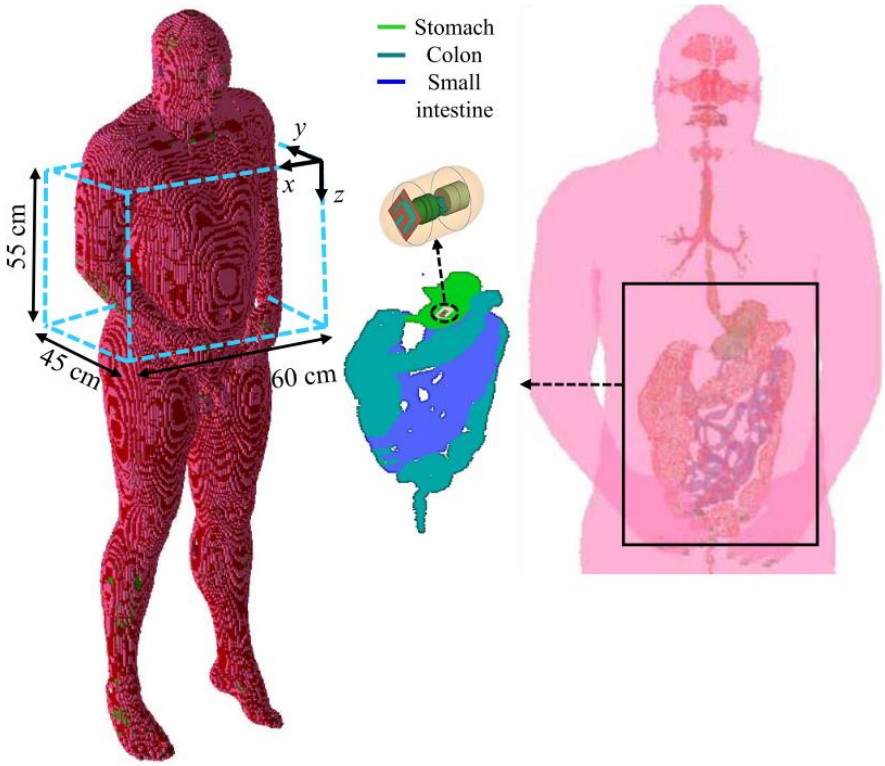

Figure 1.6 Testing of implantable device in 3D realistic human model [12].

In [38], solid phantom has been suggested for on body antenna testing. The Schmid & Partner Engineering AG (SPEAG) Posable Phantom for Electromagnetic Systems Evaluations (POPEYE) [39] is a whole body model that allows change of limb positions and spans a frequency range from 300 MHz to 6 GHz as shown in Figure 1.7. These phantoms offer useful RF dosimetry solutions, along with other models like SAM head phantoms [40]. Physically created phantoms have several disadvantages, including the difficulty of creating a heterogeneous model with intricate internal structures (such as organs or bones) and the need to cover the dielectric characteristics of human tissues over a broad frequency range.

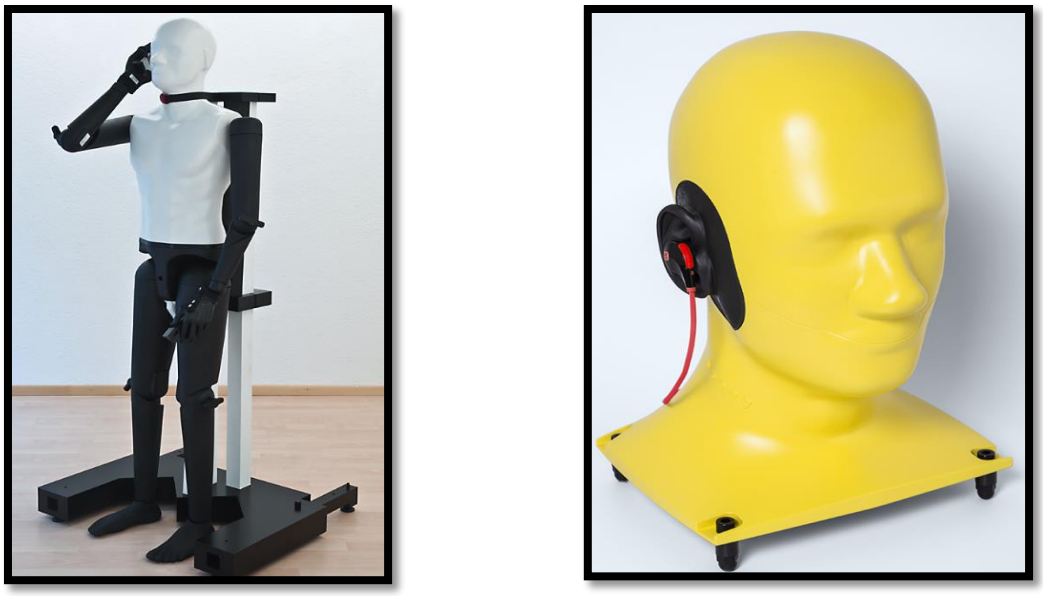

(a) (b)

Figure 1.7 Solid body phantoms developed by SPEAG (a) Whole body phantom POPEYE (b) SAM head phantom

It is challenging to compare antennas presented in various research papers because their output is heavily influenced by the phantoms used. These models differ in many ways, including geometry, size, targeted tissues, number of tissues, model accuracy, operating frequency range, placement and alignment of the implant, and thermal dependency. Temperature variations and tissue ageing both have an effect on dielectric properties. A review of variations in tissue characteristics as a function of temperature is presented in [41]. Meanwhile, a mathematical model for evaluating the effect of ageing (primarily due to variations in the water content of biological tissues with age) on tissue dielectric properties is developed, as detailed in [42]. The research presented in [43] examines the evaluation of an in-body antenna design while accounting for age dependency. The inclusion of temperature dependency in phantom models becomes much more important for thermal treatments such as microwave hyperthermia or ablation.

1.4 SUPERSTRATE AND SUBSTRATE LAYERS

For the antenna to be low profile, the dielectric constant of the substrate used must be high [2][4]. Implantable antennas must be biocompatible in order to protect the patient and prevent the implant device from becoming dislodged. Biocompatibility and the ability to resist annoying short circuits are especially the most important characteristic features in case of antennas built for long-haul implantation [7]. As a result, these implant devices are covered with a superstrate layer to protect

the human body from the adverse effects of implantable antenna. The antenna is protected from direct contact with the semiconducting tissue by the superstrate layer. Further, the superstrate is used to behave as a shield between the metallic layer and human tissues by dropping RF power at the locations of lossy human tissues. Superstrate layer must be chosen such that it should not affect or have a slight effect on the parameters of antenna. Superstrate layers applied on antenna can be same as substrate layer. Some of the commonly used superstrate layers are MACOR (ϵ_r = 6.1; tan δ = 0.005), and ceramic alumina (ϵ_r = 9.4; tan δ = 0.006) and poly-di-methyl-siloxane (PDMS) (ϵ_r = 2.2; tan δ = 0.013) at 2.45 GHz [8].

(a) (b)

Figure 1.8 (a) Elastic superstrate material (b) Antenna encased inside superstrate material [44]

When choosing a bio-compatible material for an antenna, the elasticity of substrate and superstrate is critical since the superstrate material must be able to cover the antenna's non-uniform surfaces smoothly. In several recent research papers, the substrate material is chosen to have a high value of dielectric constant of about ϵ_r = 9 to 10.2. Figure 1.8 (a) shows the elastic superstrate material for covering an antenna whereas Figure 1.8 (b) depicts an antenna coated in an elastic material Silastic MDX4-4210 Biomedical-Grade Base Elastomer. This elastic material is easy to manufacture and has an excellent viscosity for encasing the antenna [44].

1.5 TESTING OF ANTENNA

For performance verification of antenna, it can be tested using in-silico, in-vitro, ex-vivo, or in-vivo techniques, whichever possible. These testing types have been discussed in the subsections below.

1.5.1 In-silico testing

The term 'in-silico' is a modern term commonly used to refer the testing based on computer simulation. The antenna performance parameters like S_{11}, gain, directivity, bandwidth and radiation pattern etc. can be calculated using CST MWS software. The major advantage of in-silico testing is that any device's fabrication and practical testing can be done after getting an approximate idea of results, which saves cost and time. The results calculated under simulation can vary with the experimental conditions as the simulation is done under the ideal conditions of temperature and pressure. This testing can be done inside tissue models (homogenous, heterogenous, or realistic human models) as discussed in the previous Section. In [17], in-silico testing has been performed by inserting a capsule device in homogeneous layer of muscle tissue of dimensions 100 x 100 x 100 mm^3 as depicted in Figure 1.9(a). Further, in-silico testing of the antenna inside CST human model named Gustav has been illustrated in Figure 1.9(b) [26].

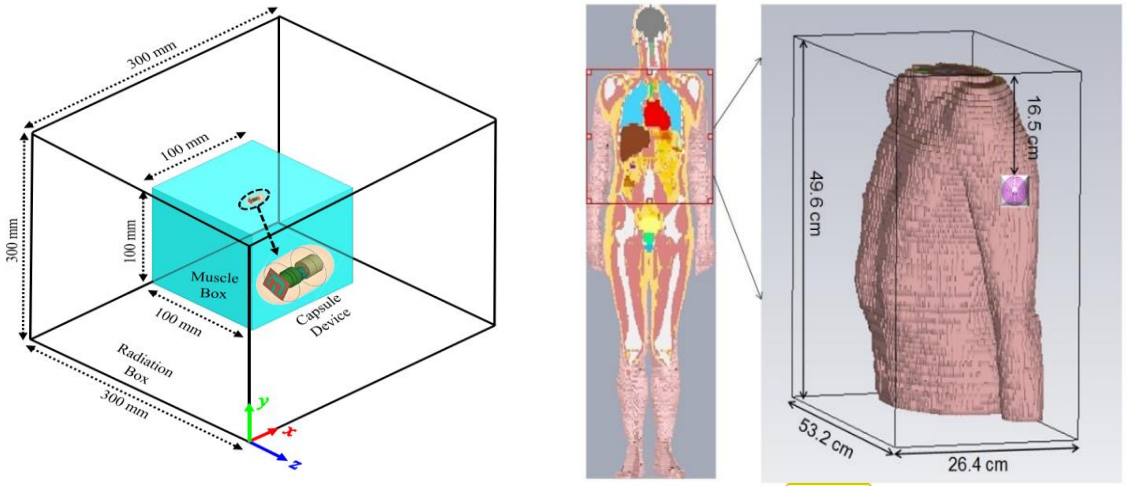

(a) (b)

Figure 1.9 In-silico testing of implantable capsule device in (a) homogeneous phantom [12] (b) human model named Gustav of CST [26]

1.5.2 In-vitro testing

When the testing of an antenna is done in body phantom that is made by preparing homogenous [single layer tissue] or inhomogeneous [multi-layer tissue] solutions of skin, muscle, bone, fat or their combinations, that type of testing is known as in-vitro testing. This type of testing of antennas made for the human body has to go through many tests before inserting them inside the body because insertion of any foreign element in the body can cause serious problems. Therefore, before inserting anything inside the body, some scientific testing must be done even after software

simulations. The body phantoms are made by the mixture of water, sugar, salt and oil, etc., for obtaining the required electrical permittivity and conductivity, which matches the properties of human body tissues. These solutions are made in cylindrical, spherical, rectangular, or square boxes depending upon the type of implantable area. In some literature, cylindrical-shaped model is depicted as a human arm [45], while spherical shapes are characterized as a human head model [46]. Figure 1.10 displays the in-vitro testing of an implantable antenna inside skin mimicking liquid. Frequency selective surface (FSS) technique had been utilized to design an antenna and it was covered using alumina to make it biocompatible [47].

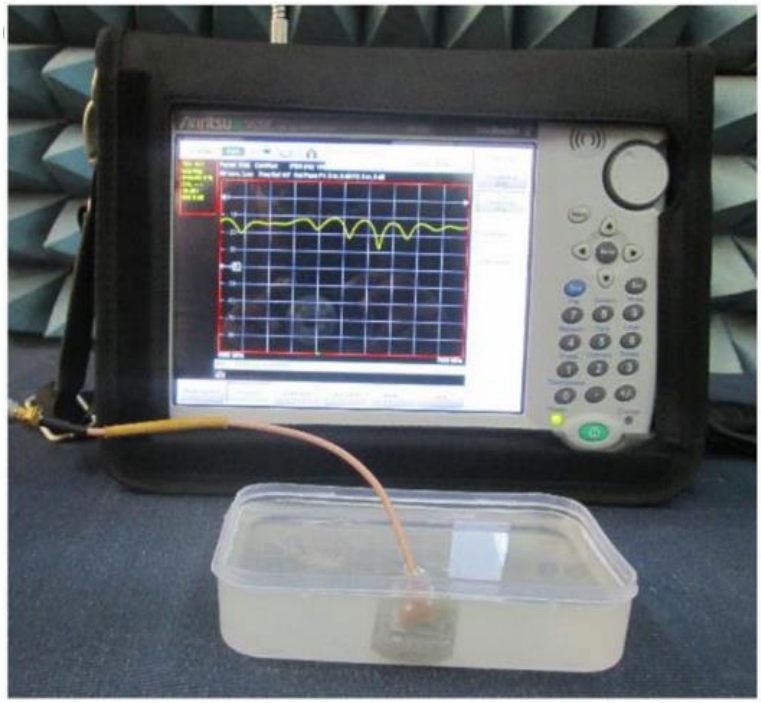

Figure 1.10 In-vitro testing inside skin mimicking liquid contained in a rectangular box [47]

1.5.3 Ex-vivo testing

If the testing is done by taking a tissue sample of an animal, it is called ex-vivo testing. Live animal is not harmed in this type of testing. Sometimes different body samples of these animals are taken and an antenna is put inside its brain, heart, skin, or any other organ, depending upon the application area. Ex-vivo testing has been successfully done on animal tissues of rat [44], pig [22], [48] etc.

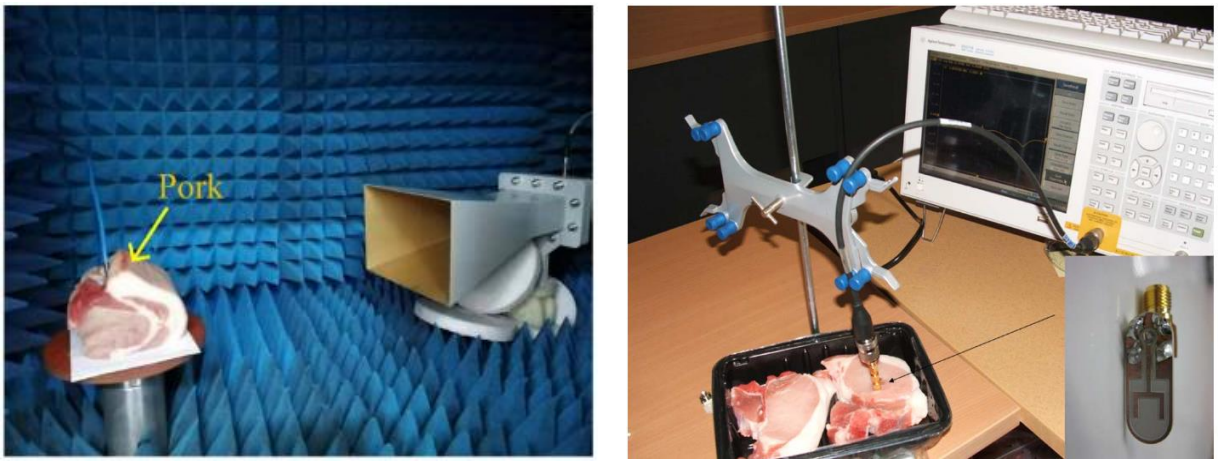

(a) (b)

Figure 1.11 (a) Ex-vivo testing inside pork sample (a) Measurement of far field patterns [22] (b) Measurement of return loss [48]

Figure 1.11 shows the experimental testing procedure of antenna inside pork samples. In Figure 1.11 (a), the ex-vivo testing is conducted for calculating the far-field results of the antenna inside an anechoic chamber, whereas in Figure 1.11 (b), the ex-vivo testing is performed inside pork chops for measuring the return loss of antenna using VNA.

1.5.4 In-vivo testing

If testing of an antenna is done inside the whole animal, then it is termed in-vivo. In this type of testing, the implantable device is surgically inserted inside live donor animals. A dual band implantable antenna is tested by injecting it inside a donor rat [44] as depicted in Figure 1.12 (a). In Figure 1.12 (b), an implantable device containing a helix antenna that works on ISM band is tested inside a donor pig [49].

The in-vitro method has several advantages. Firstly, submission of any animal protocol to Institutional Animal Care and Use Committee (IACUC) is not required. Secondly, they are preferred by pharmaceutical companies for mass production because of their ease of production as compared to animal use and economic reasons. Third, it obviates the need for a laboratory animal management specialist. But this method has the disadvantage as it is costlier than the in-vivo method for small-scale production [5]. On the other hand, the in-vivo method has benefits of providing accurate results and is cheaper than in-vitro for small-scale production. It has several disadvantages viz. constant pain in animals, requires continuous observation of animals health, and can be costly if routinely needed in an immunocompromised animal [19].

The goal of in-vivo testing is to evaluate the variables that affect measurements during a surgical procedure: the development of air gaps between the prototype that has been implanted and the surrounding tissues; the diversity of tissues surrounding the antenna and their frequency-dependent behavior; and the variation between test subjects and surgical techniques [49].

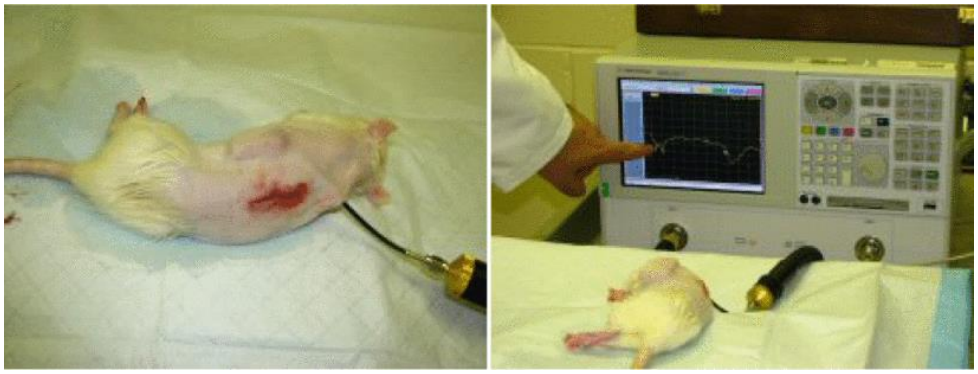

(a)

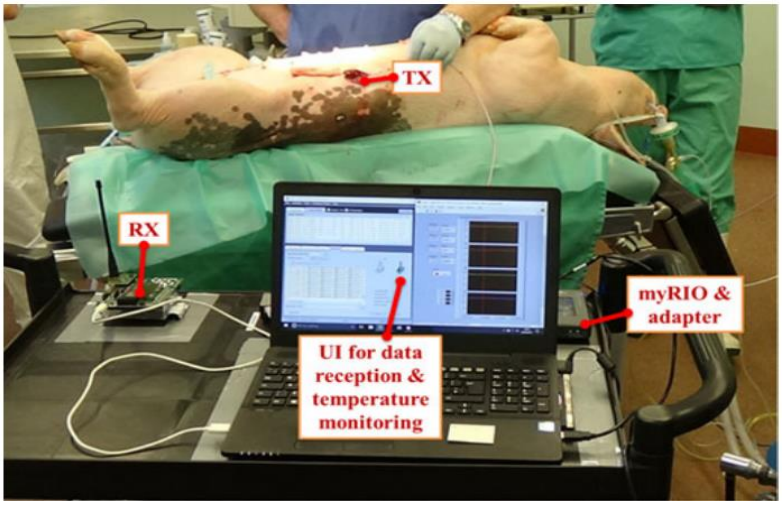

(b)

Figure 1.12 In-vivo testing (a) inside donor rat [44] (b) inside donor pig [49]

1.6 RESEARCH GAPS

The literature studied shows that the designing of an implantable antenna is still one of the most challenging part of biomedical systems. Therefore, a lot of research work is required to be done in this field to increase the performance of implantable antennas using different performance improvement technique. The main requirements of bio implantable antennas that satisfy the needs of future generations are discussed along with some research gaps:

- Size

Size is an essential issue in the designing of an implantable antenna. The antennas designed in [1,2,3,6,7,15] had noticeable results concerning return loss, but most of them suffered from a large size. As the dimensions of the biomedical devices are fixed according to applications, the area provided for embedding antennas in their geometry is too small. Therefore any antenna with appreciable parameters but larger dimensions is useless.

- High dielectric material

For designing an implantable antenna, a material with high dielectric constant is preferred. This is due to the fact that material with higher permittivity yields to smaller footprint of an antenna on a given frequency in comparison to a material having low permittivity.

- Flexible substrate

The antennas designed in [7,15,32] are made up of inflexible substrate materials that cannot withstand high pressure of anything that comes in contact with the body surface where biomedical device is implanted. It is impossible to avoid any contact with the human body. It means, any pressure less or more can cause great damage to the implantable antenna. Flexible substrates, however can avoid this problem.

- Superstrate layers

The antennas employed for implantable applications must be covered with superstrate layers on both sides, but most of the antennas in recent literature are not fully covered, making the antenna vulnerable to react with human tissues.

1.7 OBJECTIVES

The problem statement of the proposed research work is to prepare a state of the art overview of implantable antennas used for biomedical applications. For obtaining a deep understanding of implantable antennas, various antenna designs have been studied, which are already reported in the literature review. Gathering the overall knowledge about biotelemetry, a bio implantable antenna can be designed. The main objectives are designed as follows:

1. To design and simulate a novel compact microstrip antenna for MICS/ISM band.
2. Parameter extraction and fabrication of the proposed antenna.
3. Testing and validation of the proposed antenna.
4. Performance comparison of proposed antenna with the current state of art.

1.8 ORGANIZATION OF THESIS

The thesis is arranged into six chapters, and chapter wise summary is discussed below:

Chapter 1: Introduction

This chapter contains the introduction of IMD's, challenges faced while designing an implantable antenna, human models, substrate and superstrate materials, antenna testing etc. along with organization of thesis at the end.

Chapter 2: Literature survey

In this chapter, a detailed review of recent literature related to implantable antennas has been provided. Several research articles related to this work are bifurcated in three basic categories, i.e., (a) testing inside software (in-silico testing), (b) testing inside phantom (in-vitro), (c) testing inside animal tissue or live animal (ex-vivo or in-vivo) along with motivation, research gaps and objectives of the thesis. Finally, based on research gaps and objectives, methodology for the current work is decided.

Chapter 3: Skin and brain implantable inset-fed antennas at ISM and MICS bands for biotelemetry applications

In this chapter, two implantable antennas having dimensions 13.3×14.6 mm^2 have been designed and developed for biotelemetry applications at ISM and MICS bands. The in-silico results have been analyzed in both skin and brain layers and in-vitro testing is performed in skin mimicking liquid.

Chapter 4: Compact implantable antenna at ISM band for biotelemetry applications

In this chapter, a compact implantable antenna of dimensions 10.2 x 8.61 x 1.92 mm^3 and peak gain - 17.08 dBi have been designed for biotelemetry applications. SAR value for 1-g and 10-g averaged cubic tissue is considered for the security of patient from unfavourable impact of radio frequency radiations on human body.

Chapter 5: In-silico, in-vitro and ex-vivo testing of small footprint implantable biocompatible microstrip antenna for biotelemetry applications

In this chapter, a miniaturized skin implantable biocompatible microstrip antenna has been proposed for biotelemetry applications at 2.4-2.48 GHz. The volume of proposed antenna is 42.68 mm^3 with dimensions 8.2 x 6.94 x 0.75 mm^3. In-vitro testing is done in skin mimicking liquid and ex-vivo testing is done inside chicken sample.

Chapter 6: Conclusion and future scope

Finally, the proposed work's conclusions and potential future scope has been discussed in this chapter of thesis.

CHAPTER 2
LITERATURE SURVEY

In this chapter, an exhaustive literature survey on implantable antennas designed for biomedical devices application has been carried out. Depending upon the intended application, biomedical devices might be either on the body or inside the body. The decision to use one type of device over another may be influenced by economic factors, technology advancements, and research developments.

Wearable or on-body technology is already a part of our daily lives. For instance, monitoring wristbands and smart watches are already available. The emergence of other product categories such as smart footwear and body wear for sports and fitness, neckwear and jewellery for aesthetic purposes, etc., will be facilitated by new trends in wearable technology. The market for these smart wearable goods will reach over $150 billion in annual sales by 2026 [50]. Wireless on-body gadgets are being adopted into the healthcare system because they allow for non-invasive vital sign monitoring. However, other issues including compactness, security, standardization, energy efficiency, robustness, and unobtrusiveness remain unresolved [51].

The majority of in-body implants are still under development and need a particular medical prescription to be employed. When Rune Elmgvist et al. were successful in placing the first pacemaker inside a human body in 1958, these devices first became available [52]. Since then, in-body devices often referred to as Implantable Medical Devices (IMD) have filled a void where physiological parameters are only available from within the human body or where wearable devices were insufficiently potent. A few ingestible endoscopic capsules with biotelemetry capabilities and implanted pacemakers are the only in-body medical devices now on the market; the majority of them are still in the testing or prototype stages [53]–[55].

Depending on how they are inserted into the human body, in-body wireless devices are categorized as implantable, ingestible, or injectable [53]. These tools provide access to an exciting range of fresh healthcare applications. The list of obstacles to be solved for these devices is still longer and more difficult than in the case of wearable's: a higher degree of miniaturization, biocompatibility, safety considerations, powering, and so on.

A wireless biotelemetry system for either in-body or on-body devices has been proposed in this context using a number of technologies. RFID technology is one of them, and it offers a low-cost, low-power alternative to some of the issues outlined above [56], [57]. RFID technology offers integrated commercial chips and defined communication protocols that make it easier to create medical devices with wireless biotelemetry. A few RFID chips with sensing capabilities have also been just recently created [58], allowing this technology to carry out new tasks. For all of these reasons, RFID-based systems are becoming more prevalent in the healthcare system, moving from the industrial sector towards it [59]–[61], even though their adoption is still in its early phases for tracking and identifying patients [62]–[65].

Testing of an antenna is important to check various performance parameters and whether the device can withstand the guidelines of IEEE standards at particular frequency band or not. As already discussed in organization of thesis in chapter 1, testing of antenna is divided into four basic categories viz. in-silico (testing inside software), in-vitro (testing inside phantoms), ex-vivo (testing inside sample of animal tissue), or in-vivo (testing inside live animal). Based on these testing techniques the literature survey is divided into three subsections. Section 2.1 discusses about implantable antennas tested inside software simulators only. Section 2.2 discusses about fabricated implantable antennas tested inside human body tissue mimicking phantoms. Section 2.3 discusses about fabricated implantable antennas tested inside animal or sample of an animal. In all these Sections, the main discussion has been focused towards on size of antenna, type of substrate or superstrate layers used and the type of testing methods involved.

2.1 IN-SILICO TESTING (TESTING INSIDE SOFTWARE)

Sánchez et al. (2010) [20] designed a dual band implantable antenna for MICS and ISM bands using 1.27 mm thick Arlon 1000 of dielectric value 10.2 as a substrate. Results are conducted on one layered, three layered, and realistic human body models based on man's voxel dataset. The antenna is multilayered as the radiating elements and feeding line are placed on different levels.

Merli et al. (2011) [23] implemented a dual band multi-layered PIFA antenna working on MICS and ISM band for biomedical applications. The antenna is designed to be fitted in an implantable sensor accommodated with a battery and electronic circuitry of size 32 mm x 10 mm. Four layers of a Rogers TMM substrate are stacked up for making a pyramidal shape, and each layer is

separated for better perception. This antenna is simulated inside cylindrical homogenous phantoms of skin and brain layers and also inside three layered heterogeneous model of human tissues.

Sofia Bakogianni et al. (2014) [29] proposed a compact printed folded dipole antenna working on MICS band for biomedical applications with dimensions 19.6 x 2 x .254 mm^3. Canonical head and trunk models were utilized to embed the proposed antenna inside skin and muscle tissues. For minimizing the size of antenna and controlling input reactance, folding technique is used. Modeling of the antenna is done on Ansys High Frequency Structure Simulator (HFSS).

Liu et al. (2016) [31], implemented an integrated on-chip implantable antenna using 0.18 micrometer CMOS technology. Three-dimensional voxel human body was used for the implantable antenna testing inside a human head of dimensions 17.7 x 22 x 25 mm^3. A chip-to-SMA transition is designed for testing of antenna.

J. Kim et al. (2021) [66] designed an antenna for implantable device systems of cardiac pacemakers. This antenna works on 400 MHz frequency, and the results are checked at various depths of the human body model from 0.4 to 4 mm. To study the effect of battery positioning on antenna performance in the implantable device, metallic structure was added which indicated battery. There was a slight difference in results of the antenna and resembled with and without using a battery.

S. Sultana et al. (2017) [67] presented a flexible PIFA antenna for MICS band applications. The dimensions of the antenna are 20 x 24.4 mm^2 and is made using Rogers RT/duroid 3210 having dielectric constant value 10.2. The antenna is simulated in air as well as in human head phantom. The phantom is created with four layers of skin, fat, bone and brain. The peak gain obtained is 38.09 dBi, and 1 gram averaged SAR obtained is 0.55 W/kg.

Lee et al. (2015) [68] investigated a PIFA antenna working on MICS band for biotelemetry applications. The footprint of the antenna obtained is 25 mm x 9 mm and the substrate used for making antenna is FR-4. The antenna is covered with a superstrate layer of polyurethane having dielectric constant 4.8. The testing of antenna is done inside 2/3 muscle phantom. The bandwidth obtained is 226 MHz and peak gain is -27.7 dBi. The 1 gram averaged SAR obtained is 39.44 W/kg.

S. M. Asif et al. (2019) [69] designed and validated a deep implantable antenna using a wideband numerical model (WBNM) for enabling RF-power leadless pacing. This is a metamaterial based antenna that works on 2.4 GHz frequency. The simulation of antenna is done on spherical multilayered head phantom, homogenous skin phantom and inside three layered model consisting skin, fat and muscle.

R. Hasan et al. (2019) [70] implemented an antenna having dimensions 35 x 22 x 0.1 mm^3 for a pacemaker of size 40 x 30 x 10 mm^3 for ISM band applications. The substrate as well as superstrate used is Rogers RT/duroid 3010 due to its flexibility. The simulated results are analyzed by inserting the pacemaker device into a 2/3 muscle equivalent phantom. The return loss obtained is -28.37 dB at resonant frequency of 2.464 GHz.

Mohamed Behih et al. (2021) [71] presented a multiband PIFA antenna for biotelemetry applications that works on several bands, i.e., MedRadio (Medical Device Radio Communications Service) (401-406 MHz), ISM (433.1-434.8 MHz, 902.8-927 MHz, 2.4-2.48 GHz), and Wireless Medical Telemetry Service (WMTS) (1.395-1.400 and 1.427-1.432 GHz). The volume of the proposed antenna is 78.52 mm^3 and is made using Cuflon substrate of dielectric constant 2.05 and thickness 0.38 mm. The antenna is implanted inside the muscle layer by making a three layered model of human tissues.

Yazdanifard et al. (2020) [72] proposed an ultra-wideband miniaturized antenna for bidirectional-brain machine interface (Bi-BMI). The frequency range covered by the antenna is 3.08 GHz to 10.63 GHz. Defected feed line and parasitic structure on radiating patch layer were used for obtaining results. The antenna is simulated inside the DURA matter of full head voxel model. The recipient antenna is kept 20 cm away from the implantable sensor for testing.

T. Shaw et al. (2021) [73] implemented a circularly polarized antenna of volume 12.02 x 12.02 x 0.24 mm^3 working on 2.45 GHz resonant frequency for implantable applications. Different simulated results of various combinations of unit cell antenna array were checked at 40 mm of distance. Simulation environments are taken as homogeneous skin phantom, human torso, and human head. To protect human tissues from metal contact, the antenna is covered with 0.02 mm layer of alumina, which makes it biocompatible.

Alshammari et al. (2022) [74] introduced an implantable antenna working at ISM band having two co-centric rectangular split-rings with slots between them. The antenna is designed using Rogers RT/duroid 3010 substrate having thickness 0.127 mm and for size reduction shorting pin technique is used. Simulation is done inside homogenous skin tissue layer to validate the antenna.

Silue at al. (2022) [75] introduced a meandered antenna for biomedical implantable applications covering ultra-wideband (UWB), Medical Body Area Networks (MBAN), MICS, MedRadio, ISM and Wireless Medical Telemetry Service (WMTS) band. The designed antenna is cylindrical in shape with height 10 mm and radius 3.5 mm. Both 1 gram and 10 gram averaged SAR value obtained are within the permissible IEEE C95. 1-1999 and IEEE C95.1-2005 standards respectively. Simulation of the proposed antenna is done inside muscle equivalent phantom.

Nancy et al. (2022) [76] presented an implantable fractal antenna with dual ring slot structure for biomedical applications operating at ISM and WMTS band. Square shaped circular fractal geometry is utilized for obtaining wideband characteristics and miniaturized design. Alumina is used as substrate and antenna is encapsulated using Teflon material. The 1 gram averaged SAR value obtained is under safety standards. Simulation of the antenna is done inside skin phantom.

Sweety et al. (2022) [77] implemented a CPW fed double hexagonal spender shaped antenna for ISM band (5.7 GHz to 5.8 GHz). FR-4 substrate is used to design the 15 x 15 x 1.6 mm^3 antenna without using any superstrate layer. Simulation of antenna is done inside multilayered human body equivalent phantom.

M. Rahman et al. (2019) [78] implemented a compact meander shaped patch antenna at MICS band for biomedical applications. The antenna volume is 0.16 cm^3 and is made using Rogers RT/duroid 3210 substrate having 1.25 mm thickness, and the same material with 0.53 mm thickness is used as the superstrate. The antenna is designed such that it can be inserted inside the muscle layer of human chest. Simulation of antenna has been performed by inserting it inside the muscle layer of a three layered model containing skin, muscle and fat.

2.2 IN-VITRO TESTING (TESTING INSIDE PHANTOM)

Tutku et al. (2008) [20] presented an implantable antenna using Rogers RT/duroid 3210 substrate at MICS and ISM band to be used in continuous glucose monitoring applications. The reduced

antenna size obtained after using shorting pin technique is 22.5 x 22.5 x 2.5 mm^3. For obtaining better results, particle swarm optimization is used. Simulation is done inside single layer of skin and in three layer model of skin, fat and muscle. In-vitro testing has been performed by dipping the purposed antenna in skin mimicking gel.

Ha et al.(2011) [22] designed a Zeroth–Order-Resonance (ZOR) antenna for implantable biomedical applications. The frequency bandwidth obtained by the antenna is 400 - 409 MHz i.e., it operates on MICS band. The substrate used for fabrication is FR-4 with 1.6 mm thickness and dimensions of antenna are 15.9 x 12.9 x 1.6 mm^3. In-vitro testing is done inside muscle equivalent phantom.

Scarpello et al.(2011) [24], implemented a folded slot dipole flexible implantable antenna which works on ISM band using coplanar waveguide feed. In-vitro testing of the proposed antenna is performed in human muscle tissue liquid MSL2450, which mimics the dielectric properties of muscle tissue at 2.45 GHz. Biocompatible material PDMS (Poly-di-methyl-siloxane) is used as a substrate for embedding the antenna.

Asili et al.(2012) [25] presented an implantable dual band antenna for biomedical applications working on MICS and ISM (433-434.8 MHz) band. The dimensions of the antenna are 10 x 12 x 1.5 $mm^{3,}$ which is printed on FR4 substrate. It has been designed for implanting inside skin; therefore, skin mimicking gel is made for in-vitro testing.

Duan et al.(2012) [26], presented a dual band implantable antenna of dimensions 27 x 14 x 1.27 mm^3 working on MICS band for biomedical applications. Rogers RT/duroid 6010 is used both as substrate and superstrate layers of antenna. It is differentially fed at the same side for ease of connection on the differential circuitry. In-vitro testing of antenna is done in skin mimicking gel.

Yang et al. (2017) [32] proposed a circularly polarized implantable antenna for biomedical applications which works on ISM band. Rogers RT/duroid 6010 is used both as superstrate and substrate for the designed antenna. The dimensions of this compact antenna are 10 x 10 x 1.27 mm^3. In-vitro testing of the proposed antenna is done inside a cubic skin phantom, while for in-vivo testing, pork is used.

V. Gupta et al. (2020) [35] introduced a compact CPW fed implantable antenna for ISM band applications. The antenna occupies a total volume of 98 mm^3 using Rogers RT/duroid 3010 as a substrate. Two orthogonal modes TM_{01} and TM_{10} are obtained with an axial ratio bandwidth of 170 MHz and impedance bandwidth of 450 MHz. Peak gain obtained is -15.96 dB while SAR obtained is 0.494 W/kg. Simulation studies of the proposed antenna has been done by performing in-silico testing in a three layer cylindrical phantom model while ex-vivo testing is done inside pork tissue.

Liu et al. (2021) [46] introduced a compact antenna working at ISM band for wireless biotelemetry applications to fit inside microsystem device model. The antenna is simulated inside spherical head model, human heart model and homogeneous skin phantom. The size of the device is 15 x 9 x 1.6 mm^3 while antenna dimensions are π x 4^2 x 1.27 mm^3 which makes the antenna suitable for implantable applications.

S. Das et al. (2020) [47] introduced a high gain double ring slot antenna working on ISM band that uses FSS as a reflector for gain enhancement. Galinstain metal in liquid form is used for covering the antenna with a biocompatible layer. SAR value of 252 W/kg is obtained for 1g-averaged tissue on human wrist model. In-vitro testing is done on human skin mimicking model whereas ex-vivo testing is done inside pork slab.

J. Faerber et al. (2018)[49] introduced a conformal helix antenna covering an endoscopic capsule of size 10 x 30 mm^2. It can operate at 433 MHz inside human tissues. In-silico testing is done inside human muscle tissue cubic model of 190 x 190 x 190 mm^3. In-vivo trial of this endoscopic antenna is done inside porcine model by inserting it 60 cm inside a small bowel. The results are compared by inserting the device in two different pigs of different weights and ages.

Chien et al.(2010) [79] presented an implantable monopole biomedical antenna for MICS band. The antenna occupies a volume of 18 x 16 x 1 mm^3 and uses a ceramic substrate $MgTa_{1.5}$ Nb_5 O_6. Using screen printing technique and Ag/Pd paste, two prototype antennas were printed on the substrate. The 1 gram averaged SAR of both the antennas is 797 W/kg and 714 W/kg, respectively. In-vitro testing of proposed antenna is done in skin tissue fluid which was found suitable for working at MICS band for biomedical application.

C. Liu et al. (2013) [80] presented a PIFA antenna for MICS band biotelemetry applications. The antenna size attained is 10 x 16 x 1.27 mm^3 using two layers of Rogers RT/duroid 3010 dielectric material. The simulation is done inside skin phantom of different dimensions for comparison of obtained results. The 1-gram and 10-gram averaged SAR values obtained are 609.2 W/kg and 96.80 W/kg respectively. In-vitro testing of antenna is done by creating a human tissue mimicking gel.

Das et al. (2020) [81] proposed a co-planar waveguide (CPW) fed circularly polarized antenna resonating at 2.45 GHz. Corner perturbation technique is used to achieve circular polarization and an axial ratio bandwidth of 10.6 percent and peak gain of -8.6 percent is achieved. Simulation is done by inserting the antenna inside cubic skin layer while the ex-vivo testing is done inside pork slab.

Nguyen et al. (2021) [82] designed a compact size meandered antenna for 2.4 GHz ISM band medical implant applications. Taconic CER-10 (ϵ_r =10.2, σ = 0.0035) a flexible substrate material with thickness 0.64 mm is used to design the antenna with dimensions 2.5 x 2.5 x 1.28 mm^3. Antenna impedance bandwidth is increased by using 1.2 ohm chip resistor and two rectangular cuts on ground layer. SAR value is simulated on head, right leg and left arm models of human body. The return loss is measured in skin mimicking liquid as well as inside minced pork.

Michael J. Christoe et al. (2021) [83] implemented a meandered antenna compatible with ingestible capsules working at 433 MHz. Different challenges related to implantable devices were discussed in this paper. Five different designs of antenna were tested for bending on an implantable device having dimensions 11.2 x 30.2 mm^2. A 0.1 mm flexible polyimide substrate of permittivity 3.5 and loss tangent 0.0027 is used for designing the antenna with 35 µm copper tracing. A cylindrical human body homogenous phantom is used for simulating the antenna with three different types of environment found in human gut, i.e. ballistic gel (equivalent to human model tissue), saline water and neutral water. In-vitro testing of these three phantoms is also done and compared with the simulated results.

A Basir et al. (2018) [84] designed a dual band implantable antenna for both MICS and ISM band biomedical applications. The overall dimensions of antenna are 14 x 17 x 0.25 $mm^{3,}$ and In-vitro testing is conducted in saline solution of muscle equivalent phantom. The peak gain values

obtained are -33 dB and -16 dB at MICS and ISM bands respectively. Rogers RT/duroid 6010 is used as substrate to design this antenna.

Tuan-Anh Le Trong et al. (2021) [85] proposed a spiral radiator antenna for human head implantation resonating at three frequency bands of 402 MHz - 405 MHz, 1427 MHz – 1432 MHz, and 2400 MHz – 2480 MHz. The thickness of antenna is 0.5 mm, while the volume covered is 197 mm^3. Two circular layers of Taconic RF-10 substrate ($\epsilon_r = 10$ and $\tan \delta = 0.0035$) having 0.25 mm thickness and radius 11.2 mm are used. The antenna is simulated inside a homogeneous head model dimensions 100 mm x 100 mm x 60 mm. The practical testing of the antenna is done inside human tissue mimicking semisolid solution.

2.3 EX-VIVO OR IN-VIVO (TESTING INSIDE ANIMAL)

Chow et al. (2009) [4], designed a 30 mm long cylindrical stent having 5 to 6 mm of diameter with an implantable transmitter device for implanting inside the branch of pulmonary artery. This device is working on 2.4 GHz frequency which is in-vivo tested on pig. The output power of the implant acting as a transmitter is -3 dBm. Horn antenna is utilized for calculating the received power, which is placed at 10 cm ventral to the chest for antenna pattern measurement. For calculating the far-field results, the antenna is placed at a distance of 50 cm from the implant position.

S. Hayat et al. (2021) [12] proposed a dual band implantable antenna for an endoscopic capsule system working on 915 MHz and 2450 MHz. The standard size of the capsule system is 26 x 11 mm^2, while that of the designed antenna is 6.5 x 6.5 mm^2. ULTRALAM 3850HT material have dielectric constant 2.9 is used as substrate and superstrate for designing the antenna while the implantable elements are covered with ceramic alumina (Al_2O_3) of thickness 0.25 mm. The simulation is done inside a homogeneous box of dimensions 100 x 100 x 100 mm^3 filled with muscle phantom and inside the heterogeneous environment of three-dimensional human body model. The experimental work of testing is done inside saline water solution and in minced pork.

Amjad Iqbal et al. (2021) [14] implemented a self-duplexing biotelemetry antenna for biomedical implant applications. It operates at 1470 MHz and 915 MHz and is designed on 0.13 mm thin Rogers RT/duroid 3010 substrate. Simulation is done by inserting the implantable device inside

single layer of skin. In-vitro testing is done inside saline solution and ex-vivo testing is done inside pig tissues. Measurement of radiation pattern is done inside pig tissues.

Wei Wang et al. (2021) [22] designed an implantable sensor antenna for breast cancer detection at 2.45 GHz. A miniaturized shape with volume 13.2 mm^3 is obtained by making an "S"-shape on the radiating patch using a 0.254 mm thick Rogers RT duroid 6010 substrate (ϵ_r = 10.2, tan σ = 0.0035) and a CPW feed. Simulation has been carried out by inserting the antenna inside muscle layer of two layered phantom of skin and muscle. In-vitro testing is done inside tissue mimicking liquid. Ex-vivo testing is done inside pork fat and pork muscle samples which are denoted as normal and malignant breast tissue, respectively. The peak gain obtained is -8.4 dB for the proposed antenna.

Huang et al.(2011)[23] presented a multiband antenna for biomedical applications working on both MICS and ISM band. Rogers 3210 with 0.635 mm thickness is used for designing the antenna. The volume of antenna is 254 mm^3 which consists of four layers. In-vitro testing is done for skin and muscle tissue while in-vivo testing is done in minced pork (front leg of pork).

Gozasht et al.(2013) [27] designed a multiband PIFA antenna for three resonating frequencies 433 MHz, 1430 MHz, and 2400 MHz. In this paper, a shorting pin method is used to minimize the antenna size to 19 x 30 x 1.6 mm^3. Multilayered human tissue phantoms of block and cylindrical shapes are used for performing simulation of the proposed antenna. In-vivo testing is done inside the pork phantom.

Rula S. Alrawashdeh et al. (2015) [30] designed a flexible, implantable antenna for biomedical applications which operates on both MICS and ISM band. A CST Katja voxel body representing a 43 years old female of height 163 cm and weight 62 Kg is used for testing antenna in CST simulation environment. For antenna miniaturization, complementary split ring resonator (CSRR) loading technique is utilized on the patch layer. In-vivo testing is done in pork phantom and is compared with the simulated results.

Liu et al. (2018) [33] designed a circularly polarized implantable antenna having dimensions 11 x 11 x 1.27 mm^3 for biomedical applications which works on 915 MHz ISM band. Stub loading and capacitive coupling techniques are used for miniaturization of antenna. Minced pork is used for the purpose of ex-vivo testing.

L. Xu et al. (2021) [37] introduced a coaxial fed implantable antenna working on WMTS and ISM bands. The volume of antenna is π x 5.1^2 x 1.27 mm^3 and is made using Rogers RT/duroid 3010 material with 0.635 mm thickness which works as substrate as well as superstrate. Both 1-gram and 10-gram averaged SAR values are simulated at WMTS and ISM bands with different implant depths. The antenna is simulated inside skin tissue phantom while the In-vitro and ex-vivo testing was done inside tissue mimicking gel and pork respectively.

Tutku et al. (2010) [44] implemented a dual band implantable antenna of size 23 x 23 x 2.5 mm^3 for both ISM and MICS bands. Rogers RT/duroid 3210 having dielectric constant 10.2 is used as substrate and silicone (Silastic MDX4-4210) is used as a superstrate material. Comparison of silicone and Rogers RT/duroid 3210 is done for superstrate material by comparing their return loss which clearly shows that silicone is a better superstrate then Rogers RT/duroid 3210. In-vitro testing is done in skin mimicking material while in-vivo testing is done on rats.

A. Kiourti et al. (2013) [86] investigated two implantable antennas of volume 204 mm^3 and 399 mm^3 at MICS band for biomedical applications. Rogers RT/duroid 3210 material having dielectric constant 10.2 is used for designing and testing of antennas. Simulation is done inside the skin layer of a three layered model of different human tissues i.e., skin, fat, and muscle. Further, simulation is done inside the ellipsoidal trunk-shaped model for the purpose of glucose monitoring. Three different rats are used as subject for in-vivo testing of antennas at different implant depths.

Xiao et al. (2022) [87] designed a conformal implantable antenna having dimensions 30.5 x 4.6 x 0.05 mm^3 for inner walls of wireless capsule endoscope working at 915 MHz. For designing this antenna folding and vector current reversal techniques are used. The size of antenna is selected such that it fits inside endoscopic capsule of 10 mm inner diameter. Polymide material is used as substrate for making a foldable antenna due to its flexible nature and high permittivity. In-vitro testing of antenna is done inside three layered human body phantom and ex-vivo testing has been performed inside pork sample.

Abbas et al. (2022) [88] introduced a biomedical antenna for scalp implantation working on ISM band. A thick liquid crystalline polymer Roger ULTRALAM of 0.1 mm thickness and 2.9 dielectric constant is used as superstrate and substrate material. Using shorting pin technique, open-ended slots at patch and close ended slots at ground plane the volume achieved of the

designed antenna is 9.8 mm^3. The 1 gram averaged SAR obtained is 289.76 W/kg which is within the IEEE C905.1-2005 safety guidelines. Link budget investigation is done to confirm the robustness and dependability of the telemetric link within the specified range. Simulation is done inside skin phantom and 3D human body model while ex-vivo testing is done inside minced pork for the validation of results.

Syed et al. (2022) [89] presented a triple band implantable antenna for biotelemetry applications working on 902-928 MHz band, 1124-1980 MHz band and 2400-2483.5 MHz band. The volume of antenna is 7 x 5 x 0.37 mm^3 designed for flat type implantable devices architecture. Rogers RT/duroid 6010 substrate is used for the electronic elements inside device and are enclosed inside 0.2 mm thick ceramic alumina. Both SAR values of 1 gram and 10 gram averaged tissue are under standard limits. This coaxial fed antenna is tested inside homogenous skin phantom and human body model while ex-vivo testing is done inside minced pork.

Ahlawat et al. (2022) [90] implemented a scalp and heart implantable antenna for 915 MHz and 2.45 GHz ISM band biomedical applications. The volume of the designed antenna is 107.315 mm^3, designed on Rogers RT/duroid 3010 substrate. Alumina is used as superstrate for covering the top and bottom layer of proposed antenna. The antenna is designed according to the architecture of a flat type implantable device. Simulation is done inside three layered phantom and realistic human body model. SAR values for 1 gram averaged tissue are simulated on an anatomical head and torso of human body model. Ex-vivo testing is done inside pork sample for the validation of results.

Shah et al. (2022) [91] implemented a scalp and deep tissue implantable antenna for ISM band operations. The antenna volume obtained is 3.4 x 3.4 x 0.377 mm^3 and is made using Rogers RT/duroid 6010 substrate. A meandered patch with full ground plane of antenna is used for preventing the backward flow of energy and safeguarding the patient. SAR values for Both 1 gram and 10 gram averaged tissue are found to be in standard limit by calculating it on different planes of Gustav human model. Simulation is done inside single and multilayered tissue models. Ex-vivo testing is done inside minced pork.

M. Singh et al. (2021) [92] introduced a dual antenna system for ISM band biotelemetry applications. In this paper two antennas are coupled with a single Defected Ground Structure (DGS). The dimensions of a single unit are 10.5 x 10.5 x 0.635 mm^3. The simulation of the antenna

is done inside fat layer of a three layered phantom containing skin, fat and muscle. In-vitro measurement is done inside skin mimicking gel whereas ex-vivo testing is done inside pork slab. The analysis of 1 gram and 10 gram averaged SAR is done inside human head model with values 347.08 W/kg and 66.55 W/kg respectively.

Kuo Liu et al. (2021) [93] implemented a spiral shaped antenna for an implantable capsule shaped device that works on 2.4 GHz and 5.8 GHz ISM band applications. The antenna is simulated inside heart and large intestine models whereas practically the testing is done inside minced pork and inside the intestine of a pig. To prove that the antenna is working effectively, the link budget of antenna is calculated by testing the implantable antenna with an external device. The communication link transceiver distance calculated at 2.4 GHz is 14 m, while for 5.8 GHz it is 5 m when the link margin is increased.

2.4 MOTIVATION

After following a thorough review of the literature, it was determined that while a considerable research is already underway in the field of implanted antennas, there is still a room for improvement, as most articles revealed a tradeoff between one or more implantable antennas properties. The substrate chosen for designing an implantable antenna should have a high dielectric value.

However, certain antennas in recent literature have a low dielectric constant. Because of low dielectric constant, the antenna has a bigger profile, making it impossible to implant within a human body or into an implanted device.

Further, recently published implantable antennas do not have a biocompatible layer on both sides, leaving the surrounding human tissues exposed to short circuits caused by direct contact to metal layer. A quick healthcare diagnosis and treatment motivates research on implantable antennas. This area of research is still immature and thus has significant potential to be considered as one of the hot areas of exploration. Likewise, the SAR values are not estimated in certain literature, which is critical for determining whether the radiation of antenna is damaging the human body. All of these flaws prompted us to create an implanted antenna with optimal specifications that did not compromise any of its key attributes. Following that, there was a desire to develop a novel compact antenna with superstrate layers on both sides and an appropriate SAR limit that could be easily integrated into an implantable device. An attempt has been made to highlight the gaps from the

study and propose the statement of the problem for our research work based on the relevant literature study and facts.

CHAPTER 3

SKIN AND BRAIN IMPLANTABLE INSET-FED ANTENNAS AT ISM AND MICS BANDS FOR BIOTELEMETRY APPLICATIONS

In this chapter implantable inset fed patch antennas are proposed for biotelemetry applications. There are basically two bands allocated for biotelemetry; ISM and MICS band. In Section 3.1 the antenna has been designed and developed at ISM band whereas, in Section 3.2 the proposed antenna covers MICS band. As already discussed, a material having higher value of dielectric constant is preferred for designing an implantable antenna for biomedical and biotelemetry applications. When an antenna is designed with a substrate material with a greater dielectric constant, the antenna's performance suffers, but the antenna's size shrinks. In order to overcome this degradation in antenna performance in terms of gain, superstrate material has been used. Further to increase the bandwidth, slotted ground structure has been utilized. Therefore, Rogers RT/duroid 3010 is used as a substrate as well as superstrate layer with dielectric constant 10.2 and thickness 0.64 mm. The optimal dimensions of both the antennas are 13.3 x 14.6 mm^2, which has been discussed briefly with each slot position and its size in Sections 3.1.1 and 3.2.1. The fabricated antenna's performance has been checked inside in-vitro solution of skin mimicking liquid for validation of results which has been discussed in Sections 3.1.2 and 3.2.2 along with the recipe of preparation of skin mimicking liquid at each band. All performance parameters that are important for an implantable device are calculated and discussed in this paper. Return loss analysis, SAR analysis, gain, surface current distribution and comparison between simulated and measured return loss are depicted in Sections 3.1.3 and 3.2.3. Finally, a comparison of significant parameters of proposed antenna with recent literature is inferred in tabular form which validates the practical feasibility of the proposed antenna structures.

Figure 3.1 depicts the flow chart of the work done in Chapter 3, starting with design of antenna in software to analysing the performance parameters of the fabricated design. High dielectric material has been used for designing the compact biocompatible antenna. Human skin phantom has been designed for testing the antenna according to achieved frequency bands.

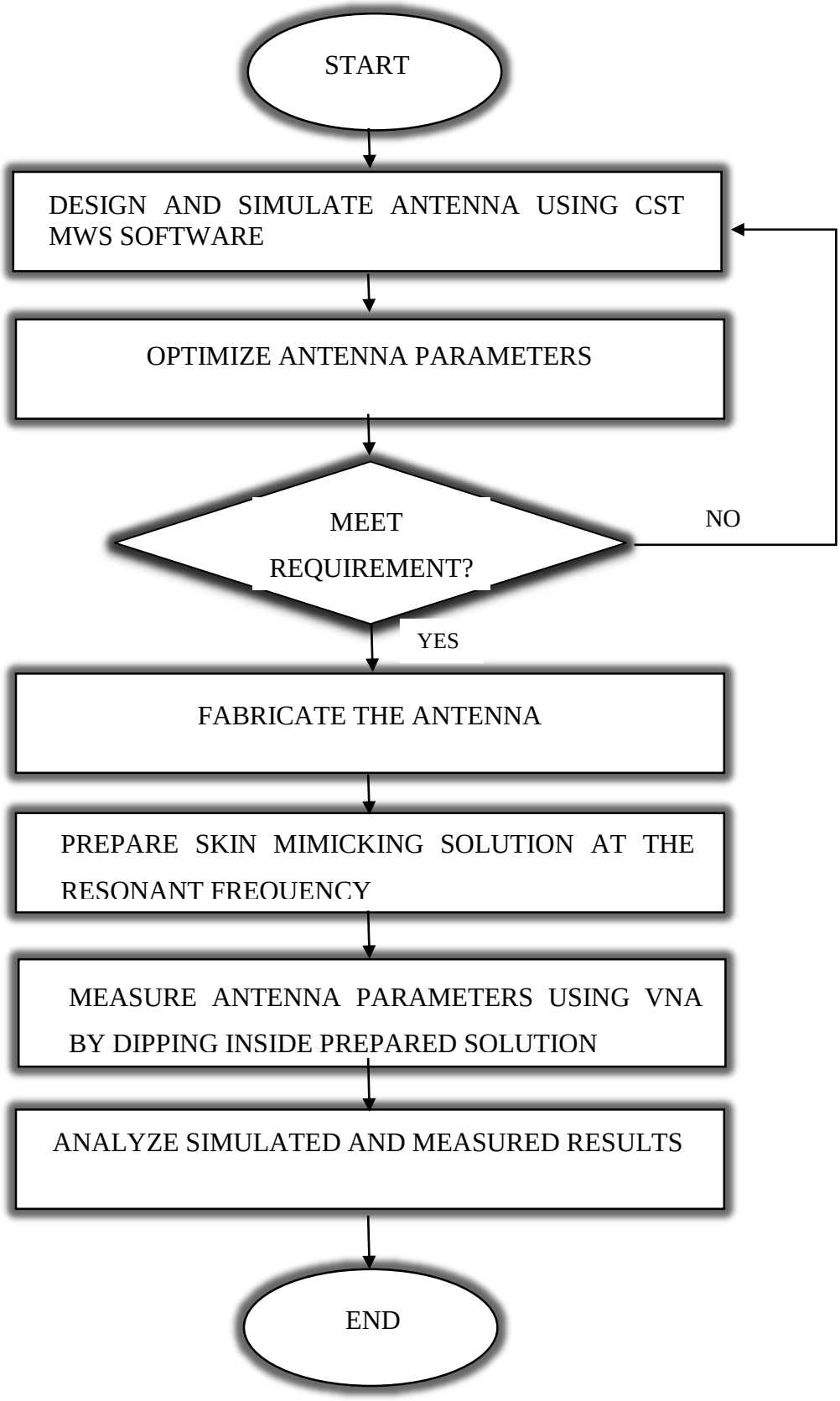

Figure 3.1 Flowchart of proposed microstrip patch antennas at MICS and ISM band.

3.1 IMPLANTABLE ANTENNA AT ISM BAND

In this section, a implantable inset-fed microstrip antenna has been proposed with a small patch size for biotelemetry applications that works on Industrial, Scientific, and Medical (ISM) (2400.0–2483.5 MHz) bands. The frequency range covered by the antenna is 2.26-2.71 GHz with an appreciable bandwidth of 18.10%, and its resonating frequency is 2.45 GHz, at which its return loss is -20.7 dB inside skin. These performance parameters of the antenna along with some more parameters like SAR, volume factor, peak gain, and the number of superstrate layers used, are compared with the recent literature in Table 3.1.3 in the results and discussion Section.

3.1.1 Antenna Design

The overall dimensions of the proposed antenna are calculated using transmission line model, which includes the size of feedline, patch and substrate. Figure 3.1.1 shows the geometry of the proposed antenna with dimensions of 13.3 x 14.6 mm^2 having a small patch size of 7.8 x 10.6 mm^2. For making it compatible with the human body, a dielectric material Rogers RT/duroid 3010 ($\epsilon_r = 10.2$ and $\tan \delta = 0.0022$) is used both as substrate as well as superstrate, having a thickness of 0.64 mm each, thus making an overall thickness of antenna as 1.92 mm. This high dielectric material also helps to reduce the size of antenna as dielectric value is inversely proportional to the size of antenna. And by adding its two more layers for perfectly covering the antenna makes the antenna size for the given frequency smaller.

Figure 3.1.1(a) shows the patch of the antenna having a circular slot of radius 1 mm. An inset feed of length 4.8 mm and width 0.66 mm is used for feeding the antenna. Moreover, two slots are presented in the ground layer below the patch in which, the first one is a rectangular slot of dimensions 3.9 x 7.8 mm^2, and another one is a semicircular slot of radius 3.2 mm that has been attached to the rectangular slot below the center of the patch as shown in Figure 3.1.1(b). The overall dimensions of the proposed antenna are shown in mm. Figure 3.1.1(c) and Figure 3.1.1(d) show the fabricated antenna without and with the superstrate layers, respectively.

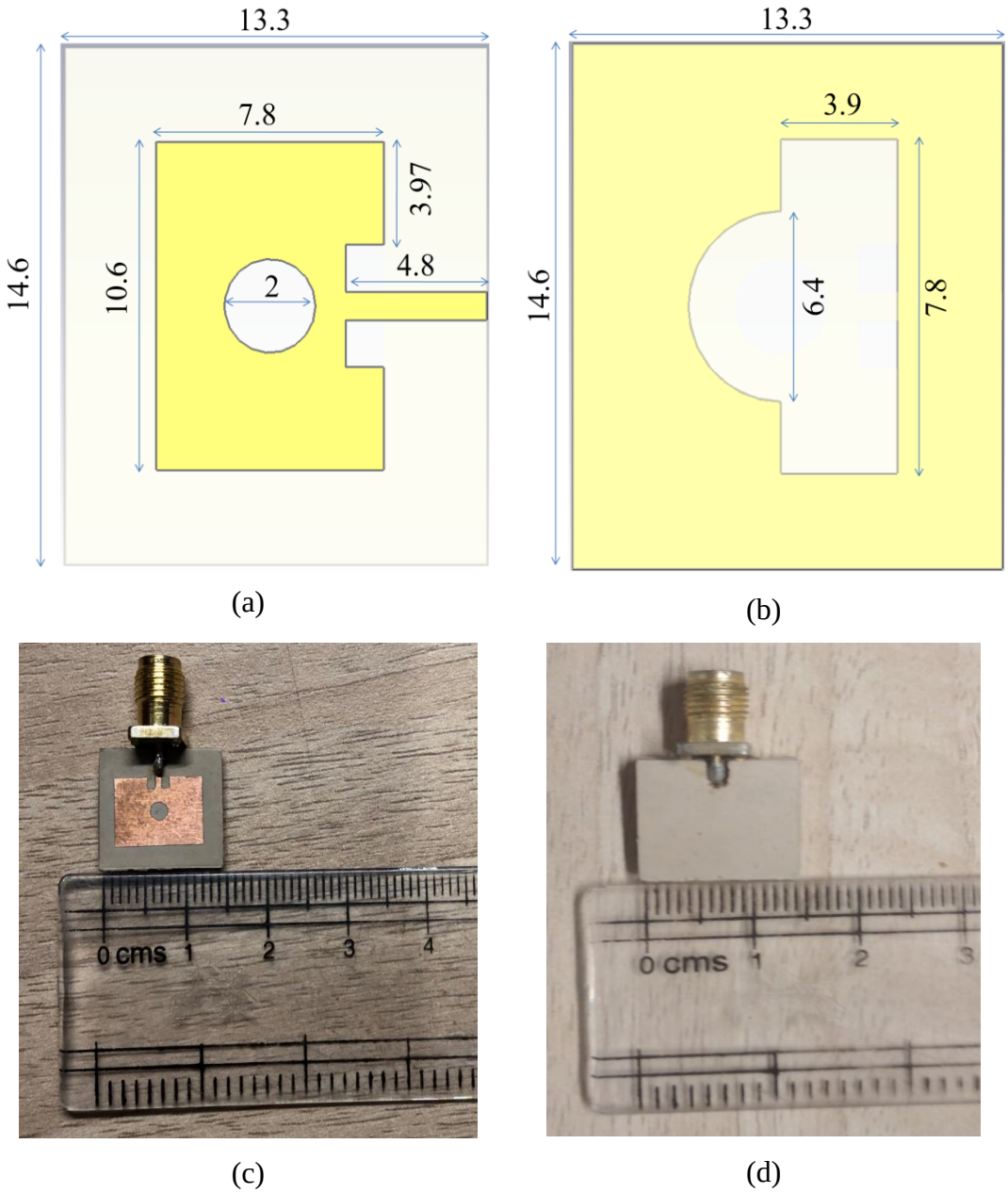

Figure 3.1.1 Geometry of proposed antenna

(a) Radiating patch
(b) Ground plane
(c) Fabricated antenna without superstrate layer
(d) Fabricated antenna with superstrate layer

3.1.2 Fabrication and Testing of Antenna

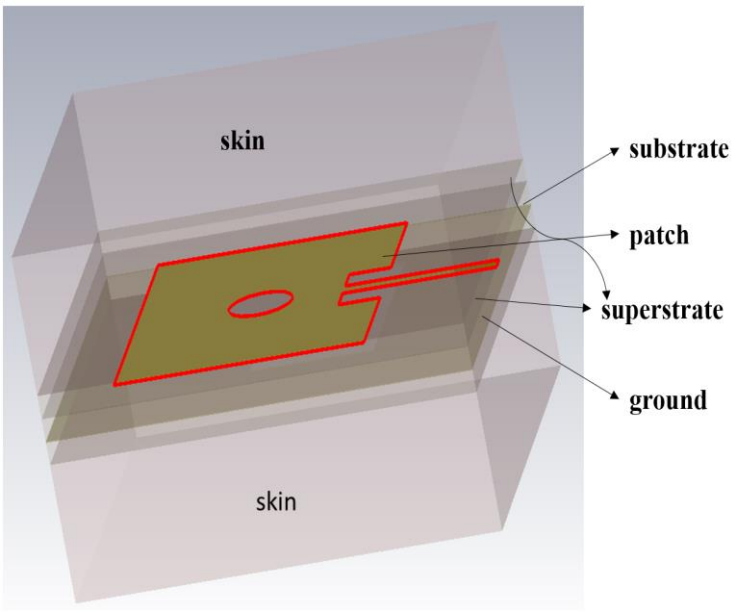

(a)

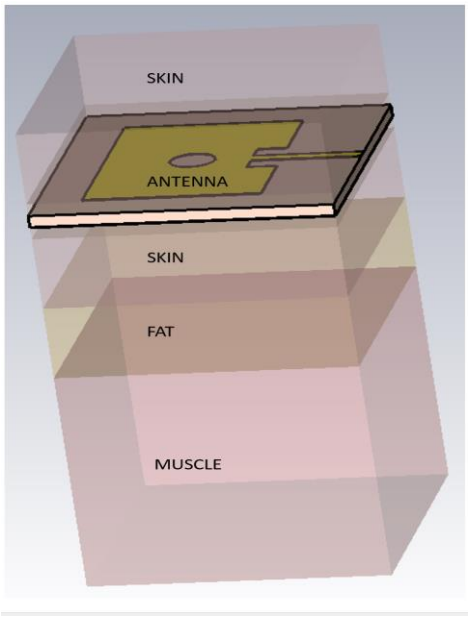

(b)

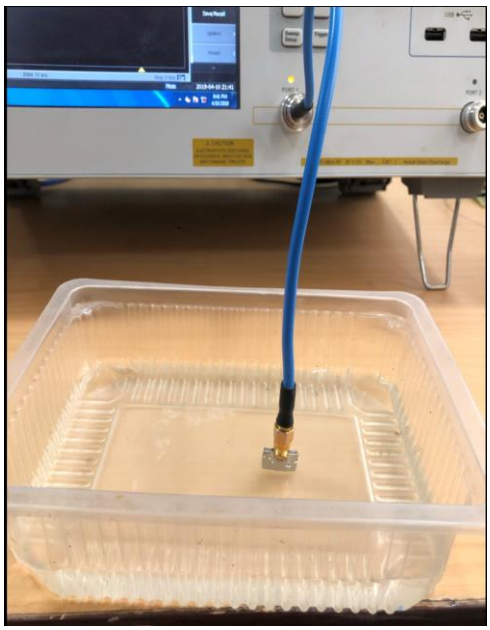

(c)

Figure 3.1.2 Testing of antenna

(a) Antenna inside skin layer
(b) Antenna inside three layer (skin-fat-muscle)
(c) Fabricated antenna testing inside skin mimicking liquid

Figure 3.1.2 shows the simulation and measurement setup of the proposed antenna. Figure 3.1.2(a) shows the antenna inserted inside a single layer of skin phantom, and Figure 3.1.2(b) shows the

same antenna inserted inside three-layer model of skin, fat, and muscle while simulating using software. Specific parameters of the human model i.e., the dielectric properties of human tissues at ISM band are depicted in Table 3.1.1. All three layers i.e., skin, fat and muscle have different dielectric values. The proposed antenna is fully functional in both models, which justifies that it can be used for implantation in most parts of the body.

Table 3.1.1 Dielectric properties of human tissues at ISM band

Human tissue layer	Permittivity	Conductivity (S/m)	Density (kg/m^3)
Skin	38.007	1.464	1020
Fat	5.280	0.105	918
Muscle	53.574	1.810	1040

Figure 3.1.2(c) shows the in-vitro testing of fabricated antenna for S_{11} using VNA inside a homogenous phantom skin mimicking liquid (made using 50% water and 50% sugar) having approximately the same electrical property as of skin whose recipe is illustrated by Sukhija et al. [3]. This phantom is inserted inside a container of size 150 x 100 x 50 mm^3 and filled such that the antenna can be easily dipped inside the liquid phantom.

3.1.3 Results and Discussions

For validating the results of the proposed antenna, gain, SAR and reflection coefficient (S_{11}) are calculated at the resonating frequency. For checking that if the antenna is biocompatible inside human body or not, the impact of SAR on nearby skin due to the designed antenna is checked for 1-g average cubic tissue at 2 mW as shown in Figure 3.1.3(a). The SAR values for 1-g average cubic tissue obtained for supply power of 2 mW is 1.55 W/kg (or for 1 W is 775.5 W/kg) which is below 1.6 W/kg according to IEEE C95. 1-1999 standard and implies that antenna is safe to use till 2 mW power according to safety standards. The color range (blue to red) being depicted in Figure 3.1.3(a) signifies the value of SAR going from minimum to maximum.

Figure 3.1.3(b) shows the comparison of return loss of proposed antenna with superstrate inside brain layer, skin layer, three-layer and without superstrate layers. This figure clearly indicates that in all the models, the antenna is resonating at ISM band except for one case when antenna is tested without superstrate. There are minor changes in the return loss of these models which shows that

our proposed antenna is perfectly and evenly working in brain layer, skin layer as well as in three layered phantom.

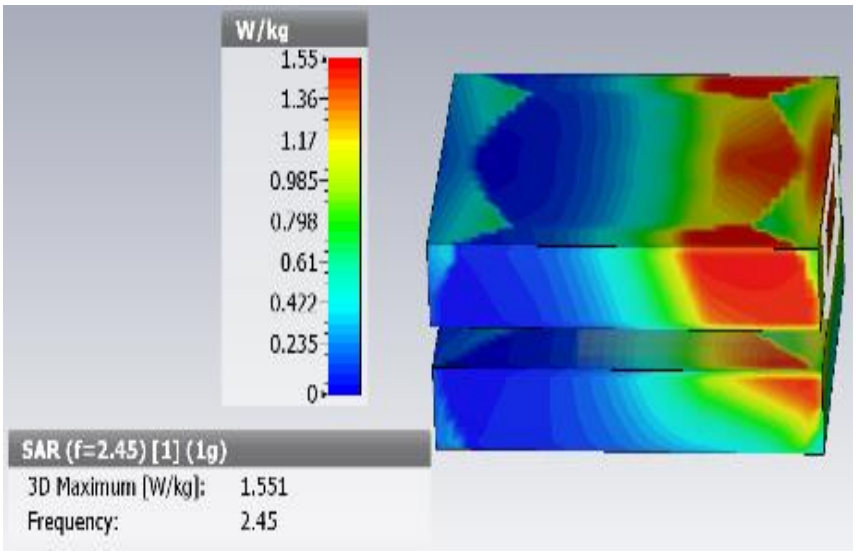

(a)

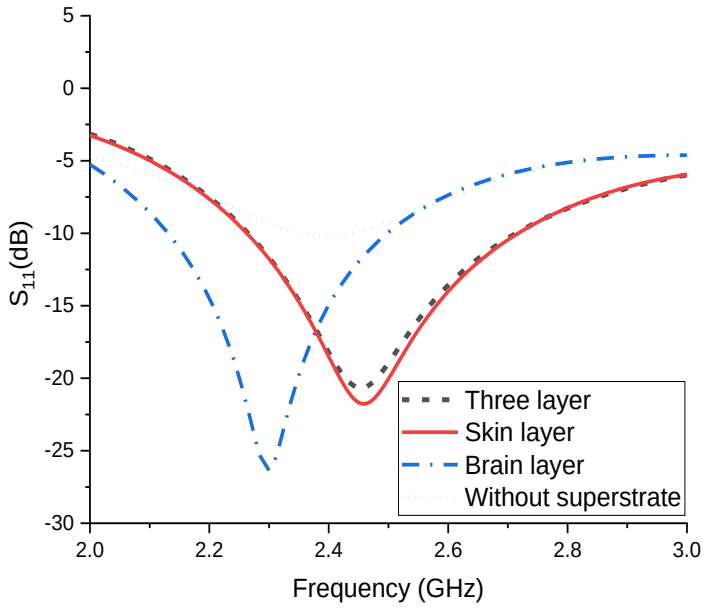

(b)

Figure 3.1.3 Simulated results of proposed antenna

(a) SAR value for 1-gram average cubic tissue at 2mW power.

(b) Comparison of return loss of proposed antenna within brain layer, single skin layer, three-layer and without superstrate

A simulated 3D gain pattern showing a peak gain of -14.9 dB at 2.45 GHz for the proposed antenna is depicted in Figure 3.1.4(a). Figure 3.1.4(b) illustrates the surface current distribution of the proposed antenna. This distribution gives us an idea about which part is mostly responsible for antenna radiation. The red color on the surface current distribution plot denotes that the maximum current is present at the feedline and the edges that are nearby the feedline on the patch. Further, on the ground layer, the area near the slots is primarily responsible for surface current distribution. The maximum value obtained for the surface current is 231 A/m.

Volume factor of antenna is described as the ratio of bandwidth (in kHz) to the volume of antenna (in mm^3) as shown in Equation (3.1.1) [16]. The volume factor of the proposed antenna is 1207 $kHz/mm^{3,}$ which is much better as compared to antennas reported for a similar application.

$$\text{Volume factor (VF)} = \text{Bandwidth (kHz)}/\text{Antenna volume } (mm^3) \qquad (3.1.1)$$

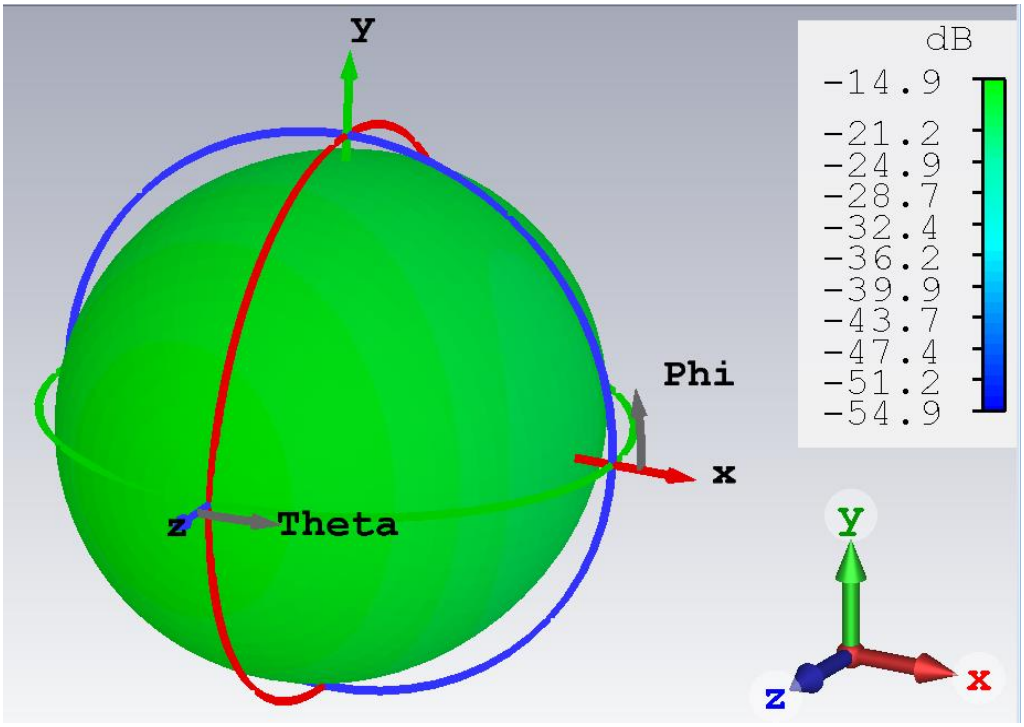

(a)

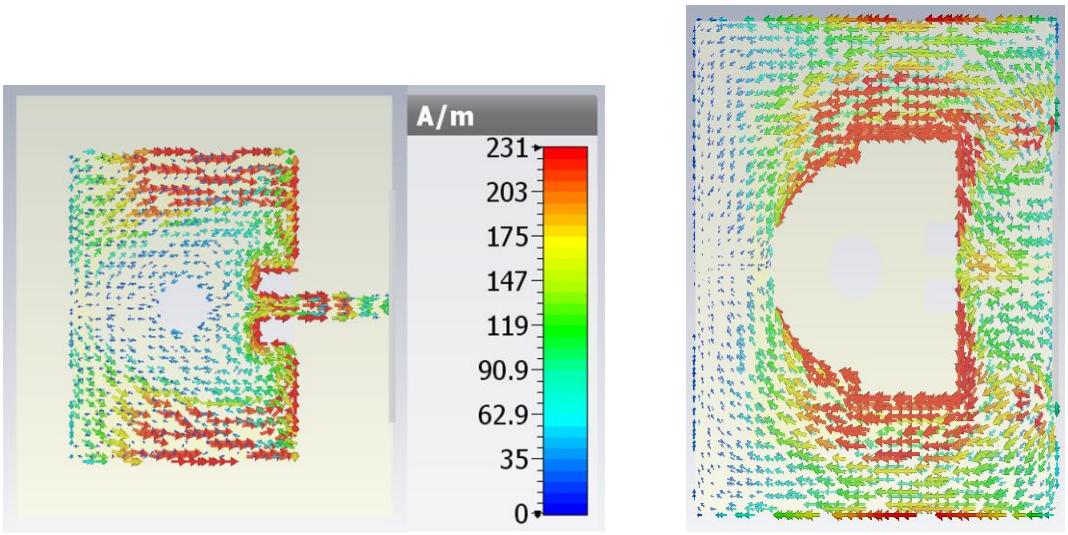

Front view Back view

(b)

Figure 3.1.4 Simulated Gain and surface current distribution of proposed antenna inside skin

(a) 3D gain

(b) Surface current distribution

The comparison between simulated and measured radiation patterns at phi = 90 degrees and phi = 0 degrees is shown in Figure 3.1.5(a). The orange line denotes the simulated value whereas the dashed black line depicts the measured value. Figure 3.1.5(b) shows the comparison of return loss of the fabricated antenna with the simulated one.

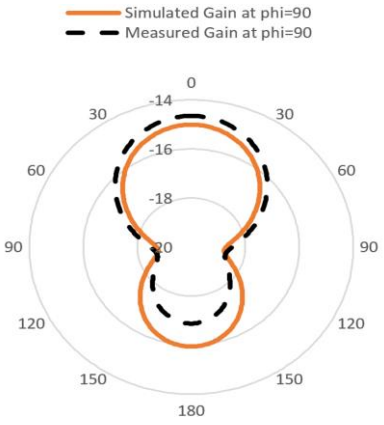

Phi = 90 degree

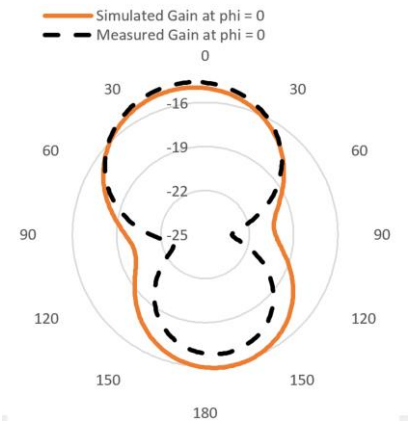

Phi = 0 degree

(a)

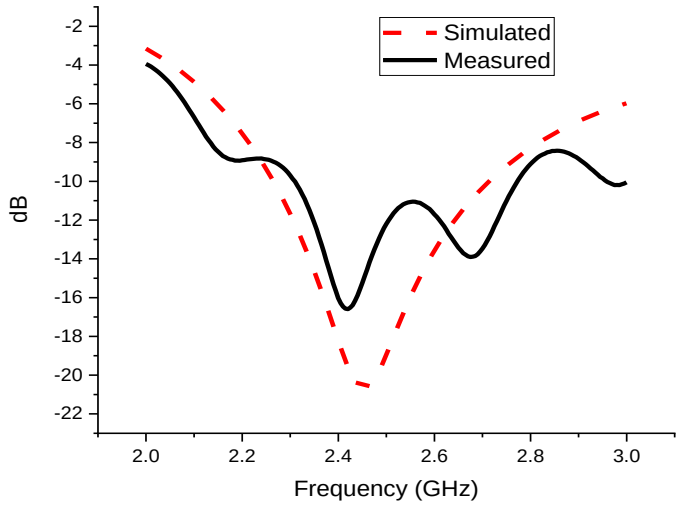

(b)

Figure 3.1.5 Comparison between simulated and measured results of proposed antenna in skin
(a) Gain
(b) Return Loss

A close agreement between simulated and measured results of the proposed antenna at ISM band is depicted inside skin except for some small differences in return loss and bandwidth as illustrated in Table 3.1.2. These differences can occur due to various reasons viz.; (a) simulation is done in ideal conditions but while measuring, temperature and pressure changes affect results, (b) poor soldering of SMA connector to the limited area of feedline of the antenna, and (c) dipping of antenna connector with antenna inside phantom solution can alter results. From bandwidth column it is clear that the antenna is resonating at ISM band in all conditions mentioned in the table.

Table 3.1.2 Comparison of simulated and measured return loss and bandwith of proposed antenna

	S_{11} (dB)	Bandwidth (GHz)
Skin	-20.7	2.26-2.71
Three layer	-21.77	2.26-2.72
Brain	-26.36	2.14-2.5
Skin (Measured)	-16.6	2.31-2.76

Table 3.1.3 Comparison of proposed antenna with recent literature

Ref.	Volume (mm^3)	Bandwidth ($\lvert S_{11} \rvert \leq$ -10 dB)	Peak Gain (dB)	SAR (1g-average) (W/kg)	Volume factor (kHz/ mm^3)	Superstrate layers	Resonant Freq. (GHz)
[45]	19x30x1.6	>8%	-13	-	219.3	single	2.4
[94]	27.5x21x1.6	12.57 %	-27.46	-	335	nil	2.44
[95]	16.5x16.5x2.54	4.4 %	-9	292	159	single	2.4
[96]	10x15x2	-	-16.3	-	-	Both sides	2.45
[97]	22x16x1.27	1.6%	-19.5	$2.15x10^{-3}$	89.5	nil	2.45
[98]	14x14x1.27	12%	-19	482	1205	single	2.34
[99]	27x9x1.27	>6%	-20	-	489.3	single	2.45
[100]	$\Pi x(7.5)^2 x1.92$	10.4%	-13.8	159.4	764	single	2.45
Proposed work	**13.3x14.6x1.92**	**18.10%**	**-14.9**	**775.5**	**1207**	**Both sides**	**2.45**

Table 3.1.3 provides a detailed comparison of our proposed work with the recent literature in terms of antenna dimensions, bandwidth, peak gain, SAR, volume factor, superstrate layers used and resonant frequency achieved. By having a close look at all the cited references in Table 3.1.3; we can observe that our proposed antenna prototype is good enough to be used in implantable devices for biotelemetry applications. In [94] and [97] the implantable antennas that have been designed have large dimensions and have not used any superstrate layer which makes the antenna unsuitable for implantable applications. In [45], [95], [98]–[100] antenna is covered with superstrate layer only on one side. Using a single superstrate layer can make the antenna more prone towards unwanted short circuit thus reducing its biocompatibility to human body tissues. Though the refs.

[45], [95], [100] have little better peak gain than the proposed antenna but bandwidth percentage is smaller. Ref. [100] has smaller footprint than the proposed one due to its circular geometry but it is having only single layer of superstrate which is again one of the shortcomings of a biomedical antenna. The antenna discussed in ref. [96] has small volume as well as it is covered from both sides with superstrates but no information about bandwidth, SAR value or volume factor has been provided and peak gain is also smaller than the proposed antenna. As shown in table the gain values obtained are negative. The negative gain is because of the dissipation caused around the human tissue. When the antenna is placed under the skin, the radiation is the off-body direction and has negative peak gain.

3.2 IMPLANTABLE ANTENNA AT MICS BAND

In this section, an implantable microstrip patch antenna has been designed and developed at MICS band for biotelemetry applications. The antenna proposed in this section has the same dimensions i.e. 13.3 x 14.6 mm^2 as was taken for the antenna discussed in Section 3.1 but in the previous Section the antenna was operating at ISM band and in this section the proposed antenna covers MICS band. Shorting pin technique and high dielectric material layers of Rogers RT/duroid 3010 (dielectric constant = 10.2) are used for making the overall antenna dimensions small enough to be fitted inside implantable devices. The step by step approach to obtain final design has been discussed in Section 3.2.1 with different evolution stages of the proposed antenna. In-silico testing of proposed antenna is carried out inside human tissue layers using software CST MWS, and practically it was tested inside in-vitro solution shown in Section 3.2.2 of this chapter. All performance parameters that are important for an implantable device are calculated and discussed in this chapter. Return loss analysis, SAR analysis, gain, surface current distribution and comparison between simulated and measured return loss is depicted in Section 3.2.3. Finally, a comparison of significant parameters of proposed antenna with recent literature is inferred in Table 3.2.2 which validates the practical feasibility of proposed structure.

3.2.1 Step by step approach to proposed antenna design

Figure 3.2.1 illustrates the dimensions of proposed antenna footprint as 13.3 x 14.6 mm^2 with a limited patch size of 7.8 x 10.6 mm^2. This is among the smallest patch size of antenna reported in recent literature working on MICS band. For biocompatibility, the substrate material used is Rogers RT/duroid 3010 (ϵ_r = 10.2 and tan δ = 0.0022) having thickness 0.64 mm. This same material has been used as a superstrate layer at the top and bottom sides for covering the antenna. Therefore, the overall thickness of antenna becomes 1.92 mm due to three layers (one substrate and two superstrate layers). These high dielectric superstrate layers are the key components in reducing the overall dimensions of antenna. Shorting pin of 0.2 mm diameter is used at the top left of patch connecting it to ground as shown in Figure 3.2.1(a) and Figure 3.2.1(b). Radiating patch of antenna is shown in Figure 3.2.1(a). Inset feed of 4.8 mm length and 0.66 mm width is used for exciting the antenna. A circular slot of 2 mm diameter is made at the center of radiating patch of antenna. Moreover, two rectangular slots with dimensions 0.5 x 9.6 mm^2 (shown vertically) and 4.8 x 0.5 mm^2 (shown horizontally) are made in the patch element. Figure 3.2.1(b) shows the

ground layer of antenna which is complex in structure with a circular ring shaped slot of 0.5 mm width just below the center of radiating patch between a circle of radius 1.5 mm and a circular ring of 1.2 mm width. Figure 3.2.1(c) illustrates the fabricated antenna without superstrate whereas Figure 3.2.1(d) shows the fabricated antenna with superstrate.

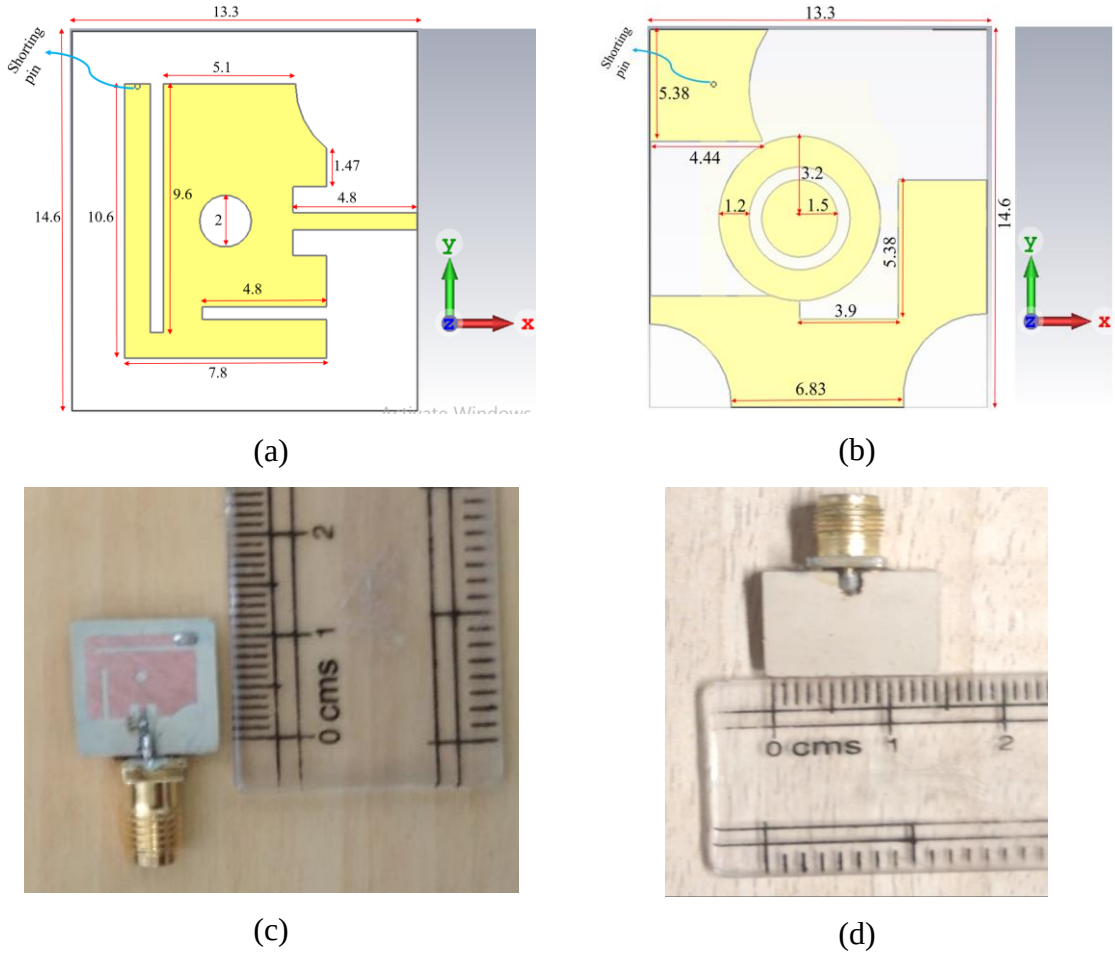

(a) (b)

(c) (d)

Figure 3.2.1 Geometry of proposed antenna

(a) Radiating patch
(b) Ground plane
(c) Fabricated antenna without superstrate layer
(d) Fabricated antenna with superstrate layer

Figure 3.2.2(a) shows the step-by-step approach to achieve the final structure of proposed antenna. It depicts the evolution stages of proposed antenna with four different cases. Case 1 shows the antenna without using shorting pin as well as without segmentation of ground layer. In Case 2, a segmented ground structure is formed in place of plane ground without shorting pin. Case 3 is the final structure of proposed antenna which is obtained after using segmentation as well as shorting

pin which resonates at MICS band. Case 4 is not shown in Figure 3.2.2 but it is similar to Case 3 without superstrate layers. The plot for Case 4 depicted in Figure 3.2.2(b) shows that the proposed antenna doesn't resonate at the required MICS band without superstrate layers. The comparison of return loss of all these four cases is illustrated in Figure 3.2.2(b).

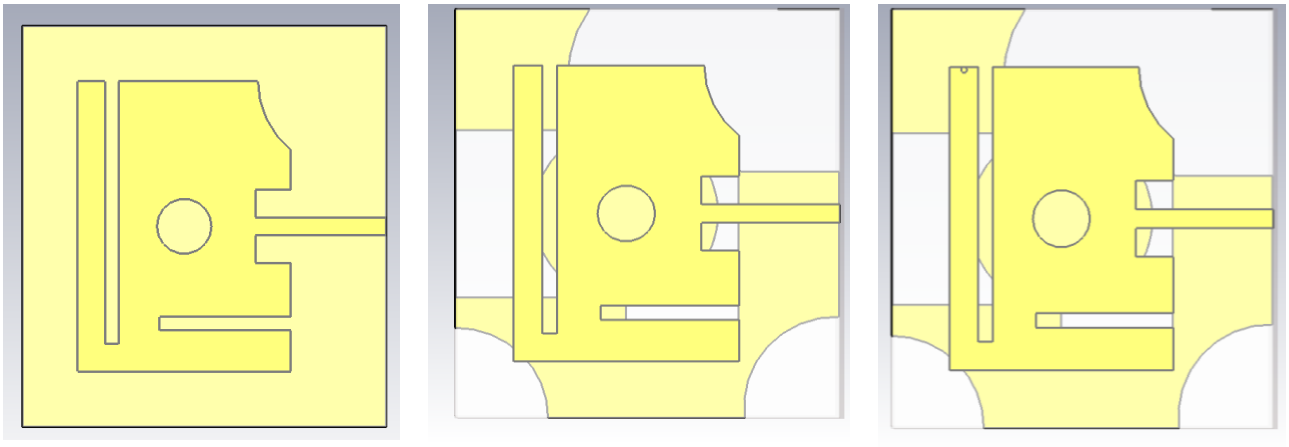

Case 1 Case 2 Case 3

(a)

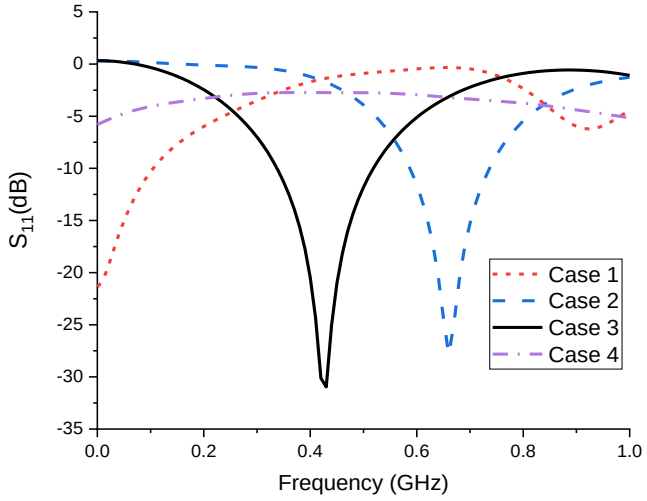

(b)

Figure 3.2.2 Evolution of proposed antenna

(a) Evolution stages of proposed antenna

(b) Return loss curves for four different cases

3.2.2 Testing of antenna

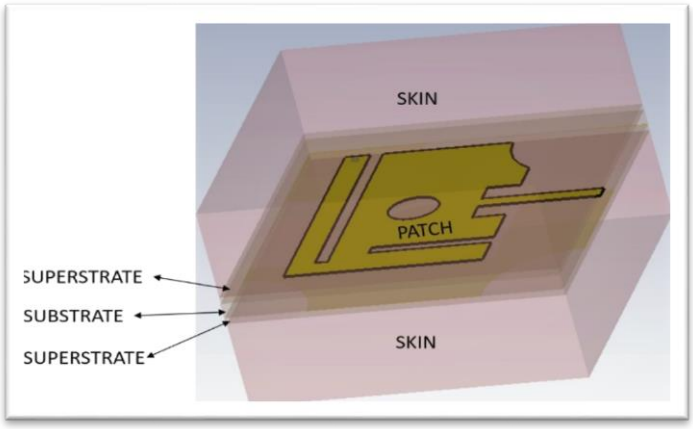

(a)

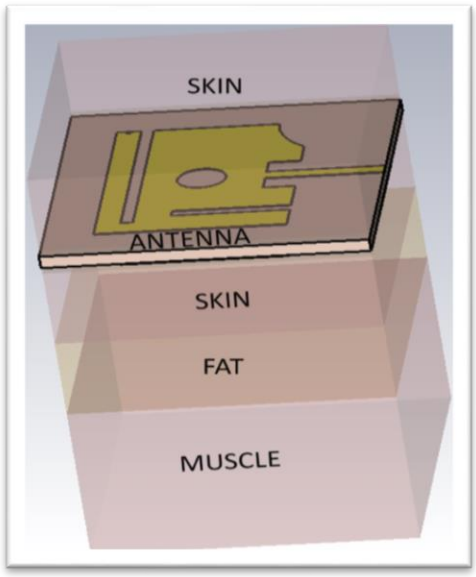

(b)

(c)

Figure 3.2.3 Testing of antenna

(a) Antenna inside skin layer
(b) Antenna inside three layer (skin-fat-muscle)
(c) Fabricated antenna testing inside skin mimicking liquid

Simulation and measurement setup of proposed antenna is shown in Figure 3.2.3. Figure 3.2.3(a) and Figure 3.2.3(b) shows the in-silico testing of proposed antenna inside homogenous skin phantom and heterogeneous three layered phantom of skin, fat and muscle respectively. In both phantoms, the antenna is inserted inside skin layer, but to show that the resonance of antenna is not affected in the presence of other tissue layers (because practically every tissue layer will be

present near antenna inside human body during implantation) simulation is done including fat and muscle layers as shown in Figure 3.2.3(b). In-silico testing is done using software. In both models the antenna is placed inside skin but for checking if antenna can work in heterogeneous environment of human body with nearly similar results on MICS band, testing on three-layer model is done. The skin and fat layer both are 4 mm in height whereas muscle layer is 8 mm in height.

In Figure 3.2.3(c), in-vitro testing of fabricated antenna is shown on VNA for calculating return loss (S_{11}). A homogeneous skin mimicking liquid phantom is made using 50% water and 50% sugar as stated by [94]. This skin phantom has electrical properties equivalent to skin tissues. Testing is done inside container of dimensions 150 x 100 x 50 mm^3 in which the liquid phantom is filled and antenna is fully dipped inside it.

3.2.3 Results and discussions

For authenticating the proposed antenna working on MICS band for implantable devices, reflection coefficient (S_{11}), SAR and gain is calculated. In-silico testing has been performed for the proposed antenna in homogenous skin, homogeneous brain and three-layer tissue models which has been depicted in Figure 3.2.4. It is clear from the graph that the antenna can operate evenly on MICS band either operated in homogenous or heterogeneous environment of human models.

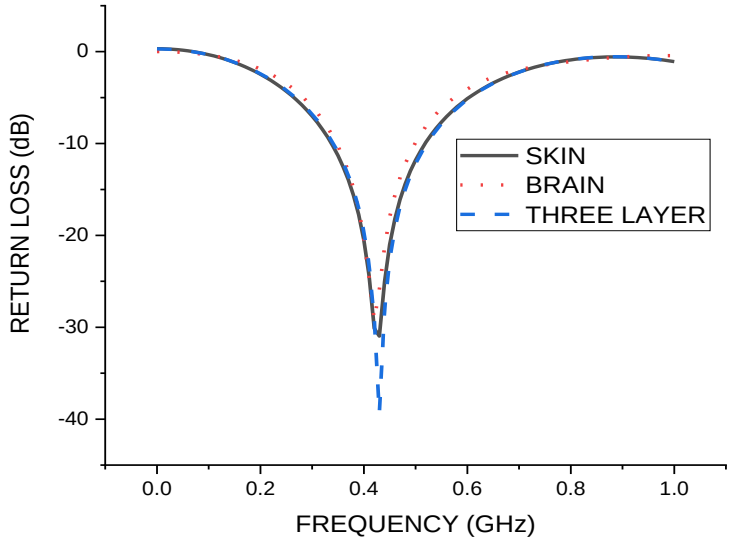

Figure 3.2.4 Comparison of return loss of proposed antenna within brain layer, homogeneous skin layer and three-layer phantom

The return loss and bandwidth of antenna in different tissue models is depicted in Table 3.2.1.

Table 3.2.1 Comparison of simulated and measured return loss and bandwith of proposed antenna

Biological tissue phantom	S_{11} (dB)	Bandwidth (GHz)
Skin	-30.95	0.34-0.51
Three layer	-39.33	0.35-0.52
Brain	-29.20	0.35-0.49
Skin (Measured)	-28.23	0.14-0.79

Biocompatibility of antenna in human body is checked by calculating SAR according to IEEE C95.1-1999 standards. Figure 3.2.5 shows that the 1g-averaged SAR value of antenna calculated at 1 W is 636.6 which means maximum input power to antenna can be given as 2.51 mW to operate under 1.6 W/kg which is strictly as per the limit specified by IEEE C95.1-1999 standards. The area highlighted in red color is portraying peak value of SAR while blue color portrays the lowest value of SAR. From this color coding we can say that the area nearby feedline is responsible for peak SAR.

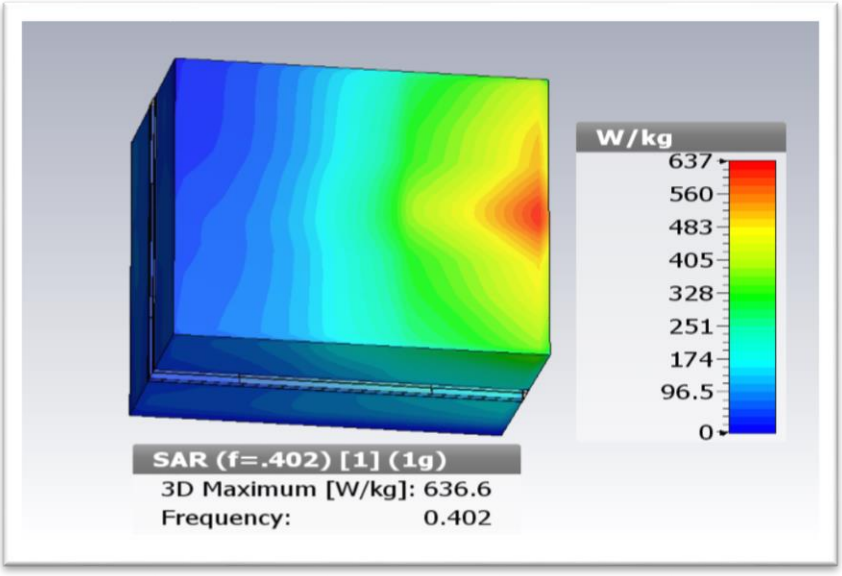

Figure 3.2.5 SAR value for 1-gram averaged cubic tissue at 1W power.

Figure 3.2.6(a) shows the simulated gain vs frequency pattern of antenna with gain of -22.14 dB at 402 MHz frequency. Surface current distribution of antenna is illustrated in Figure 3.2.6(b). This is used to find the particular area of antenna mostly responsible for radiation. From Figure 3.2.6(b) it is clear that the area near feedline is responsible for highest surface current in both patch as well as ground layers as the red color shows maximum current in the picture. Peak value of surface current obtained is 600 A/m. Volume factor of 456 is calculated from the simulated results of the proposed antenna inside skin which is better than other recently reported antennas.

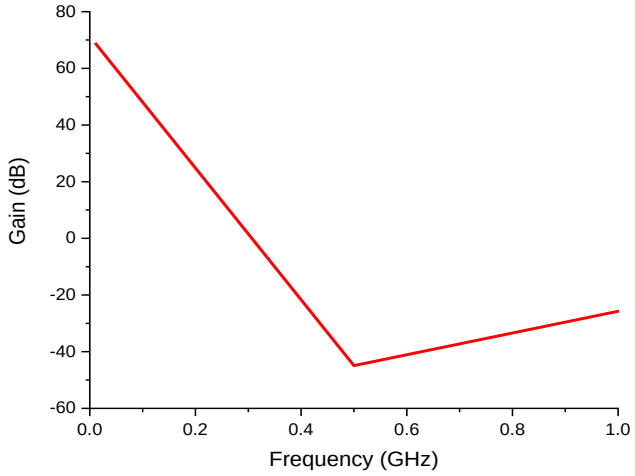

(a)

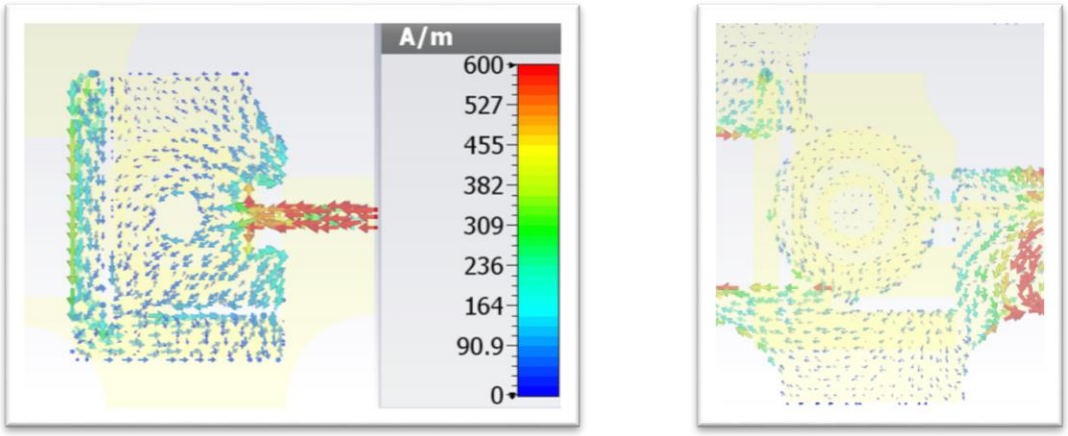

Front view Back view

(b)

Figure 3.2.6 Simulated results of proposed antenna

(a) Gain vs frequency

(b) Surface current distribution

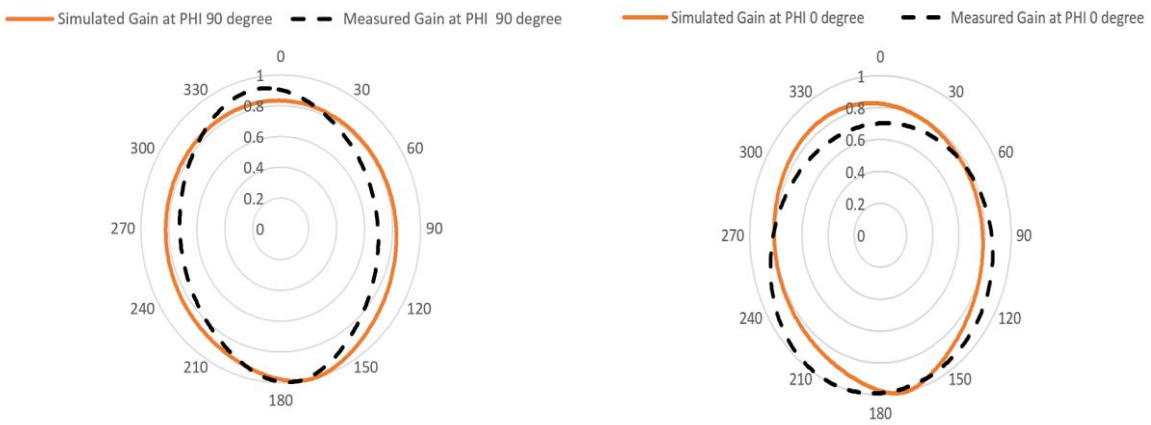

(a)

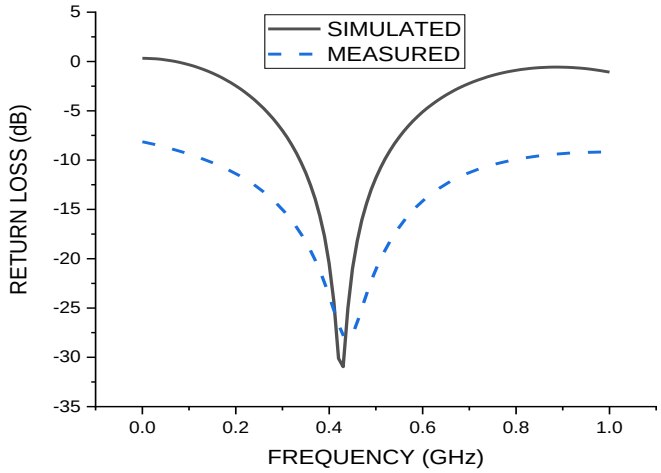

(b)

Figure 3.2.7 Comparison between simulated and measured results
(a) Gain at phi 90 degree and phi 0 degree
(b) Return Loss of proposed antenna in skin

Figure 3.2.7(a) shows simulated versus measured radiation pattern at phi 90 degrees and phi 0 degrees. In Figure 3.2.7(b) the comparison of return loss of the fabricated antenna with simulated one inside skin phantom is illustrated. There is a very close agreement in the simulated and measured results of proposed antenna with marginal difference in return loss and bandwidth which is depicted in Table 3.2.1. Moreover, the comparison of proposed antenna with recent literature on implantable antenna at MICS band is done in Table 3.2.2 in terms of volume, bandwidth, peak gain, SAR, superstrate layers used and volume factor of antenna. By performing the comparison of different parameters for different implantable antennas available till today we can say that this is the only antenna avoiding direct contact to skin by using superstrate layers on

both sides. Further, the proposed antenna is best among the recent literature provided in terms of volume factor too. This comparison makes the proposed antenna much suitable for implantable devices.

It is clear from comparison table that [101] is having highest percentage bandwidth on MICS band among all but antennas with low SAR value and good gain, but it is not covered with any superstrate layer. Ref. [95], [96], [102], [103], [104] are partially covered with superstrate layer with [96] and [102] having a good volume factor. Antennas in [96] and [102] are having lower volume than the proposed one but in terms of bandwidth, gain and insulation on both sides the proposed antenna is better.

Table 3.2.2 Comparison of proposed antenna with recent literature

Ref.	Volume (mm^3)	Bandwidth ($\lvert S_{11} \rvert \leq$ -10dB)	Gain (dB)	SAR (1g-average) (W/kg)	Volume factor (kHz/mm^3)	Superstrate layers
[95]	16.5x16.5x2.54	13 %	-31.5	318	101.2	Single
[96]	$\pi x(7.5)^2 x1.92$	28%	-	239.5	335.29	Single
[101]	22x16x1.27	52.6%	-18.5	.352	268.4	Nil
[102]	14x14x1.27	23.5%	-46	338	401.7	Single
[103]	27x9x1.27	>7.5%	-39.46	-	103.7	Single
[104]	19x30x1.6	>3.8%	-32	-	17.5	Single
This work	**13.3x14.6x1.92**	**40%**	**-22.14**	**636.6**	**456**	**Both sides**

CONCLUSION

In this chapter, two implantable antennas of similar size 13.3 x 14.6 x 1.92 mm^3 are designed and fabricated for biotelemetry applications at ISM and MICS bands. A high dielectric material Rogers

RT/ duroid 3010 ($\epsilon_r = 10.2$) is used as a substrate material for making the antennas biocompatible. The same material is used as superstrate layer that is applied on both sides of antenna for completely avoiding the contact of metal (patch and ground layers) to human tissue on implantation. Shorting pin technique is utilized in addition to slotting so as to make the antenna resonant at MICS band while being miniaturized and thus making it a novel structure too. Generally, resonating at lower frequency increases the antenna size but here the antenna dimensions are the same as they were for antenna resonating at ISM band (discussed in Section 3.1). For the validation of results, in-vitro testing is done inside skin phantom which is in accordance to simulated results with a small but acceptable variations. The SAR value for both antennas has been obtained below 1.6 W/kg for 1-g average cubic tissue which is considered safe according to IEEE C95. 1-1999 standards and prevents the patients from adverse effects of radiation of radio frequency on the human body. Volume factor, size and bandwidth percentage of both the antennas are best among the recently reported literature at the given frequency bands. The proposed antennas have perceptible performance parameters keeping in mind the safety of human beings that makes it a preferable choice for implantation inside the human body.

CHAPTER 4

COMPACT IMPLANTABLE ANTENNA AT ISM BAND FOR BIOTELEMETRY APPLICATIONS

This chapter proposes a miniaturized superstrate-loaded slotted implantable antenna working at ISM band for biotelemetry applications that is capable of monitoring Intracranial Pressure (ICP) when inserted inside the scalp on the top of brain. Slotting technique is used in the radiating patch and ground plane to reduce the size of antenna and to increase the bandwidth. The overall size of proposed antenna is 10.2 x 8.61 x 1.92 mm^3 which is considerably smaller than the previous two designs discussed in chapter 3.1 and 3.2 of chapter 3 and the present available literature. A high dielectric biocompatible material Rogers RT/duroid 3010 having dielectric constant 10.2 is used in making and encasing the proposed antenna. The small size and coverage of antenna with biocompatible layers on both sides makes the antenna structure novel as well as the best contender to be used in implantable devices. The design and fabrication of proposed antenna is discussed in detail, along with its evolution and parametric sweep in Section 4.1. In-silico testing is done inside homogeneous as well as heterogeneous layers in simulations, while in-vitro testing is done for the fabricated antenna using a single layer skin mimicking liquid which is discussed in an another Section 4.2 of this chapter. The proposed antenna produces appreciable results in terms of bandwidth, peak gain, SAR and volume factor. A detailed comparison of antenna performance parameters with the latest literature is demonstrated in Table 4.8 included in Section 4.2 of this chapter.

4.1 ANTENNA DESIGN

Figure 4.1 shows the geometrical representation of the proposed antenna with dimensions 10.2 x 8.61 mm^2 having a small patch size of 6.2 x 4.5 mm^2. A high dielectric biocompatible material, Rogers RT duroid 3010 (ϵ_r = 10.2 and tan δ = 0.0022) having thickness of 0.64 mm is used both as a substrate as well as superstrate for making the antenna compatible with human body tissues. Thus making overall thickness of the antenna as 1.92 (0.64 x 3 = 1.92) mm.

Figure 4.1(a) shows the radiating patch of suggested antenna having a circular slot of radius 1 mm with a semi-circular slot of radius 1.5 mm at the bottom of patch. An inset feed line of length 2.86 mm and width 0.66 mm is used for feeding the antenna. The advantage of using an inset feed line over other feeding methods is that it is simple to model as well as can easily be fabricated. It

also helps to achieve good impedance matching. Two vertical rectangular slots with different dimensions viz. 4.1 x 2.25 mm^2 and are introduced in the ground plane below the patch. Moreover, a circular slot of radius 1.5 mm is introduced at the centre of the ground plane, which makes the overall defect to resemble as if it is a quadrant shaped slot; reason behind this is that it merges with the two rectangular slots as depicted in Figure 4.1(b). The proposed antenna without and with superstrate layers is shown in Figure 4.1(c) and Figure 4.1(d), respectively. The detailed parametric dimensions of the radiating patch and ground plane along with slots are listed in Table 4.1.

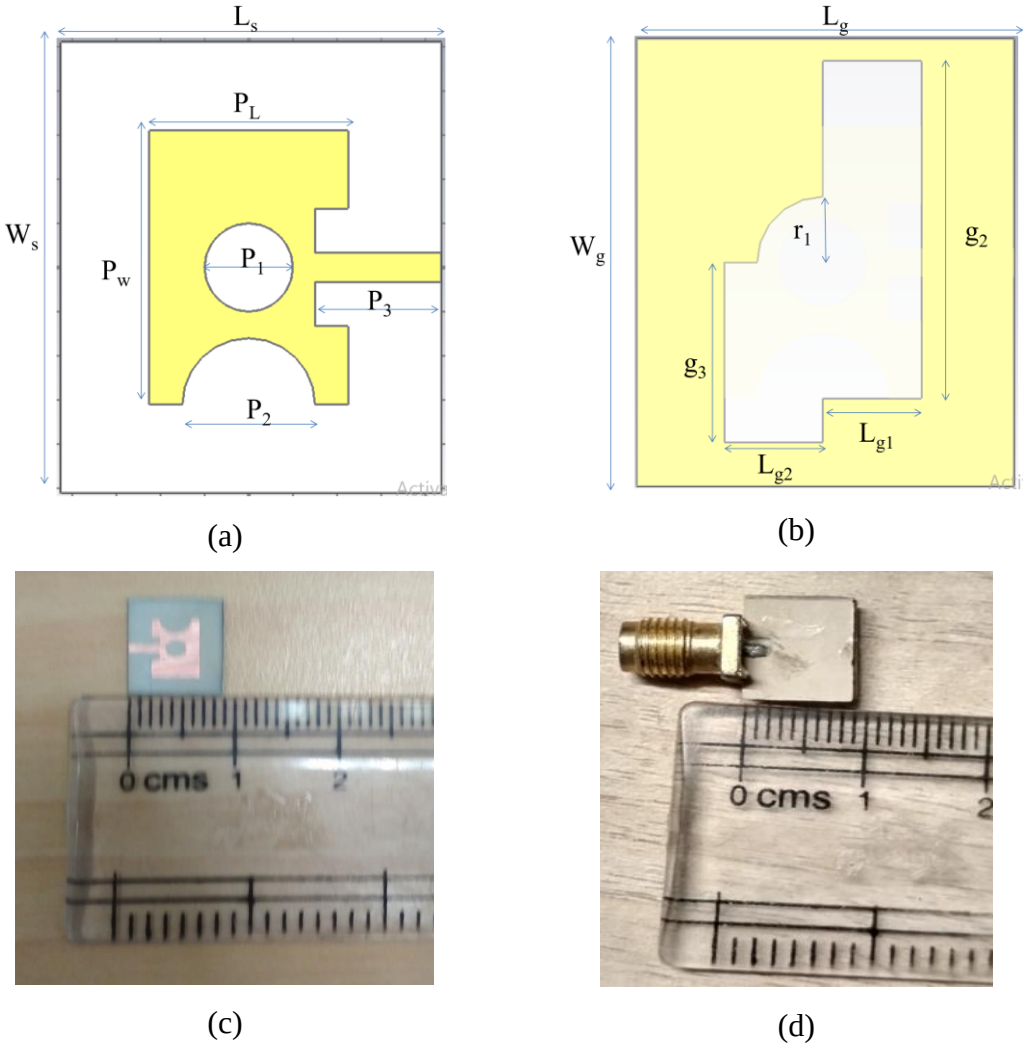

Figure 4.1 Geometrical representation of the proposed antenna
(a) Radiating patch
(b) Ground plane
(c) Fabricated antenna without superstrate layer
(d) Fabricated antenna with superstrate layer

Table 4.1 Geometrical dimensions of proposed antenna in mm

Parameter	Value	Coordinates	
L_s	8.61	(-4.25,5.1)	(4.36,5.1)
W_s	10.2	(-4.25,-5.1)	(-4.25,5.1)
P_L	4.5	(-2.25,3.1)	(2.25,3.1)
P_w	6.2	(-2.25,-3.1)	(-2.25,3.1)
P_1	2	(-1,0)	(1,0)
P_2	3	(-1.5,-3.1)	(1.5,-3.1)
P_3	4.86	(1.5,-0.33)	(4.36,-0.33)
L_g	8.61	(-4.25,5.1)	(4.36,5.1)
W_g	10.2	(-4.25,-5.1)	(-4.25,5.1)
r_1	1.5	(0,0)	(0,1.5)
g_2	7.7	(2.25,-3.1)	(2.25,4.6)
g_3	4.1	(-2.25,-4.1)	(-2.25,0)
L_{g1}	2.25	(0,-3.1)	(2.25,-3.1)
L_{g2}	2.25	(-2.25,-4.1)	(0,-4.1)

4.1.1 Evolution of the ground plane of proposed antenna

Figure 4.2 shows the evolution of ground plane of proposed antenna. Slotting technique is applied in the ground plane to obtain the desired results at ISM band for the proposed antenna. The ground plane basically consists of two vertical rectangular slots having different dimensions 7.7 x 2.25 mm^2 and 6.4 x 2.25 mm^2 along with one circular slot of radius 1.5 mm, which has been just introduced below the centre of radiating patch. The resonant behaviour of these three slots in the ground plane analysed in terms of return loss has been depicted in Figure 4.3 as four cases: Case 1, Case 2, Case 3 and Case 4, and the results obtained are illustrated in Table 4.2. In Case 1, the antenna with full ground plane has been shown without applying any kind of slotting technique. Figure 4.3 clearly shows that without slotting, the antenna does not resonate. In Case 2, a rectangular slot with dimensions 7.7 x 2.25 mm^2 is constructed in the ground plane for which the resonant frequency obtained is 2.63 GHz covering a bandwidth of 2.44-2.87 GHz with a return loss of -30.79 dB. As can be visualized from the bandwidth spectrum achieved in Figure 4.3, the desired ISM band (2.4-2.48 GHz) is not fully covered. Therefore, this configuration of slotted

ground plane is not good enough to satisfy our application. In Case 3, another rectangular slot with dimensions 6.4 x 2.255 mm^2 is embedded in the ground plane in addition to the rectangular slot configured in Case 2. Case 3 shows a return loss of -16.30 dB at the resonant frequency 2.42 GHz covering a bandwidth of 2.28-2.57 GHz. To get better results in terms of return loss within ISM band, Case 4 has been considered in which one more circular slot of radius 1.5 mm has been added just below the centre of radiating patch in addition to the two rectangular slots embedded in Case 3. Further, Case 4 depicts a return loss of -20.02 dB at the resonant frequency 2.475 GHz covering a bandwidth of 2.31-2.65 GHz. In the configuration pertaining to ground plane discussed in Case 4; the results obtained are good enough to satisfy the ISM band at the specific resonant frequency covering the required bandwidth. Thus Case 4 is considered as the final configuration of ground plane of the proposed antenna.

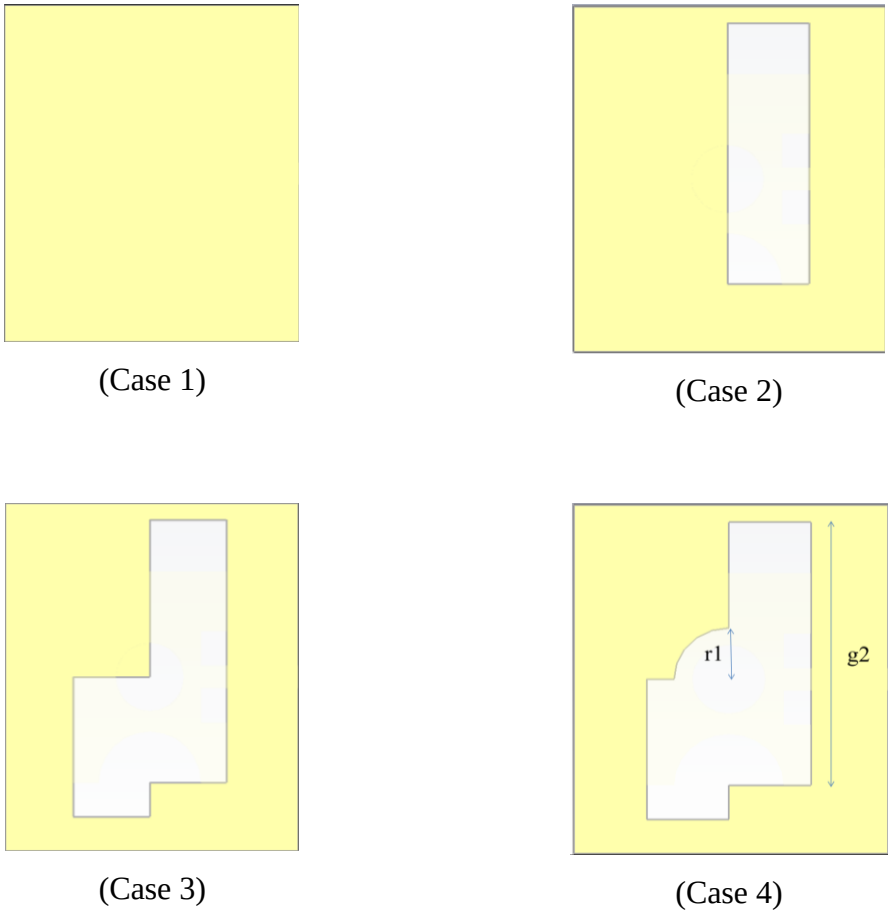

(Case 1) (Case 2)

(Case 3) (Case 4)

Figure 4.2 Evolution of the ground plane of proposed antenna

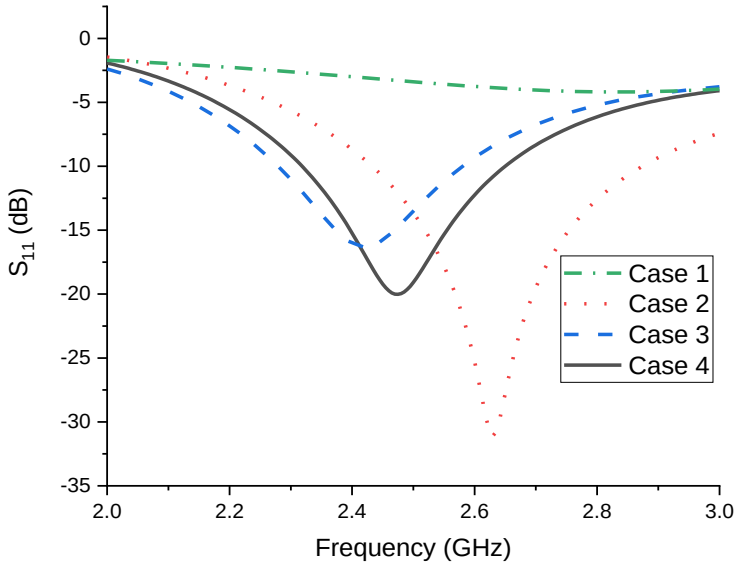

Figure 4.3 Comparison of return loss for four different configurations of ground plane of proposed antenna

Table 4.2 Performance characteristics of the ground plane of antenna for four different cases

	S_{11} (dB)	Bandwidth (GHz)	Resonant frequency (GHz)
Case 1	-	-	-
Case 2	-30.79	2.44-2.87	2.63
Case 3	-16.30	2.28-2.57	2.42
Case 4	-20.02	2.31-2.65	2.475

4.1.2 Parametric Sweep with different r_1 and g_2

Figure 4.4(a) shows the variation in return loss of antenna with the corresponding change in radius of circular slot in ground plane from $r_1 = 0.5$ to $r_1 = 3$. The return loss at $r_1=1.5$ is best suited for the proposed antenna as its resonant frequency falls in the desired bandwidth allocated to ISM band. Table 4.3 depicts the performance characteristics of proposed antenna with different values of radius of circular slot embedded exactly at the centre of ground plane below the radiating patch. Moreover, Figure 4.4(b) shows the corresponding change in return loss of antenna with change in length g_2 of bigger rectangular slot in the ground plane from $g_2 = 7.2$ to $g_2 = 8.2$. From Table 4.4, it is clear that return loss at $g_2 = 7.7$ and its corresponding resonant frequency obtained is best suited for our desired ISM band.

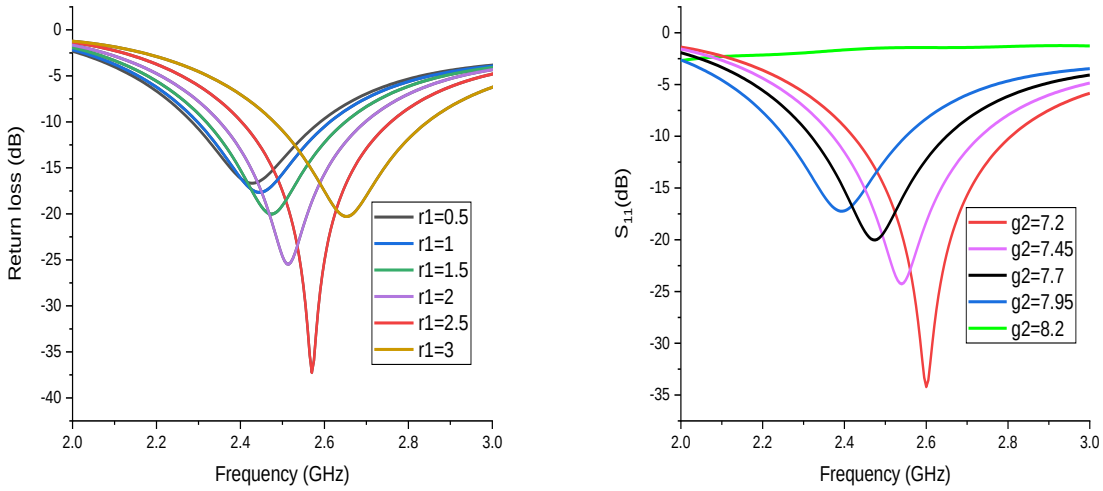

(a) (b)

Figure 4.4 Parametric sweep for the different slots embedded in the ground plane of proposed antenna

(a) Return loss of the proposed antenna with varying r_1

(b) Return loss of the proposed antenna with varying g_2

Table 4.3 Performance characteristics of the proposed antenna with different values of r_1 (radius of circular slots)

r_1 (mm)	S_{11} (dB)	Bandwidth (GHz)	Resonant frequency (GHz)
0.5	-16.66	2.28-2.59	2.43
1	-17.67	2.3-2.6	2.45
1.5	-20.02	2.31-2.65	2.475
2	-25.47	2.35-2.69	2.52
2.5	-37.25	2.4-2.75	2.56
3	-20.27	2.48-2.84	2.65

Table 4.4 Performance characteristics of the proposed antenna with different values of g2 (length of bigger rectangular slot)

g_2 (mm)	S_{11} (dB)	Bandwidth (GHz)	Resonant frequency (GHz)
7.2	-34.21	2.43-2.8	2.6
7.45	-24.26	2.38-2.73	2.54
7.7	-20.02	2.31-2.65	2.475
7.95	-17.24	2.25-2.55	2.39
8.2	-	-	-

4.2 SIMULATION AND MEASUREMENT SET UP OF THE PROPOSED ANTENNA

Figure 4.5 shows the simulation setup of the proposed antenna. The proposed antenna has been simulated using CST MWS. Figure 4.5(a) shows the antenna inside single-layer model of skin phantom with 4 mm skin layers at both sides whereas, in Figure 4.5(b) the antenna is simulated inside three-layer model of skin, fat and muscle with height 4 mm, 4 mm and 8 mm respectively and in Figure 4.5(c) the antenna is simulated inside single-layer model of 4 mm brain layers at both sides.

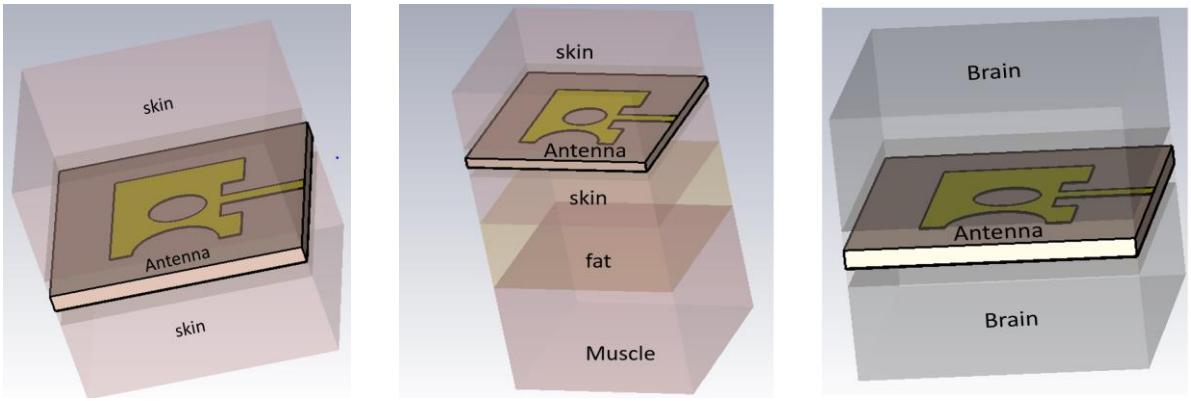

(a) (b) (c)

Figure 4.5 Simulation setup of proposed antenna
(a) Antenna inside skin layer
(b) Antenna inside three layer model of skin, fat and muscle
(c) Antenna inside brain layer

Figure 4.6 illustrates the simulated return loss characteristics of the proposed antenna along with superstrate inside the brain layer, skin layer and three-layered model. One more return loss curve has been shown here that corresponds to antenna simulated without superstrate layer. From all these return loss plots it can be clearly observed that in all the models, the antenna is resonating at the desired ISM band excluding the case when antenna is not covered with superstrate layers. There are minimal changes in the return loss of first three models which shows that the antenna is perfectly and evenly working in brain layer, skin layer as well as in three layered phantoms. Table 4.5 shows the dielectric properties of these human tissues at ISM band. Further, Table 4.6 shows the values of return loss and bandwidth achieved by the proposed antenna within brain layer, skin layer and three-layer phantom models.

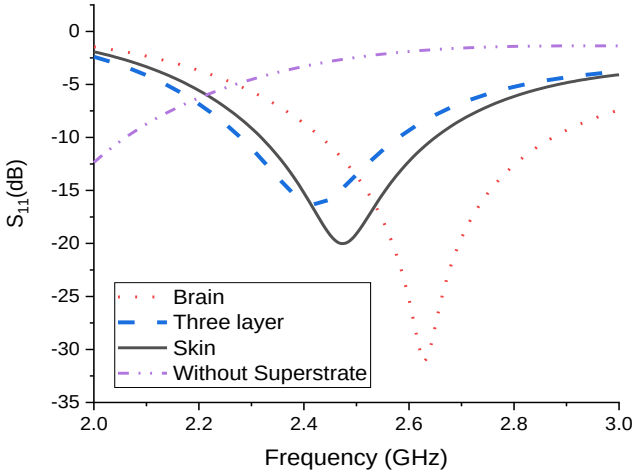

Figure 4.6 Comparison of simulated return loss characteristics of the proposed antenna

Table 4.5 Dielectric properties of human tissues at ISM band

Human tissue layer	Permittivity	Conductivity (S/m)	Density (kg/m^3)
Skin	38.007	1.464	1020
Fat	5.280	0.105	918
Muscle	53.574	1.810	1040

Table 4.6 Performance of the proposed antenna in brain layer, single skin layer and three layer phantom models

	S_{11} (dB)	Bandwidth (GHz)	Resonant frequency (GHz)
Skin	-20.02	2.31-2.65	2.475
Brain	-30.61	2.35-2.68	2.51
Three layer	-17.04	2.24-2.56	2.38

4.2.1 Surface Current Distribution

Figure 4.7(a) shows the surface current distribution on the radiating patch and ground plane of the proposed compact superstrate loaded slotted implantable antenna. The red color signifies the highest surface current value and blue color indicates the lowest surface current value. This gives an idea about those parts of antenna that are mostly responsible for radiation. It can be observed that the current intensity is maximum across the feedline which is attached to the radiating patch and across a semi-circular slot embedded at the bottom corner of radiating patch. Two rectangular slots and one circular slot are etched from the ground plane to attain the property of the defected ground structure. The current density is increased near the edges of slots, which means that the inserted slots play a vital role to obtain the desired resonance at ISM band without affecting the bandwidth.

4.2.2 Specific Absorption Rate (SAR)

The impact of the proposed compact superstrate loaded slotted implantable antenna on human tissue, described by SAR was also examined. SAR value depends on the geometry of human tissue, antenna positioning, dielectric properties of tissue, transmitting input power and spacing between the antenna and human tissue. The basic formula of SAR is given in Equation 4.1.

$$\text{SAR (W/kg)} = \frac{\sigma \times E^2}{\rho} \tag{4.1}$$

where, σ is the conductivity of tissue (S/m), E is the root mean square value of electric field (V/m) induced in the tissue and ρ is the tissue density (kg/m^2). The American standard for SAR analysis

is used i.e., the SAR value averaged over 1 gram and 10 gram of tissue should be less than 1.6 W/kg and 2 W/kg respectively. For validating the results of the proposed antenna, SAR (1-gram averaged and 10-gram averaged) are calculated at the resonating frequency. For checking that if the antenna is biocompatible inside the human body or not, the SAR values for 1W are shown in Figure 4.7(b). The SAR value is presented from minimum to maximum using color code of blue to red respectively. The area near the feedline is red which means SAR is maximum near the feedline of antenna. The SAR value for 1g-averaged cubic tissue obtained for supply power of 1W is 900 W/kg means a supply of less than 1.78 mW should be applied to obtain a value of SAR below 1.6 W/kg within the permissible limit. Similarly, the SAR value for 10g-averaged cubic tissue obtained for supply power of 1W is 82.1 W/kg means a supply of less than 24.4 mW should be applied to obtain a value of SAR below 2 W/kg within the permissible limit.

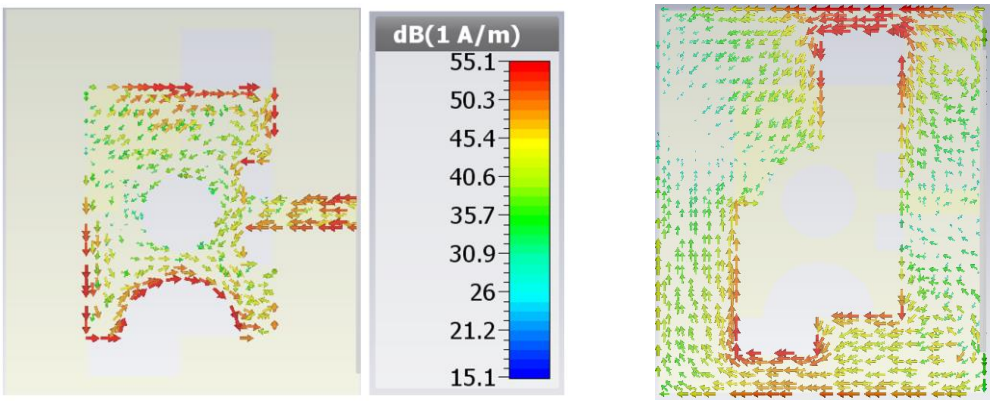

(a)

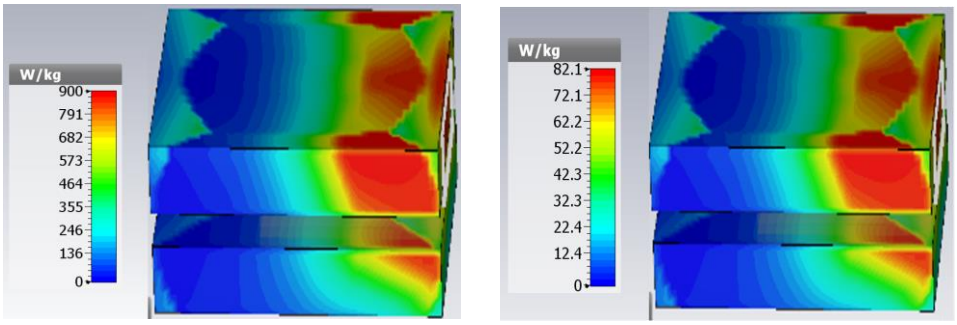

1-gram averaged SAR 10-gram averaged SAR

(b)

Figure 4.7 Surface current and SAR of proposed antenna
(a) Surface current distribution on radiating element and ground plane
(b) SAR value for 1-gram averaged and 10-gram averaged tissue

Figure 4.8 shows the impedance vs. frequency plot of proposed antenna within the frequency of range 2-3 GHz. A marker is shown here to depict the resonating frequency of proposed antenna satisfying the desired ISM band. The real part of impedance is 49.33 ohm as shown in Figure 4.8(a) whereas the imaginary part of impedance is -6.02 ohms at the resonating frequency 2.475 GHz as shown in Figure 4.8(b). These results clearly justify the radiating behaviour of antenna with perfect impedance matching of approximately 50 ohms and negligible reactive power, thus making the proposed antenna suitable for ISM band applications.

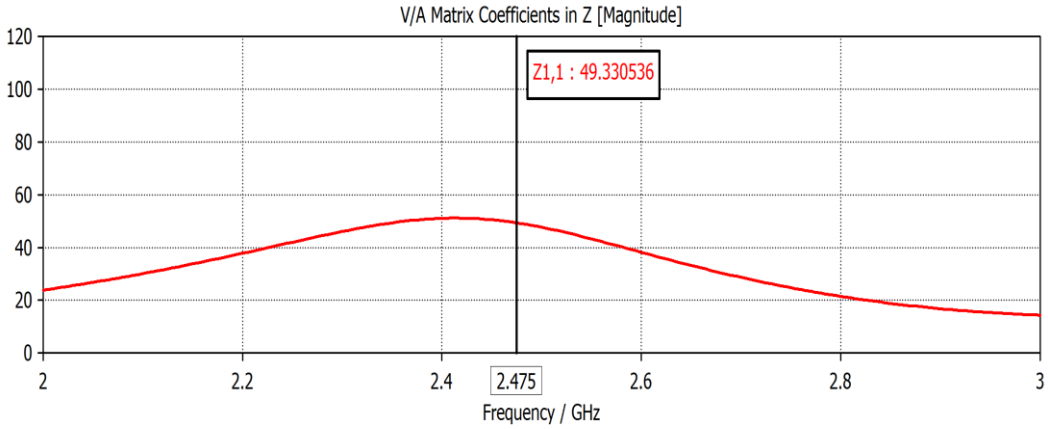

(a)

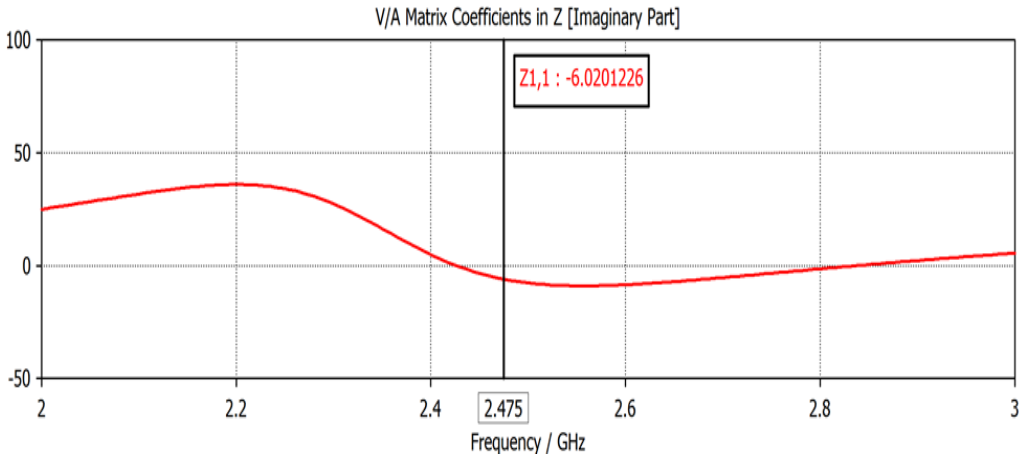

(b)

Figure 4.8 Impedance vs frequency plot of proposed antenna
(a) Real part
(b) Imaginary part

Figure 4.9(a) depicts the simulated gain vs frequency plot of proposed antenna in a single skin layer. A peak gain of -17.08 dBi at 2.475 GHz is reported. Figure 4.9(b) and Figure 4.9(c) illustrate the simulated E-plane and H-plane polar plots in relation to co-polarization and cross-polarization at phi = 90 degrees and phi = 0 degrees of the proposed antenna, respectively [105]. The green line denotes the cross-polarization, whereas the dashed black line denotes co-polarisation. The E-plane pattern is bidirectional, whereas the H-plane pattern is omnidirectional in nature [106].

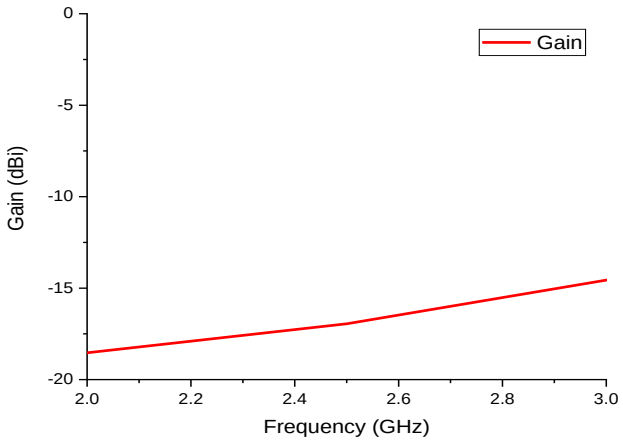

(a)

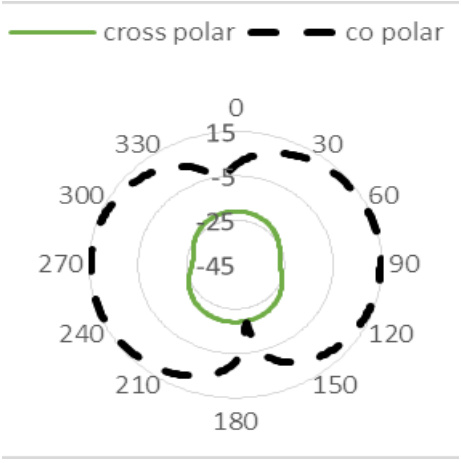

(b)

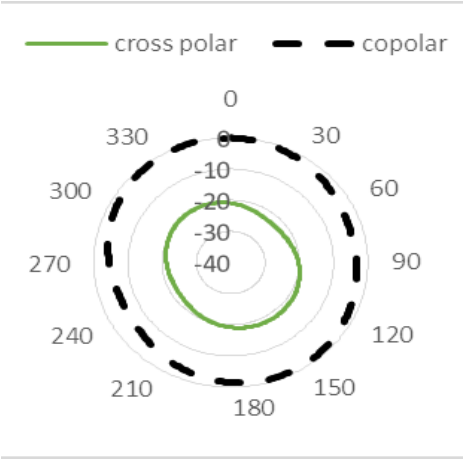

(c)

Figure 4.9 Gain plot and Radiation pattern of the proposed antenna

(a) Simulated gain vs frequency

(b) Simulated co-polarization and cross-polarization for E-plane at phi = 90 degrees

(c) Simulated co-polarization and cross-polarization for H-plane at phi = 0 degrees

(a)

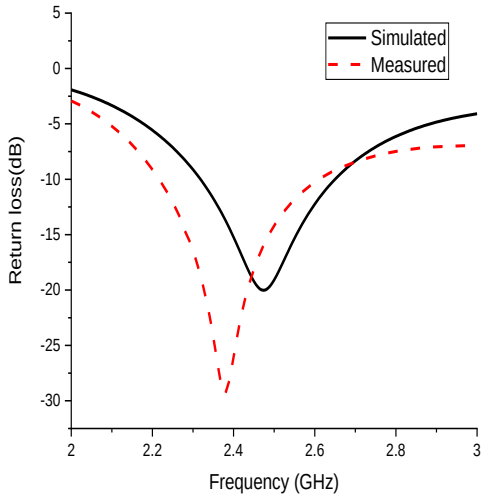

(b)

Figure 4.10 Testing and set-up of the proposed antenna

(a) Fabricated antenna testing inside skin mimicking liquid

(b) Comparison of simulated and measured return loss of the proposed antenna in skin

Figure 4.10 shows the testing set-up of proposed antenna using VNA and comparison of the simulated and measured return loss of the proposed antenna in skin layer. The return loss of the fabricated antenna is measured using Agilent E5071C vector network analyzer available in Antenna Research Laboratory, Department of Electronics and Communication Engineering, Thapar Institute of Engineering and Technology, Patiala, as shown in Figure 4.10(a). To test the antenna, a homogenous phantom of skin mimicking liquid (made using 50% water and 50% sugar) is made with approximately the same electrical properties as that of skin whose recipe has been discussed in [94]. This phantom is put inside a container of size 150 x 100 x 50 mm^3 and filled such that the antenna can easily be dipped inside the liquid phantom. Figure 4.10(b) shows the comparison of simulated and measured return loss of the proposed antenna inside a single layer skin phantom. A close agreement between the simulated and measured results of the proposed antenna at ISM band inside skin can be seen except for some small differences in return loss and bandwidth as illustrated in Table 4.7. These differences can occur due to various reasons viz.; (a) simulation is done in ideal conditions but while measuring, temperature and pressure changes affect results, (b) poor soldering of SMA connector to the limited area of feedline of the antenna, and (c) dipping of antenna connector with antenna inside phantom solution can alter results.

Table 4.7 Simulated and measured return loss and bandwith of the proposed antenna inside single layered skin phantom

	S_{11} in dB	Bandwidth in GHz
Skin (simulated)	-20.02	2.31-2.65
Skin (measured)	-29.28	2.22-2.61

Table 4.8 Comparison of performance parameters of proposed antenna with recently reported literature

Ref.	Dimensions (mm^3)	Bandwidth ($\lvert S_{11} \rvert \leq$ -10 dB) at ISM band	Peak Gain (dBi)	SAR (1g-average) at 1W power	SAR(10g-average) at 1W power	Volume factor	Superstrate layers
[94]	27.5x21x1.6	12.57 %	-27.46	-	-	335	nil
[95]	16.5x16.5x2.54	4.4 %	-9	292	-	159	Single
[96]	10x15x2	-	-16.3	-	-	-	Both sides
[97]	22x16x1.27	1.6%	-19.5	2.15x10^-3	-	89.5	Nil
[107]	10x10x1.27	10.84 %	-21	710.65	84.6	826	Single
This work	**10.2x8.61x1.92**	**13.7 %**	**-17.08**	**900**	**82.1**	**2016**	**Both sides**

Table 4.8 illustrates the comparison of performance parameter of the proposed antenna with recently reported literature. Bandwidth, peak gain, SAR (1g-averaged and 10g-averaged) and volume factor are some of the performance measures used for comparing the proposed antenna with previous available literature. In [94] and [97], the developed implantable antennas have large dimensions with low volume factor and are designed without any superstrate layer. The antenna proposed in [95] is covered with a superstrate layer on single side having very small bandwidth percentage and volume factor at ISM band. In [107], the volume of antenna is lower than our

proposed design but it is again partially covered with superstrate layer. Both sides of the compact sized antenna discussed in [96] are covered with superstrate layer but the parameters such as SAR and bandwidth are not been analyzed. Our proposed antenna is fully insulated with superstrate layers thus making it biocompatible and has a miniaturized size with best bandwidth percentage and volume factor among the recent literature available.

Volume factor of antenna is defined as the ratio of bandwidth to the volume of antenna as depicted in Equation 4.2 [21].

$$\text{Volume factor (VF)} = \text{Bandwidth (in kHz)}/\text{Antenna volume (mm}^3\text{)} \quad (4.2)$$

CONCLUSION

In this work, a compact implantable antenna working at ISM band has been proposed for biotelemetry applications. The overall size of proposed antenna is 10.2 x 8.61 x 1.92 mm^3 which is considerably small with a peak gain –17.08 dBi. Slotting strategy has been utilized both in the radiating patch as well as in ground ground plane because of which an appreciable bandwidth of 13.7% is accomplished. A high dielectric biocompatible material Rogers RT/duroid 3010 is used in making and encasing the proposed antenna. As the antennas size is small and it is covered with biocompatible superstrate layers on both sides. Therefore our proposed antenna is considered novel as well as best contender to be used in implantable devices. The measured results obtained from the in-vitro testing of fabricated antenna performed inside skin phantom are in close agreement with the simulated results with a little yet satisfactory variation. SAR value for 1-gram and 10-gram averaged cubic tissue is considered for the security of patient from unfavourable impact of radio frequency radiations on human body. Table 4.8 gives a point to point correlation of this work with the ongoing literature in terms of performance parameters antenna dimensions, bandwidth, peak gain, SAR and volume factor which shows that the presented antenna is quite adequate for implantable devices and circuits.

CHAPTER 5

IN-SILICO, IN-VITRO AND EX-VIVO TESTING OF SMALL FOOTPRINT IMPLANTABLE BIOCOMPATIBLE MICROSTRIP ANTENNA FOR BIOTELEMETRY APPLICATIONS

In this chapter, a biocompatible microstrip antenna at ISM band for biotelemetry applications is proposed. The main feature of this antenna is its compact size of 8.2 x 6.94 x 0.75 mm^3 which is small enough to be easily fitted inside an implantable device. A high dielectric material Rogers RT/Duroid 3010 (ϵ_r = 10.2, tan δ = 0.0022) of thickness 0.25 mm, is used both as superstrate and substrate. The design and evolution of proposed antenna are discussed along with fabrication in the Section 5.1 of this chapter. The antenna is covered with a biocompatible layer of superstrate on both sides in order to avoid any direct contact of the metal layer (radiating patch and ground) with human body tissue keeping in mind the safety of patients. In most of the recent designs, either the size of antenna is too big or the antenna is covered with superstrate on a single side only. In this work, size has been taken care of in addition to biocompatibility issues. Further, three types of testing are done for validating the proposed antenna that is covered in the Section 5.2 of this chapter. In-silico testing is done using three-dimensional simulation software CST MWS. The in-vitro and ex-vivo testing is done inside skin mimicking liquid and in animal tissue (chicken) respectively. This design is better than previous designs discussed in chapters 3 and 4 in terms of miniaturization and further ex-vivo testing has been performed for this design for better validation of results. The essential performance parameters of the proposed antenna for biotelemetry applications such as SAR, peak gain, surface current distribution, and return loss are measured, calculated, and discussed briefly in Section 5.3. These obtained results are compared with the recently reported literature in Table 5.2.

5.1 DESIGN AND EVOLUTION OF PROPOSED ANTENNA

Figure 5.1(a) and Figure 5.1(b) depict the geometry and dimensions of radiating patch and ground plane of the antenna, respectively. The footprint of this antenna is 8.2 x 6.94 mm^2 with 0.75 mm thickness making it too compact than recent literature and thus easy to implant. The substrate material used for making a biocompatible antenna is Rogers RT/Duroid 3010 (ϵ_r = 10.2, tan δ = 0.0022) with 0.25 mm thickness. Two more layers of the same material are used for covering the

antenna from top and bottom to avoid direct contact with human tissue. Therefore, the final thickness of the antenna is 0.75 mm. In Figure 5.1 (a), we can clearly see that the inset feed of 2.86 mm length is connected with a patch to power the antenna. The patch size is 4.2 x 2.5 mm^2 with a semi-circular slot of radius 1 mm at the left edge. Figure 5.1 (b) depicts the ground plane of the antenna with three rectangular and three circular slots. All the three rectangular slots vary in size viz. 4.9 x 3.5 mm^2, 1.7 x 1.75 mm^2 and 1.1 x 1.25 mm^2 and among the three circular slots, one has 0.5 mm radius while the other two slots are of 0.8 mm radius each, which are embedded slightly nearby the rectangular slots. Figure 5.1 (c) shows the fabricated antenna without superstrate layers, while Figure 5.1 (d) shows the fabricated antenna with superstrate layers on both sides and a 50-ohm SMA connector.

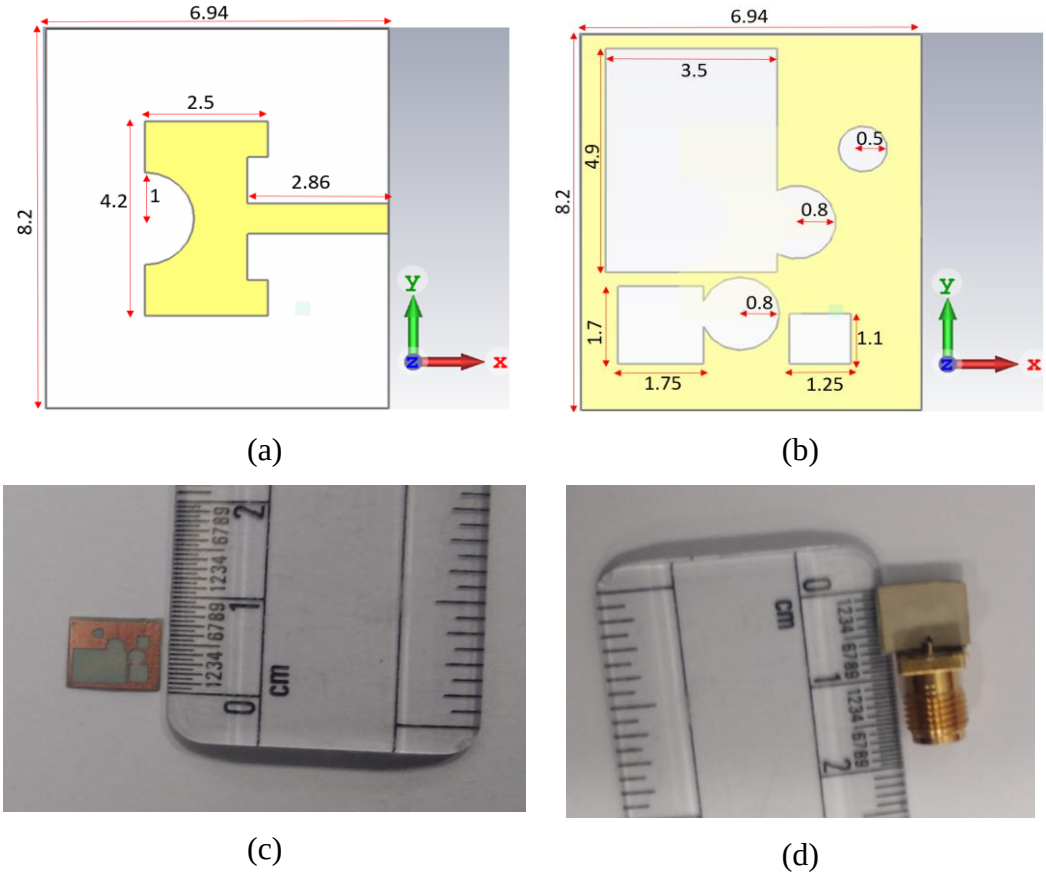

Figure 5.1 Geometry of proposed antenna

(a) Radiating patch
(b) Ground plane
(c) Fabricated antenna without superstrate layer
(d) Fabricated antenna with superstrate layer

Figure 5.2 (a) represents the three different cases of antenna evolution. Case 1 shows the antenna without any type of slot in patch or ground. In Case 2 rectangular and circular slots are

etched in the ground plane which are responsible for better return loss. Case 3 represents the final proposed antenna represented with slots in ground plane as well as semi-circular slot in patch that allows the antenna to radiate at desired frequency with good return loss at ISM band. Figure 5.2 (b) depicts the return loss graph of different cases of antenna evolution discussed in Figure 5.2 (a). From this graph we can see that the antenna does not resonate in Case 1, while in Case 2, the return loss curve signifies that antenna is resonating definitely, but the resonating frequency is far away from the desired ISM band. The evolution of proposed antenna with respect to Case 4 is not shown in Fig 5.2 (a) as it is similar to Case 3 but superstrate layers are not been used. In all other cases viz. Case 1, Case 2 and Case 3, superstrate layers have also been used. In Case 4, when the antenna is not encased with superstrate layers on both sides, there is no resonance obtained at the desired ISM band.

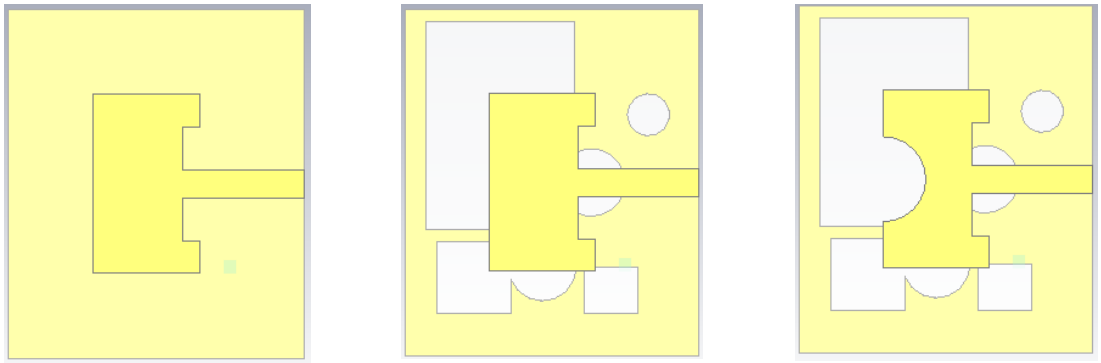

(a)

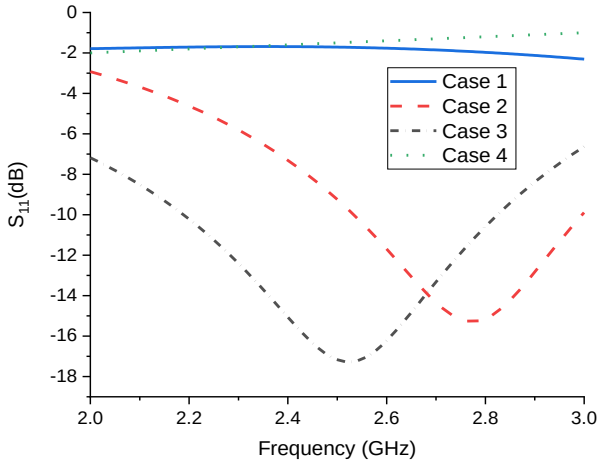

(b)

Figure 5.2 Evolution of proposed antenna

(a) Different cases leading to the final structure of proposed antenna

(b) Return loss curves corresponding to four different cases

5.2 TESTING OF PROPOSED ANTENNA

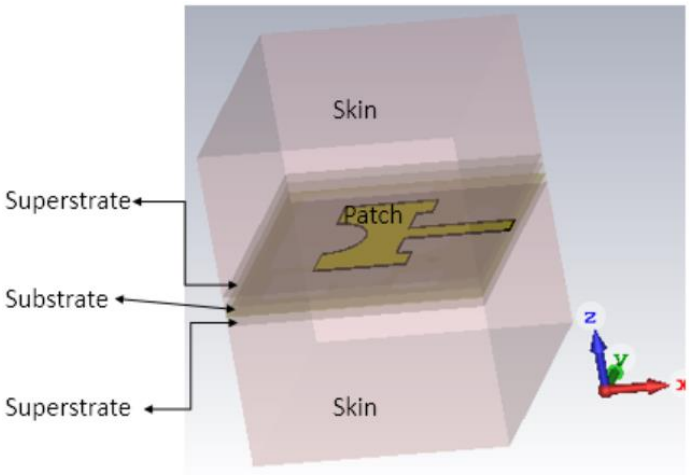

(a)

(b)

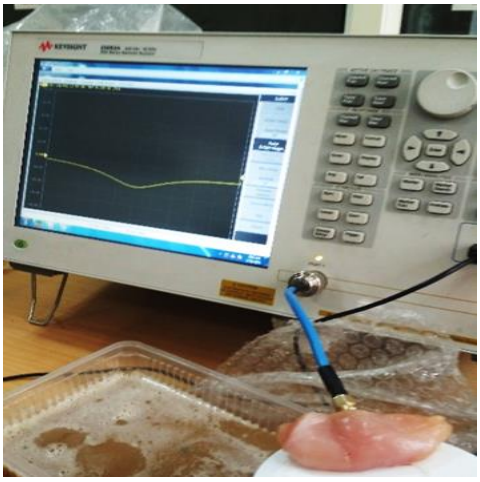

(c)

Figure 5.3 Testing of proposed antenna

(a) In-silico testing inside skin layer
(b) In-vitro testing inside skin mimicking liquid
(c) Ex-vivo testing inside animal tissue (chicken)

The proposed antenna undergoes three types of testing approaches for proper validation of simulated and measured results. The first one is in-silico testing of the antenna inside software as shown in Figure 5.3 (a), which has been performed by applying skin layer on both sides of the antenna and then evaluating the results. The second type of testing is in-vitro, which means testing

of antenna is performed in homogenous human tissue mimicking solution. For the proposed antenna, the testing is done inside skin mimicking liquid using water and sugar in equal proportion, as stated by [94]. This liquid is filled in a container of dimensions 140 x 90 x 50 mm^3 up to the level such that the antenna can be completely dipped inside the solution. This setup of antenna testing in solution using VNA can be seen in Figure 5.3 (b). The third type of testing performed is ex-vivo, which means that the testing is done inside a sample of animal tissue. For the proposed antenna, the ex-vivo, which testing is done inside a small sample of animal tissue (chicken), as shown in Figure 5.3 (c).

5.3 RESULTS AND DISCUSSION

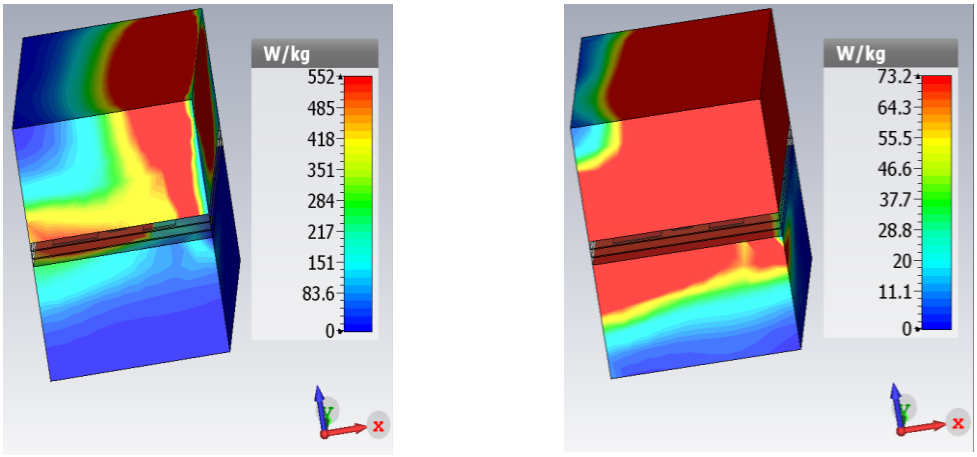

(a) (b)

Figure 5.4 Simulated results of proposed antenna
(a) SAR for 1-gram averaged cubic tissue at 1W power
(b) SAR for 10-gram averaged cubic tissue at 1W power

In order to validate the proposed antenna, the parameters like return loss, SAR, surface current distribution, and gain are calculated at ISM band. The SAR value is checked according to IEEE C95.1-1999 and IEEE C95.1-2005 standards so that the antenna radiation doesn't affect or harm the human body. The SAR range from minimum to maximum is denoted by the color scale from blue to red respectively. The SAR for 1g-averaged tissue is calculated as 552 W/kg at 1W as depicted in Figure 5.4 (a), which means that we can operate our proposed antenna up to 2.89 mW so that it can remain under 1.6 W/kg (permissible limit for 1g-averaged tissue). Figure 5.4 (b) shows the SAR for 10g-averaged tissue calculated as 73.2 W/kg at 1W, which implies that we can operate our proposed antenna up to 27.32 mW so that it can remain under 2 W/kg (permissible limit for 10g-averaged tissue) according to IEEE standards.

Figure 5.5 (a) represents the surface current distribution on radiating patch and ground plane of the proposed antenna. The value of surface current obtained is 488 A/m. The red colored arrows specify the area which is mostly responsible for radiation from the antenna. Therefore we conclude that feedline from which the antenna is being fed and that edge of patch which connects the feedline (front view) and area near the feedline and bigger rectangular slot in the ground layer (back view) are mostly responsible for radiation [108]. Figure 5.5 (b) depicts the three dimensional representation of gain of proposed antenna. This graph shows that at ISM band the gain of antenna is -21.6 dB.

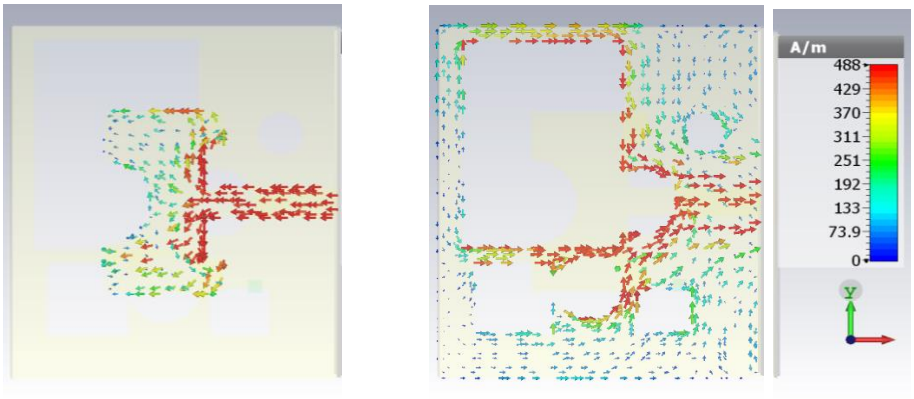

Front view Back view

(a)

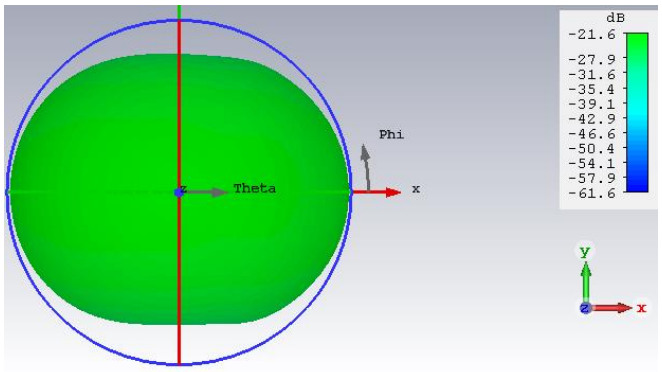

(b)

Figure 5.5 Simulated results of proposed antenna

(a) Surface current distribution

(b) 3D pattern of gain

A comparison of return loss obtained with respect to in-silico, in-vitro and ex-vivo testing is done as represented in Figure 5.6. From this figure, it is clear that the antenna is resonating perfectly at ISM band in all testing scenarios with only a little deviation. Table 5.1 illustrates the

values for return loss and bandwidth obtained during in-silico, in-vitro and ex-vivo testing. Further, in Table 5.2 all important parameters related to biotelemetry applications of antenna are compared with recent available literature. These parameters are antenna volume, bandwidth, peak gain, SAR (1g-averaged and 10g-averaged), volume factor, and number of superstrate layers. Antennas discussed in [94],[101] are not insulated with any superstrate layer and have larger antenna dimensions in comparison to all the papers tabulated in Table 5.2. but the obtained impedance bandwidth of [94] is better than [101]. While antennas in [45], [95], [96], [102], [103], [104] are covered only on single side with a superstrate layer. Both SAR values for 1 gram and 10 gram averaged tissue are calculated only in [45] and [96] other than the proposed antenna. In recent literature pertaining to [109] and [110], antennas are covered with superstrate layers on both sides, with [109] having bandwidth percentage of 18.10%. Table 5.2 clearly shows that the proposed antenna is best in terms of size (8.2 x 6.94 x 0.75 mm^3), bandwidth percentage (16.1%), and volume factor (9371.8) than previous works and is fully covered with superstrate layers on both sides to avoid contact with human tissues.

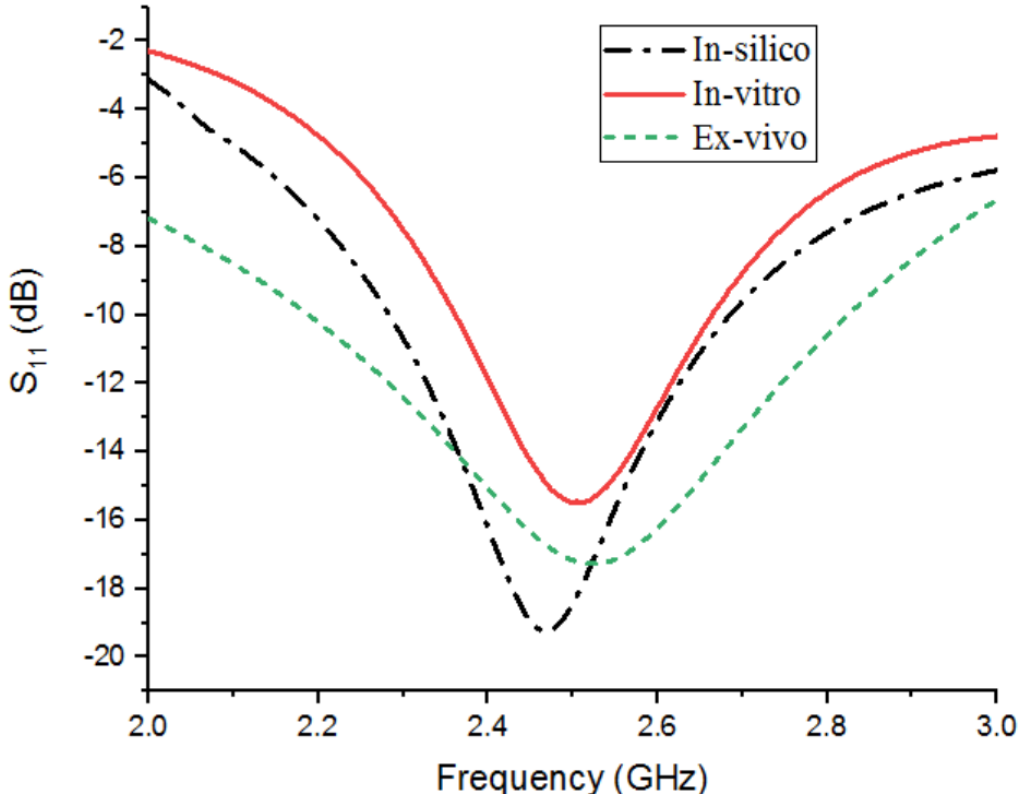

Figure 5.6 Return Loss curves of proposed antenna during in-silico, in-vitro and ex-vivo testing

Table 5.1 Return loss and bandwidth obtained during in-silico, in-vitro and ex-vivo testing.

Type of Testing	S_{11} in dB	Bandwidth in GHz
In-silico	-19.24	2.285-2.685
In-vitro	-15.48	2.365-2.66
Ex-vivo	-17.27	2.19-2.82

Table 5.2 Comparison of proposed antenna with recent available literature

Ref.	Volume (mm^3)	Bandwidth ($\lvert S_{11} \rvert \leq$ -10dB)	Peak Gain (dB)	SAR (1g-averaged)	SAR (10g-averaged)	Volume factor (kHz/mm^3)	Superstrate layers
[46]	$3.14x(4)^2x1.27$	15.9%	-37.02	849.14	91.21	6112.4	Single
[94]	27.5x21x1.6	12.57 %	-27.46	-	-	335	Nil
[95]	16.5x16.5x2.54	4.4 %	-9	292	-	159	Single
[96]	$3.14x(7.5)^2x1.92$	10.4%	-13.8	159.4	34.75	764	Single
[101]	22x16x1.27	1.6%	-19.5	$2.15x10^{-3}$	-	89.5	Nil
[102]	14x14x1.27	12%	-19	482	-	1205	Single
[103]	27x9x1.27	>6%	-20	-	-	489.3	Single
[104]	19x30x1.6	>8%	-13	-	-	219.3	Single
[109]	13.3x14.6x1.92	18.10%	-14.9	775.5	-	1207	Double
[110]	10x15x2	-	-16.3	-	-	-	Double
This work	**8.2x6.94x0.75**	**16.1%**	**-21.6**	**552**	**73.2**	**9371.8**	**Double**

CONCLUSION

In this chapter, a miniaturized biocompatible implantable antenna of dimensions 8.2 x 6.94 x 0.75 mm^3 is proposed for ISM band biotelemetry applications. For patient's safety, both sides of the antenna are covered with thin superstrate layers of Rogers RT/Duroid 3010 (ϵ_r = 10.2, tan δ = 0.002) with 0.25 mm thickness. This makes it fully encased within the biocompatible layers having high dielectric constant and thin superstrate layers makes the proposed antenna highly miniaturized making it novel and superlative from other implantable antennas. An appreciable bandwidth of 16.1% is achieved for our proposed antenna, which is considered best among recently reported implantable antennas. The volume factor of the antenna is also far better than recent antennas available in literature. SAR values of both 1g and 10g-averaged cubic tissues are determined, which are shown to be attained within the permissible limit specified by IEEE standards. The proposed antenna has been observed to be in the fully functional mode under all the three testing approaches, i.e., in-silico, in-vitro and ex-vivo, with close and maximum agreement among the results. This shows that the fabricated antenna is ready to use with immediate effect and can prove to be helpful in implantable devices for biotelemetry applications.

CHAPTER 6
CONCLUSIONS AND FUTURE SCOPE

6.1 CONCLUSIONS

Biomedical telemetry is significantly gaining interest due to the real time monitoring of patient's health. Cardiac care, capsule endoscopy, cochlear implants, health parameter monitoring (i.e., heart rate, cholesterol, sugar and temperature), and several other applications are aided by various implantable and wearable devices. In comparison to wearable gadgets, the implanted device offers a one-of-a-kind tool for accessing essential signals from within the human body at life-threatening moments. Implantable device design is extremely difficult and requires the integration of several tiny components. Although the majority of the implantable device sub-components are efficient at small sizes, the implantable antenna is not. Usually, limiting the size of an antenna degrades its electromagnetic performance. As a result, some novel structures are discussed to address these contradicting requirements in this thesis. Slotting technique, shorting pin technique, using of high dielectric material, and introduction of superstrate layers helped to achieve the final four designs in this work at ISM (2.4 - 2.48 GHz) and MICS (402 – 405 MHz). In-silico, in-vitro , and ex-vivo testing procedures are utilized for validating the fabricated designs. Each chapter of this thesis provides a significant contribution and achievement in this area, which can be summarized as follows:

In chapter 3, two implantable antennas of having same dimensions as 13.3 x 14.6 x 1.92 mm^3 are made for biotelemetry applications. A high dielectric (ϵ_r = 10.2) material Rogers RT/duroid 3010 is used as substrate material for making these antennas biocompatible. Superstrate layer is applied at both sides for completely avoiding the contact of metal (patch and ground layers) with human tissues on implantation. Both antennas are discussed in Sections 3.1 and 3.2 which are designed for ISM band and MICS band respectively. In Section 3.1 slotting technique is used in patch as well as ground plane due to which an appreciable bandwidth of 18.10% is achieved and for validation of results in-vitro testing is done inside skin phantom which is in accordance to simulated results with small but acceptable variations. The SAR value for 1-g averaged cubic tissue is considered for safety of patient from adverse effects of radiations of radio frequency on human body, therefore SAR value at 2 mW is calculated as 1.55 W/kg which is in accordance with safety regulations. Volume factor of 1207 kHz/mm^3 has been achieved for this antenna design. On the

other hand, in Section 3.2 for designing an antenna at MICS band shorting pin technique is used to reduce the overall size at low frequency. Bandwidth of 40% is achieved in this design which is much better than most of the designs reported earlier in literature operating at MICS band. Appreciable results are obtained when in-silico testing of proposed antenna is performed in three different tissue models which is further validated by doing in-vitro testing in skin mimicking liquid phantom. Both sides of antenna are covered with biocompatible layers of high dielectric material to protect nearby tissues of human body. Further SAR value for 1g average is checked according to IEEE C95.1-1999 standards to ensure full safety of patient.

In chapter 4, a compact implantable antenna of dimensions 10.2 x 8.61 x 1.92 mm^3 and peak gain –17.08 dBi is made for biotelemetry applications at ISM band. Slotting strategy is utilized both in patch as well as ground plane because of which an appreciable bandwidth of 13.7% is accomplished. SAR value for 1-gram and 10-gram averaged cubic tissue is considered for the security of patient from unfavorable impact of radio frequency radiations on the human body. The measured results obtained from in-vitro testing of fabricated antenna done inside skin phantom are in close agreement to the simulated results with a little yet satisfactory variation.

In chapter 5, a more miniaturized biocompatible implantable antenna of dimensions 8.2 x 6.94 x 0.75 mm^3 is proposed at ISM band for biotelemetry applications. In this antenna design also, both sides of antenna are covered with thin superstrate layers of Rogers RT/Duroid 3010 (ϵ_r = 10.2, tan δ = 0.0022) with 0.25 mm thickness to ensure patient's safety. An appreciable bandwidth of 16.1% is achieved for our proposed antenna which is in fact the best among recently reported implantable antennas at ISM band. Volume factor of the antenna is also far better than other antennas reported in the literature so far. SAR values of both 1g and 10g-averaged cubic tissues are determined, which are shown to be attained within the permissible limits specified by IEEE standards. The proposed antenna has been observed to be in full functional mode under all the three testing approaches, i.e., in-silico, in-vitro and ex-vivo, with close and maximum agreement among the results.

6.2 FUTURE SCOPE

This thesis covers a wide range of implantable antennas operating at MICS and ISM band for biotelemetry applications. Other challenges in the following categories, however, may be considered for future investigations:

- Wireless power transfer (WPT) is a promising technology for powering implantable antennas, which can be used to monitor and transmit important health data wirelessly in real-time. WPT enables the transfer of electrical energy from a power source to an implantable device without the need for physical connections or wires, allowing for continuous power supply and eliminating the need for frequent battery replacements or invasive surgical procedures. WPT can be integrated with implantable devices, such as pacemakers and insulin pumps, to enhance their functionality and reliability, this work could explore the design and optimization of WPT systems for implantable antennas, as well as their performance in different environments and applications.
- An important future research line is the development of a full implantable device that can transport data from inside the human body to an external receiver. This demands working on different segments which integrate medicine and engineering. Designing a gadget that includes wireless power transmission and a wake-up receiver will be a very challenging task which will be used to keep a regular watch and diagnose the medical conditions of the patient.
- Another futuristic approach is to design a flexible, tissue-independent biocompatible implantable antenna with enhanced gain and more expanded SAR distribution that can operate in a random and dynamic environment for in-body communications. This means it should be able to operate effectively in any tissue type and does not depend upon specific patient’s attributes such as age, sex and weight etc. i.e., it must be able to work effectively if the antenna environment changes with time.
- The deployment of 5G networks can enable high-speed wireless communication between implantable devices and healthcare providers, enabling remote monitoring and management of patients. This technology can also facilitate the transfer of large amounts of health data, such as high-resolution medical images or video streams, for real-time analysis and diagnosis.
- The integration of artificial intelligence (AI) with implantable antennas can enable real-time analysis of health data and more accurate prediction of potential health issues. This technology can also provide personalized recommendations for lifestyle changes or medical treatments based on an individual's unique health data.

- The integration of machine learning (ML) with implantable antennas can further enhance the capabilities of these devices by enabling advanced data analysis and predictive modeling. ML algorithms can be trained on large datasets of patient health data to detect patterns and relationships that may not be apparent through traditional statistical analysis. This can enable more accurate and personalized predictions of potential health issues and more effective recommendations for medical treatments or lifestyle changes. In addition to predictive modeling, ML can also be used to optimize the design and performance of implantable antennas. ML algorithms can analyze the electromagnetic properties of different antenna designs and optimize them for maximum efficiency and performance in specific applications and environments.

REFERENCES

[1] T. A. Aleef, Y. B. Hagos, V. H. Minh, S. Khawaldeh, and U. Pervaiz, "Design and simulation-based performance evaluation of a miniaturised implantable antenna for biomedical applications," *Micro Nano Lett.*, vol. 12, no. 10, pp. 821–826, 2017.

[2] C. J. Sánchez-Fernández, O. Quevedo-Teruel, J. Requena-Carrión, L. Inclán-Sánchez, and E. Rajo-Iglesias, "Dual-band microstrip patch antenna based on short-circuited ring and spiral resonators for implantable medical devices," *IET Microwaves, Antennas Propag.*, vol. 4, no. 8, pp. 1048–1055, 2010.

[3] S. Bhattacharjee, S. Maity, S. K. Metya, and C. T. Bhunia, "Performance enhancement of implantable medical antenna using differential feed technique," *Eng. Sci. Technol. an Int. J.*, pp. 1–9, 2015.

[4] B. Rana, J. Shim, and J. Chung, "An Implantable Antenna With Broadside Radiation for a Brain – Machine Interface," *IEEE Sens. J.*, vol. 19, no. 20, pp. 9200–9205, 2019.

[5] K. S. Guillory and R. A. Normann, "A 100-channel system for real time detection and storage of extracellular spike waveforms," *J. Neurosci. Methods*, vol. 91, pp. 21–29, 1999.

[6] D. Wessels, "Implantable Pacemakers and Defibrillators : Device Overview & EM1 considerations ' C," *2002 IEEE Int. Symp. Electromagn. Compat.*, vol. 2, pp. 911–915, 2002.

[7] T. Buchegger, O. Gerald, R. Alexander, H. Erwin, and A. Andreas, StelzerSpringer, "Ultra-Wideband Transceivers for Cochlear Implants," *EURASIP J. Appl. Signal Processing*, pp. 3069–3075, 2005.

[8] K. Gosalia, G. Lazzi, and M. Humayun, "Investigation of a Microwave Data Telemetry Link for a Retinal Prosthesis," *IEEE Trans. Microw. Theory Tech.*, vol. 52, no. 8, pp. 1925–1933, 2004.

[9] Y. Zhang, C. Liu, and K. Zhang, "Design and in-vivo testing of a low-cost miniaturized capsule system for body temperature monitoring," *Int J RF Microw Comput Aided Eng.*, no. March, pp. 1–10, 2019.

[10] N. M. Neihart, R. R. Harrison, and A. W. P. Supply, "Micropower Circuits for Bidirectional Wireless Telemetry in Neural Recording Applications," *IEEE Trans. Biomed. Eng.*, vol. 52, no. 11, pp. 1950–1959, 2005.

[11] B. Tiwari, S. Hak, and G. Vipin, "Investigation on Performance of Wearable Flexible On - Body Ultra - Wideband Antenna Based on Denim for Wireless Health Monitoring," *J. Electron. Mater.*, no. 0123456789, 2021.

[12] S. Hayat, S. Ahson, A. Shah, and H. Yoo, "Miniaturized Dual-Band Circularly Polarized Implantable Antenna for Capsule Endoscopic System," *IEEE Trans. Antennas Propag.*, vol. 69, no. 4, pp. 1885–1895, 2021.

[13] C. Wu, T. Chien, C. Yang, and C. Luo, "Design of Novel S-Shaped Quad-Band Antenna for MedRadio / WMTS / ISM Implantable Biotelemetry Applications," *Int. J. antennas propogation*, vol. 2012, pp. 1–12, 2012.

[14] A. Iqbal, M. Al-hasan, and A. Basir, “Biotelemetry and Wireless Powering of Biomedical Implants Using a Rectifier Integrated,” *IEEE Trans. Microw. Theory Tech.*, vol. 69, no. 7, pp. 3438–3451, 2021.

[15] R. Birok and R. Kapoor, “Design of Low Cost Bio-impedance Measuring Instrument,” *Int. J. Adv. Comput. Sci. Appl.*, vol. 13, Jan. 2022.

[16] P. Kamalvand, G. K. Pandey, and M. K. Meshram, “A single-sided meandered-dual-antenna structure for UHF RFID tags,” *Int. J. Microw. Wirel. Technol.*, vol. 9, no. 7, pp. 1419–1426, 2017.

[17] A. P. S. Pharwaha and S. Rani, “A Novel Antenna Design for Telemedicine Applications,” *Int. J. Comput. Inf. Eng.*, vol. 7, no. 12, pp. 1665–1669, 2013.

[18] M. K. Sharma *et al.*, “Experimental Investigation of the Breast Phantom for Tumor Detection Using Ultra-Wide Band – MIMO Antenna Sensor (UMAS) Probe,” *IEEE Sens. J.*, vol. 20, no. 12, pp. 6745–6752, 2020.

[19] A. Damaj, H. M. El Misilmani, and S. A. Chahine, “Implantable Antennas for Biomedical Applications : An Overview on Alternative Antenna Design Methods and Challenges,” *2018 Int. Conf. High Perform. Comput. Simul.*, pp. 31–37, 2018.

[20] T. Karacolak, A. Z. Hood, and E. Topsakal, “Design of a dual-band implantable antenna and development of skin mimicking gels for continuous glucose monitoring,” *IEEE Trans. Microw. Theory Tech.*, vol. 56, no. 4, pp. 1001–1008, 2008.

[21] M. Yousaf, I. B. E. N. Mabrouk, M. Zada, A. Akram, and Y. Amin, “An Ultra-Miniaturized Antenna With Ultra-Wide Bandwidth Characteristics for Medical Implant Systems,” *IEEE Access*, vol. 9, 2021.

[22] W. Wang, X. Xuan, W. Zhao, and H. Nie, “An Implantable Antenna Sensor for Medical Applications,” *IEEE Sens. J.*, vol. 21, no. 13, pp. 14035–14042, 2021.

[23] F. Merli, L. Bolomey, J. F. Zürcher, G. Corradini, E. Meurville, and A. K. Skrivervik, “Design, realization and measurements of a miniature antenna for implantable wireless communication systems,” *IEEE Trans. Antennas Propag.*, vol. 59, no. 10, pp. 3544–3555, 2011.

[24] M. P. Mohan, M. F. Karim, H. Cai, A. Alphones, and A. Q. Liu, “A Compact mmWave Butler Matrix for Wireless Power Transfer,” in *2019 IEEE Asia-Pacific Microwave Conference (APMC)*, 2019, pp. 1595–1597.

[25] E. Khansalee, Y. Zhao, E. Leelarasmee, and K. Nuanyai, “A dual-band rectifier for RF energy harvesting systems,” in *2014 11th International Conference on Electrical Engineering/Electronics, Computer, Telecommunications and Information Technology (ECTI-CON)*, 2014, pp. 1–4.

[26] C. Wang, G. A. Covic, and O. H. Stielau, “Power Transfer Capability and Bifurcation Phenomena of Loosely Coupled Inductive Power Transfer Systems,” *IEEE Trans. Ind. Electron.*, vol. 51, no. 1, pp. 148–157, 2004.

[27] J. Garnica, R. A. Chinga, and J. Lin, “Wireless Power Transmission : From Far Field to Near Field,” *Proc. IEEE*, vol. 101, no. 6, pp. 1321–1331, 2013.

[28] P. Li and R. Bashirullah, “A Wireless Power Interface for Rechargeable Battery,” *IEEE Trans. circuits Syst.*, vol. 54, no. 10, pp. 912–916, 2007.

[29] C. Wang, O. H. Stielau, and G. A. Covic, “Design Considerations for a Contactless Electric Vehicle Battery Charger,” *IEEE Trans. Ind. Electron.*, vol. 52, no. 5, pp. 1308–1314, 2005.

[30] R. Jegadeesan and Y. Guo, “Topology Selection and Ef fi ciency Improvement of Inductive Power Links,” *IEEE Trans. Antennas Propag.*, vol. 60, no. 10, pp. 4846–4854, 2012.

[31] M. Kod, J. Zhou, Y. Huang, M. Hussein, A. P. Sohrab, and C. Song, “An Approach to Improve the Misalignment and Wireless Power Transfer into Biomedical Implants Using Meandered Wearable Loop Antenna,” *Wirel. Power Transf.*, vol. 2021, 2021.

[32] R. Jegadeesan, K. Agarwal, Y. Guo, and S. Yen, “Wireless Power Delivery to Flexible Subcutaneous Implants Using Capacitive Coupling,” *IEEE Trans. Microw. Theory Tech.*, vol. 65, no. 1, pp. 280–292, 2017.

[33] R. Das and H. Yoo, “A Multiband Antenna Associating Wireless Monitoring and Nonleaky Wireless Power Transfer System for Biomedical Implants,” *IEEE Trans. Microw. Theory Tech.*, vol. 65, no. 7, pp. 2485–2495, 2017.

[34] W. Lei, H. Chu, and Y. Guo, “Design of a Circularly Polarized Ground Radiation Antenna for Biomedical Applications,” *IEEE Trans. Antennas Propag.*, vol. 64, no. 6, pp. 2535–2540, 2016.

[35] V. K. Gupta and D. Thakur, “Design and performance analysis of a CPW-fed circularly polarized implantable antenna for 2 . 45 GHz ISM band,” *Microw. Opt. Technol. Lett.*, no. March, pp. 1–8, 2020.

[36] M. L. Scarpello *et al.*, “Design of an implantable slot dipole conformal flexible antenna for biomedical applications,” *IEEE Trans. Antennas Propag.*, vol. 59, no. 10, pp. 3556–3564, 2011.

[37] L. Xu, Z. Chu, L. Zhu, and J. Xu, “Design and Analysis of Dual-Band Implantable Antennas Based on Effective Relative Permittivity Calculation,” *IEEE Trans. Antennas Propag.*, vol. 69, no. 5, pp. 2463–2472, 2021.

[38] K. Ito, C.-H. Lin, and H.-Y. Lin, “Evaluation of Wearable and Implantable Antennas with Human Phantoms,” in *Handbook of Antenna Technologies*, Z. N. Chen, D. Liu, H. Nakano, X. Qing, and T. Zwick, Eds. Singapore: Springer Singapore, 2016, pp. 2239–2268.

[39] A. G. Miquel, “Antenna Design and Characterization for Biomedical Applications Doctoral thesis.”

[40] J. Xi, C. Rowell, J. M. Fortes, F. Rouholahnejad, and B. Derat, “Optimization of SAM Head Phantom for Compact Antenna Test Ranges,” *URSI Radio Sci. Lett.*, vol. 2, pp. 20–23, 2020.

[41] C. Rossmann and D. Haemmerich, “Review of temperature dependence of thermal properties, dielectric properties, and perfusion of biological tissues at hyperthermic and ablation temperatures,” *Crit. Rev. Biomed. Eng.*, vol. 42, no. 6, 2014.

[42] J. Wang, O. Fujiwara, and S. Watanabe, “Approximation of aging effect on dielectric tissue properties for SAR assessment of mobile telephones,” *IEEE Trans. Electromagn. Compat.*,

vol. 48, no. 2, pp. 408–413, 2006.

[43] K. M. S. Thotahewa, J.-M. Redouté, and M. R. Yuce, "SAR, SA, and temperature variation in the human head caused by IR-UWB implants operating at 4 GHz," *IEEE Trans. Microw. Theory Tech.*, vol. 61, no. 5, pp. 2161–2169, 2013.

[44] T. Karacolak, R. Cooper, J. Butler, S. Fisher, and E. Topsakal, "In-vivo verification of implantable antennas using rats as model animals," *IEEE Antennas Wirel. Propag. Lett.*, vol. 9, pp. 334–337, 2010.

[45] F. Gozasht, M. D. Hossain, and A. S. Mohan, "Miniaturized Slot PIFA Antenna for Tripleband Implantable Biomedical biomedical applications," *2013 IEEE MTT-S Int. Microw. Work. Ser. RF Wirel. Technol. Biomed. Healthc. Appl.*, vol. 2, pp. 1–3, 2013.

[46] R. Liu *et al.*, "A Wideband Circular Polarization Implantable Antenna for Health Monitor Microsystem," *IEEE Antennas Wirel. Propag. Lett.*, vol. 20, no. 5, pp. 848–852, 2021.

[47] S. Das, D. Mitra, B. Mandal, and R. Augustine, "Implantable antenna gain enhancement using liquid metal - based reflector," *Appl. Phys. A*, pp. 1–7, 2020.

[48] Tharaka Dissanayake, "Dielectric Loaded Impedance Matching for Wideband Implanted Antennas," *IEEE Trans. Microw. Theory Tech.*, vol. 1, no. 1, pp. 2480–2487, 2009.

[49] J. Faerber *et al.*, "In-vivo Characterization of a Wireless Telemetry Module for a Capsule Endoscopy System Utilizing a Conformal Antenna," *IEEE Trans. Biomed. Circuits Syst.*, vol. 12, no. 1, pp. 95–105, 2018.

[50] J. Hayward, G. Chansin, and H. Zervos, "Wearable Technology 2016–2026 Markets, players and 10-year forecasts," *IDTechEx*, 2016.

[51] Y.-L. Zheng *et al.*, "Unobtrusive sensing and wearable devices for health informatics," *IEEE Trans. Biomed. Eng.*, vol. 61, no. 5, pp. 1538–1554, 2014.

[52] R. Elmgvist, J. Landegren, S. O. Pettersson, Å. Senning, and G. William-Olsson, "Artificial pacemaker for treatment of Adams-Stokes syndrome and slow heart rate," *Am. Heart J.*, vol. 65, no. 6, pp. 731–748, 1963.

[53] A. Kiourti, K. S. Nikita, and S. Member, "A Review of In - Body Biotelemetry Devices : Implantables, Ingestibles, and Injectables," *IEEE Trans. Biomed. Eng.*, vol. 64, no. 7, pp. 1422–1430, 2017.

[54] M. R. Yuce and T. Dissanayake, "Easy-to-swallow antenna and propagation," *IEEE Microw. Mag.*, vol. 14, no. 4, pp. 74–82, 2013.

[55] E. Y. Chow, M. M. Morris, and P. P. Irazoqui, "Implantable RF medical devices: The benefits of high-speed communication and much greater communication distances in biomedical applications," *IEEE Microw. Mag.*, vol. 14, no. 4, pp. 64–73, 2013.

[56] W. Yao, C.-H. Chu, and Z. Li, "The adoption and implementation of RFID technologies in healthcare: a literature review," *J. Med. Syst.*, vol. 36, pp. 3507–3525, 2012.

[57] S. Rao *et al.*, "Miniature implantable and wearable on-body antennas: Towards the new era of wireless body-centric systems [antenna applications corner]," *IEEE Antennas Propag. Mag.*, vol. 56, no. 1, pp. 271–291, 2014.

[58] A. Class, “Sensory Tag Chip—For Automatic Data Logging,” in *AMS*, 3AD, vol. 5, no. 2016, pp. v1-07.

[59] S. Parlak, A. Sarcevic, I. Marsic, and R. S. Burd, “Introducing RFID technology in dynamic and time-critical medical settings: Requirements and challenges,” *J. Biomed. Inform.*, vol. 45, no. 5, pp. 958–974, 2012.

[60] A. M. Wicks, J. K. Visich, and S. Li, “Radio frequency identification applications in hospital environments,” *Hosp. Top.*, vol. 84, no. 3, pp. 3–9, 2006.

[61] S.-W. Wang, W.-H. Chen, C.-S. Ong, L. Liu, and Y.-W. Chuang, “RFID application in hospitals: a case study on a demonstration RFID project in a Taiwan hospital,” in *Proceedings of the 39th Annual Hawaii International Conference on System Sciences (HICSS’06)*, 2006, vol. 8, pp. 184a-184a.

[62] E. Drazen and J. Rhoads, “Using tracking tools to improve patient flow in hospitals, issue brief,” *Calif. Healthc. Found.*, vol. 4, no. 1, 2011.

[63] M. McKee and W. H. Organization, “Reducing hospital beds: what are the lessons to be learned?,” 2004.

[64] J. A. Fisher and T. Monahan, “Evaluation of real-time location systems in their hospital contexts,” *Int. J. Med. Inform.*, vol. 81, no. 10, pp. 705–712, 2012.

[65] K. S. Pasupathy and T. R. Hellmich, “How RFID technology improves hospital care,” *Harv. Bus. Rev.*, 2015.

[66] J. Kim, “Implanted Antenna Design on Pacemaker with Characteristic Mode Analysis,” *2021 Int. Appl. Comput. Electromagn. Soc. Symp.*, vol. 1, pp. 400–402, 2021.

[67] S. Sultana, M. M. Miran, S. M. A. Uddin, M. M. Naby, and M. Haque, “Performance analysis of a modified implantable PIFA operates at MICS band for human head phantom model,” *3rd Int. Conf. Electr. Inf. Commun. Technol. EICT 2017*, vol. 2018-Janua, no. December, pp. 1–5, 2018.

[68] J. H. Lee, D. W. Seo, and H. S. Lee, “Design of implantable antenna on the dielectric/ferrite substrate for wireless biotelemetry,” *2015 Int. Symp. Antennas Propagation, ISAP 2015*, pp. 10–12, 2016.

[69] S. M. Asif, A. Iftikhar, and K. Maile, “A Wide-Band Tissue Numerical Model for Deeply Implantable Antennas for RF-Powered Leadless Pacemakers,” *IEEE Access*, vol. 7, pp. 31031–31042, 2019.

[70] R. R. Hasan, A. Rahman, S. Sinha, N. Uddin, and T. R. Niloy, “In Body Antenna for Monitoring Pacemaker,” *Int. Conf. Autom. Comput. Technol. Manag.*, pp. 2019–2022, 2019.

[71] M. Behih, F. Bouttout, T. Fortaki, and C. Dumond, “A novel multifunction implantable antenna design for biomedical telemetry,” *2021 Int. Appl. Comput. Electromagn. Soc. Symp. ACES 2021*, pp. 1–4, 2021.

[72] S. Yazdanifard and R. A. Sadeghzadeh, “A Miniaturized Design of Dual-band Antenna for Bidirectional Brain Machine Interface Applications,” *IETE J. Res.*, 2020.

[73] T. Shaw, G. Samanta, and D. Mitra, “Efficient Wireless Power Transfer System for Implantable Medical Devices Using Circular Polarized Antennas,” *IEEE Trans. Antennas Propag.*, vol. 69, no. 7, pp. 4109–4122, 2021.

[74] A. Alshammari, A. Iqbal, T. A. Denidni, and I. Mabrouk, “A Miniaturized Implantable Antenna for ISM band Biomedical Application,” *IEEE Int. Symp. Antennas Propag. Usn. Radio Sci. Meet.*, no. 1, pp. 109–110, 2022.

[75] D. Silue, “Enhanced Meander antenna for in-body telemetry applications,” *18th Int. Conf. Wirel. Mob. Comput. Netw. Commun. 2022*, pp. 278–283, 2022.

[76] N. Nancy and K. R. Singh, “Biomedical Implantable Antenna with Fractal Geometry,” *2022 2nd Asian Conf. Innov. Technol. (ASIANCON). IEEE*, pp. 2–6, 2022.

[77] T. J. Sweety and T. R. Arun, “CB - CPW Fed Double Hexagonal Spender Shape Antenna for ISM Band Applications,” *Third Int. Conf. Intell. Comput. Instrum. Control Technol. 2022*, pp. 1335–1338, 2022.

[78] M. Rahman, F. Ahmed, and A. M. A. Rahman, “A compact MICS band operated implantable antenna for biomedical applications,” *4th Int. Conf. Electr. Eng. Inf. Commun. Technol. iCEEiCT 2018*, pp. 148–151, 2019.

[79] T. F. Chien, C. M. Cheng, H. C. Yang, J. W. Jiang, and C. H. Luo, “Development of nonsuperstrate implantable low-profile CPW-fed ceramic antennas,” *IEEE Antennas Wirel. Propag. Lett.*, vol. 9, pp. 599–602, 2010.

[80] C. Liu, Y. Guo, and S. Xiao, “A Hybrid Patch / Slot Implantable Antenna for Biotelemetry Devices,” *IEEE Antennas Wirel. Propag. Lett.*, vol. 11, pp. 1646–1649, 2013.

[81] S. Das and D. Mitra, “Design of a compact circular polarized implantable ring slot antenna for biomedical applications,” *Electromagnetics*, vol. 40, no. 2, pp. 83–92, 2020.

[82] D. Nguyen and C. Seo, “An Ultra-Miniaturized Antenna Using Loading Circuit Method for Medical Implant Applications,” *IEEE Access*, vol. 9, pp. 111890–111898, 2021.

[83] M. J. Christoe, N. Phaoseree, J. Han, and A. Michael, “Meandering Pattern 433 MHz Antennas for Ingestible Capsules,” *IEEE Access*, vol. 9, pp. 91874–91882, 2021.

[84] A. Basir, A. Bouazizi, and M. Zada, “A dual-band implantable antenna with wide-band characteristics at MICS and ISM bands,” *Microw Opt Technol Lett.*, no. April, pp. 1–5, 2018.

[85] T. Le Trong, S. Imran, H. Shah, G. Shin, S. M. Radha, and I. Yoon, “A Compact Triple-Band Antenna With a Broadside Radiation Characteristic for Head-Implantable,” *IEEE Antennas Wirel. Propag. Lett.*, vol. 20, no. 6, pp. 958–962, 2021.

[86] A. Kiourti, K. A. Psathas, P. Lelovas, N. Kostomitsopoulos, and K. S. Nikita, “In-vivo tests of implantable antennas in rats: Antenna size and intersubject considerations,” *IEEE Antennas Wirel. Propag. Lett.*, vol. 12, pp. 1396–1399, 2013.

[87] C. Xiao, S. Hao, and Y. Zhang, “915 MHz Miniaturized Loop Conformal Antenna for Capsule Endoscope,” *IEEE Trans. Antennas Propag.*, vol. 70, no. 11, pp. 10233–10244, 2022.

[88] N. Abbas, S. Ahson, A. L. I. Shah, G. S. Member, H. Yoo, and S. Member, "Miniaturized Antenna for High Data Rate Implantable Brain-Machine Interfaces," *IEEE Access*, vol. 10, pp. 66018–66027, 2022.

[89] S. Manaf, A. Shah, M. Zada, and J. Nasir, "Ultraminiaturized Triband Antenna With Reduced SAR for Skin and Deep Tissue Implants," *IEEE Trans. Antennas Propag.*, vol. 70, no. 9, pp. 8518–8529, 2022.

[90] S. Ahlawat *et al.*, "Design and Performance Measurement of Implantable Differential Integrated Antenna for Wireless Biomedical Instrumentation Applications," *IEEE Trans. Instrum. Meas.*, vol. 71, 2022.

[91] S. Manaf, A. L. I. Shah, M. Zada, and G. S. Member, "Electrically-Small Antenna With Low SAR for Scalp and Deep Tissue Biomedical Devices," *IEEE Access*, vol. 10, no. July, pp. 90971–90981, 2022.

[92] M. S. Singh, J. Ghosh, and S. Ghosh, "Miniaturized Dual-Antenna System for Implantable Biotelemetry Application," *IEEE Antennas Wirel. Propag. Lett.*, vol. 20, no. 8, pp. 1394–1398, 2021.

[93] R. Liu, W. Cui, H. Zheng, and E. Li, "Design of Conformal Spiral Dual-Band Antenna for Wireless Capsule System," *IEEE Access*, vol. 9, pp. 117349–117357, 2021.

[94] S. Shikha and R. K. Sarin, "Low-profile patch antennas for biomedical and wireless applications," *J. Comput. Electron.*, vol. 16, no. 2, pp. 354–368, 2017.

[95] C. Liu, Y. Guo, and S. Xiao, "Compact Dual-Band Antenna for Implantable Devices," *IEEE Antennas Wirel. Propag. Lett.*, vol. 11, pp. 1508–1511, 2012.

[96] B. Aslam, U. Hasan, K. Muhammad, A. Azam, and Y. Amin, "A compact implantable RFID tag antenna dedicated to wireless health care," *Int J RF Microw Comput Aided Eng.*, no. November 2016, pp. 1–11, 2017.

[97] K. Yeap, C. Voon, T. Hiraguri, and H. Nisar, "A compact dual-band implantable antenna for medical telemetry," *Microw. Opt. Technol. Lett.*, vol. 61, no. 9, pp. 2105–2109, 2019.

[98] M. Usluer and B. Cetindere, "Compact implantable antenna design for MICS and ISM band biotelemetry applications," no. July, pp. 1–7, 2019.

[99] W. Lei and Y. X. Guo, "Miniaturized differentially fed dual-band implantable antenna: Design, realization, and In-vitro test," *Radio Sci.*, vol. 50, no. 10, pp. 959–967, 2015.

[100] A. E. Mohamed, "Implanted dual-band circular antenna for biomedical applications," pp. 1125–1132, 2018.

[101] S. Bakogianni and S. Koulouridis, "An Implantable Planar Dipole Antenna for Wireless MedRadio-Band Biotelemetry Devices," *IEEE Antennas Wirel. Propag. Lett.*, vol. 15, pp. 234–237, 2016.

[102] J. H. Lee and D. W. Seo, "Compact and tissue-insensitive implantable antenna on magneto-dielectric substrate for wireless biotelemetry," *J. Electromagn. Waves Appl.*, vol. 33, no. 18, pp. 2449–2461, 2019.

[103] P. M. T. Ikonen, K. N. Rozanov, A. V Osipov, P. Alitalo, and S. A. Tretyakov,

"Magnetodielectric Substrates in Antenna Miniaturization : Potential and Limitations," *IEEE Trans. Antennas Propag.*, vol. 54, no. 11, pp. 3391–3399, 2006.

[104] A. E. Mohamed, A. H. Muqaibel, M. S. Sharawi, and S. Arabia, "Superstrate loaded miniaturized patch for biomedical telemetry," *Microw. Opt. Technol. Lett.*, vol. 59, no. 5, pp. 1212–1218, 2017.

[105] M. A. Malek, S. Hakimi, S. K. A. Rahim, and A. K. Evizal, "Dual-band CPW-fed transparent antenna for active RFID tags," *IEEE Antennas Wirel. Propag. Lett.*, vol. 14, pp. 919–922, 2014.

[106] M. Samsuzzaman, M. T. Islam, J. S. Mandeep, and N. Misran, "Printed Wide-Slot Antenna Design with Bandwidth and Gain Enhancement on Low-Cost Substrate," *Sci. World J.*, vol. 2014, 2014.

[107] S. Ahlawat, "Design of skin implantable radiator with capacitive and CSRR loadings for ISM band applications," *Int. J. Inf. Technol.*, 2019.

[108] M. Ameen, O. Ahmad, and R. K. Chaudhary, "Bandwidth and gain enhancement of triple-band MIMO antenna incorporating metasurface-based reflector for WLAN/WiMAX applications," *IET Microwaves, Antennas Propag.*, vol. 14, no. 13, pp. 1493–1503, 2020.

[109] G. Singh and J. Kaur, "Skin and brain implantable inset-fed antenna at ISM band for wireless biotelemetry applications," *Microw. Opt. Technol. Lett.*, vol. 63, no. 2, pp. 510–515, 2021.

[110] C. Lee, T. Yo, and C. Luo, "Compact broadband stacked implantable antenna for biotelemetry with medical devices," *IEEE Annu. Wirel. Microw. Technol. Conf.*, pp. 6–9, 2006.